INVESTIGATION OF DRILLING PERFORMANCE AND PENETRATION MECHANISM USING PASSIVE VIBRATION ASSISTED ROTARY DRILLING TECHNOLOGY

by
© Md. Shaheen Shah

A Thesis submitted to the
School of Graduate Studies
in partial fulfillment of the requirements for the degree of

Master of Engineering

Department of Oil and Gas Engineering
Faculty of Engineering and Applied Science
Memorial University of Newfoundland

October 2020

St. John's   Newfoundland

Abstract

Drilling performance is an essential goal in the petroleum and mining industry. Drilling Rate of Penetration (ROP) is influenced by the operating parameter: torque, Weight on Bit (WOB), fluid flow rate, Revolution per Minute (rpm), rock related parameters (rock type, rock homogeneousness, rock anisotropy orientation), and mechanical parameters (bit type, configuration of the Bottom Hole Assembly (BHA)). The Drilling Technology Laboratory (DTL) at Memorial University of Newfoundland has incorporated the passive Vibration Assisted Rotational Drilling Technology (pVARD) as a drilling tool. This tool includes three parts within a compliant part, a part that dampens and a torque transmitting unit that is inside the BHA of the drill string. This tool utilizes the natural vibrations of the drilling process to increase drilling efficiency and rate of penetration. In this thesis, laboratory and field drilling tests have been conducted by first and second generation pVARD tools respectively which could play a positive role in improving drilling penetration rate through modified bit-rock compliance from conventional drilling. This research aims to develop a fundamental guideline for rock strength measurement and to interlink mechanical tests for the purpose of evaluating drilling performance. The compressive rock strength has an inverse relationship with drilling efficiency. The average Unconfined Compressive Strength (UCS) and Indirect Tensile Strength (ITS) of the granite were obtained to be 168.4 MPa and 16.3 MPa respectively by the mechanical loading frame in the laboratory parameters following American Society for Testing and Materials (ASTM) standard.

The pVARD operational details are important for optimal configuration and best drilling results. The study focused on designing pVARD to be consistent with a Large Drilling Simulator (LDS) selecting optimal Belleville springs. Compression tests and numerical studies have been carried out using a mechanical frame and simulation analysis respectively, for different Belleville Spring stacking scenarios. Mechanical and simulation studies with details of pre-planned drilling experiments can provide important guidelines for optimizing pVARD basics. The hysteresis effect analysis of LDS-pVARD springs also provided a coherent idea of energy dissipation during the cycle test. Depending on the rock type and drilling parameters can provide pre-settings and configurations of pVARD for optimal drilling performance.

Finally, this dissertation focuses on the effects of vibration on the performance of a diamond coring bit when drilling on hard rock with a first-generation small lab scale vibration tool pVARD. Thereafter, Drill off Tests (DOTs) have been performed using a Small Drilling Simulator (SDS) with axial vibrations on the drill string in laboratory conditions. The vibration properties have been adjusted to various settings of spring compliance and dampening (rubber) material. The results of the evaluation of the experimental data show that the ROP increased by a maximum of 28% keeping WOB within the operational limits.

The results and knowledge obtained from this study will help to design third generation pVARD tools.

Keywords: Rate of Penetration (ROP), Drilling Efficiency, passive Vibration Assisted Rotational Drilling Technology (pVARD), Rock Strength, Belleville Spring, Drill off Tests.

Acknowledgements

Table of Contents

List of Figures

List of Tables

List of Symbols, Nomenclature or Abbreviations

MUN	Memorial University of Newfoundland
DTL	Drilling Technology Laboratory
VARD	Vibration Assisted Rotational Drilling
pVARD	passive Vibration Assisted Rotational Drilling
ASTM	American Society for Testing and Materials
ROP	Rate of Penetration
RPM	Revolution Per Minute
WOB	Weight on Bit
UCS	Unconfined Compressive Strength
CCS	Confined Compressive Strength
ITS	Indirect Tensile Strength
BHA	Bottom Hole Assembly
FEA	Finite Element Analysis
LDS	Large Drilling Simulator
SDS	Small Drilling Simulator
DRIL	Drilling Research Investigation Limited
VNI	Union Drilling Institute
MSE	Mechanical Specific Energy
DOC	Depth of Cut
MRR	Material Removal Rate
PQ	Performance Qualifier
CPF	Cost Per Foot
FPD	Feet Per Day
BC	Bit Cost
RR	Rig Rate
PDC	Polycrystalline Diamond Compact
POT	Pump off Test
DOT	Drill off Test
NPT	Non-Productive Time
INPT	Invisible Non-Productive Time
BHP	Bottom Hole Pressure
BHC	Bottom Hole Cleaning
AOGT	Axial Oscillation Generator Tool
DEM	Distinct Element Method
DOD	Downhole Oscillating Device
FOS	Factor of Safety
SinSoft	Single Soft Springs
SinStiff	Single Stiff Springs
DouStiff	Double Stiff Springs
LVDT	Linear Variable Differential Transformer

Chapter 1:   Introduction

1.1.   Research Background

Drilling is essential for exploration, and production of hydrocarbon. Drilling efficiency, productivity and cost-effectiveness have also become important for oil and gas companies because of low hydrocarbon price. Increasing the rate of penetration (ROP) has been a matter of great interest in the oil and gas industry and different technologies have been developed in the last century to achieve this goal. For the Rotary drilling operation, the borehole is drilled by rotating a bit, and cuttings are removed by continuous circulation of the drilling fluid in which natural bit vibration is generated when the bit penetrates the formation [1]. The technology uses natural bit vibration or additional vibration to enhance drilling performance. The most important variables influencing the ROP have been identified: bit type, formation characteristics, drilling fluid properties, bit operating conditions, bit tooth wear, bit hydraulic.

There have been numerous research reporting vibration related issues to oil and gas drilling. These reports have mainly highlighted the negative effect of vibrations induced in the oil and gas wells while drilling that reduce the tool's life time, damage downhole tools, increase the nonproductive time, decrease the drilling rate of penetration, and eventually increase the overall drilling cost. However, a segment of publications shows a positive influence of vibrations on enhancing drilling performance, reducing the Non-Productive Time (NPT), and decreasing overall drilling cost.

NPT which is the main reason for delays in planned drilling projects. There are numerous incidents or events that cause the stoppage of drilling operations or the progress of drilling progress resulting in NPT. In some cases, NPT can be anonymous and difficult to detect which is called Invisible Non-Productive Time (INPT). Vieira et al. [2] showed the drilling time and the effect of INPT overall drilling costs of a well drilled in the Middle East that is in Figure *1.1*.Undoubtedly, the introduction of NPT detection and methods for its elimination reduces the overall cost of wells and consequently indicates additional costs in developing other wells or exploring other fields.
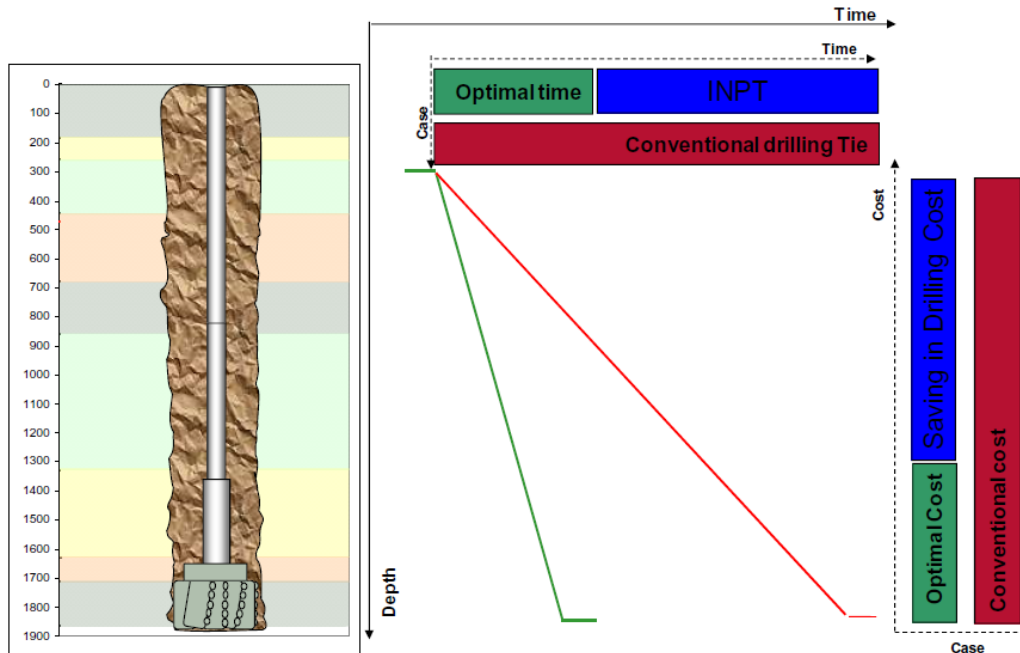
Figure 1.1: The consequence of INPT on the drilling time and the overall drilling cost [2]

The passive Vibration Assisted Rotary Drilling (pVARD) investigation at the Drilling Technology Laboratory (DTL) of Memorial University of Newfoundland started by examining how to further improve the drilling efficiency of drill string vibrations by affecting rock penetration. In its continuity DTL has designed, manufactured, and conducted lab and field trials using a novel drilling passive vibration tool for use in the Bottom Hole Assembly (BHA) of a drill string. It is selected to utilize naturally occurring vibrations for the drilling process to increase drilling efficiency without damage/wear to the bit. This pVARD technology improves bit-rock interaction and increases ROP by integrating spring compliance between drill strings.

A diamond coring bit is used as the primary bit for the simulation, experiment, and study. The diamond core drilling bit is used extensively to drill circular or annular holes in a variety of material. The diamond core drill bit was patented by Jedick and Ohio [3] and has revolutionized the drilling industry—resulting directly in the discovery of many minable orebodies that could have gone otherwise unnoticed. Before the introduction of the diamond core bit, drilling was still largely dependent on the search for rock outcrops through the different indirect petro-physical methods, with little information available about the ore density below the surface.

2

pVARD tool has not previously been tested on granite using coring bits. pVARD is comprised of compliance components that distinguish it from conventional drilling performance. Initially, laboratory and field tests in the DTL show that pVARD technology is promising compared to rotary drilling performance. In some experimental relationships in the DTL research, it is proposed to describe ROP-related parameters such as weight-on-bit (WOB), rotary speed, and rock strength, which have been designated as 'The Perfect-Cleaning Theory'. Some numerical and simulation analysis has been done for pVARD in rotary drilling. However, a study is needed on the investigation for the increase in ROP and drilling process in rotary drilling using pVARD. In addition, an evaluation is required to develop a guideline for rock compressive strength measurement for the purpose of evaluating drilling performance.

One of the main goals of this thesis is to develop the empirical mechanisms following American Society for Testing and Materials (ASTM) standards that use a mechanical test frame to measure granite strength. Thereafter, the focus of this thesis is to further improve drilling performance by understanding one key variable, drill string vibration using a pVARD tool in experimental investigation. This study will help develop the different scales of the pVARD tool to increase drilling efficiency beyond the current limit of optimization of existing drilling parameters.

1.2. Research Purpose and Objectives

For the drilling operation with optimum efficiency, the control of cutting force, vibration force, and advancing direction of drill bits is critical. Therefore, systematic analysis of working forces of drill bits and force direction control can be necessary and useful for drilling setup design, and be helpful for understanding and optimizing passive Vibration Assisted Rotary Drilling (pVARD). Preliminary laboratory and field tests have shown that pVARD technology is promising compared to rotary drilling. The main focus of this research is therefore to design passive vibration-assisted rotary drilling experiments such that:

➢ Evaluate the strength of the granite with standard unconfined compressive and indirect tensile tests by a mechanical loading frame.

➢ Schematic design of the laboratory scale pVARD to be mechanically compatible with LDS by selecting optimal Belleville Springs.

➢ Conduct the mechanical and simulation studies to optimize Belleville Springs stacking and LDS-pVARD configurations for drilling performance applications.

➢ Evaluate the hysteresis effect on the LDS Belleville springs with experimental load-deflection cyclic analysis.

➢ Investigate the application and performance of the passive vibration-assisted rotary drilling (pVARD) tool with a Diamond coring bit on granite sample and compared to drilling using the conventional system "rigid".

1.3. Thesis Outline

This thesis focuses on the design, improvement, and experimentation of passive Vibration Assisted Rotary Drilling (pVARD) equipment. This work also develops fundamental planning for rock strength measurement for the purpose of evaluating drilling performance.

Chapter 2 provides an extensive literature review about the rotary drilling, drilling efficiency and rate of penetration, factor affecting ROP, diamond coring bit and its penetration mechanisms. It also covers the drill hole vibrations and bit-rock interaction. This chapter also describes the current state of knowledge around pVARD technology.

Chapter 3 explains the background study of the effect of vibration on ROP. It also describes the previous generation of the VARD and pVARD analysis.

Chapter 4 focuses on describing the research methodology of the main four chapters.

Chapter 5 covers the standard unconfined compressive and indirect tensile strength measurement of the granite rock by mechanical loading frame in the laboratory conditions.

Chapter 6 suggests the schematic design of the third generation means LDS-pVARD tool. It also describes the mechanical and simulation studies on various scenarios of Belleville Spring stacking as vibrational element.

Chapter 7 investigates the hysteresis effect on the LDS-pVARD spring with experimental load-deflection cyclic analysis.

Chapter 8 evaluates the effect of the vibration on the granite using the SDS-pVARD tool with a diamond coring bit for measuring drilling performance and compares it to conventional system drilling without pVARD.

Chapter 9 highlights the accomplished summary and conclusions of this research. It also suggests some recommendations for the third generation pVARD to produce an optimal operational range for the drilling applications.

Chapter 2:   Literature Review

2.1.   Rotary Drilling Technique

Rotary drilling is one of the most widely used drilling techniques in the oil and gas industry. The rotary drilling process is shown in Figure *2.1*. The main components of rotary drilling consist of a rotary table and kelly. A drill pipe is attached to the kelly which is led by a rotary table. Torque is transferred from the drill bit at the bottom of the drill pipe. Weights are applied on the drill bit which is termed as WOB and rock is fractured by the bit-rock interaction. Drilling mud is circulating from the mud tank. The bit is elevated in pressure by passing the mud pump through the inner hole of the drill pipe, then through the bit nozzle, and back up the mud tank to the wellbore with the annulus in the drill pipe. Thus, the drilling cuttings are removed with repeat drills through the annulus from the bottom thereby cleaning the bottom holes making the drilling smooth. Rate of Penetration (ROP), is a key parameter for evaluating the entire drilling performance. ROP enhancement is the main goal of drilling activity [1].
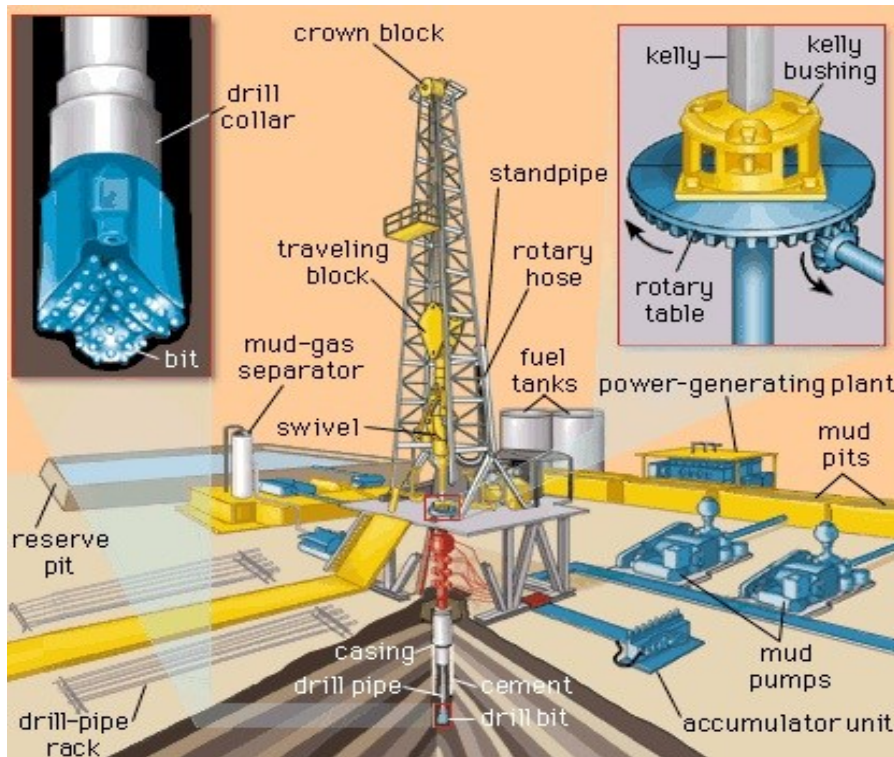
Figure 2.1: Mechanisms of the Rotary Drilling Technique *[4]*

2.2. Drilling Efficiency & Rate of Penetration

Empirical relationships were proposed by the researchers to describe ROP-related factors. Maurer [5] found that ROP relates with the rotary speed, weight on the bit , the bit diameter , and the strength of the rock being drilled, the relationship known as "perfect cleaning". This relationship is imperfect because it does not include other drilling parameters such as bottom-hole-pressure (BHP), flow rate, and cutting cleaning efficiency. In addition, Bauer and Calder [6] showed that a good correlation could be obtained between penetration rate and rock uniaxial compressive strength, provided sufficient tests were conducted to obtain a statistically meaningful rock strength. Bourgoyne and Young [7] introduced a model that is accomplished through multiple regression analyses of detailed drilling data taken over short intervals that include formation strength, depth, compaction, and pressure differential across the hole bottom, bit diameter and weight, wear, rotary speed, and bit hydraulics. Warren [8] developed an imperfect cleaning model to predict ROP while accounting for the hydraulic effect for hole cleaning although it does not include cuttings-removal effects. Detournay et al. [9] completed the bit-rock interface model of the drilling response with a set of relations between the weight-on-bit, the torque, the angular velocity, and the rate of penetration that followed the bit-rock interaction. Based on these empirical relationships, researchers have been performing and determining drilling efficiency.

Taylor et al. [10] discussed drilling efficiency focusing on ROP. In most cases, ROP is considered equal to the drilling efficiency or other parameters that are related to the drilling efficiency although there are some exceptions.

Drilling efficiency is defined by Wilmot et al. [11] as the construction and delivery of a useable well while achieving the operational conditions needed to gain the lowest cost. This definition specifies that there is no single Performance Qualifier (PQ) which is equal to drilling efficiency and that evaluates all PQs and its effects on each other to give maximum efficiency.

To quantify, drilling efficiency has been measured on the Cost Per Foot (CPF), Feet Per Day (FPD), and Mechanical Specific Energy (MSE).

CPF takes into account the Rate of Penetration (ROP), Bit Cost (BC), the Rig Rate (RR), Trip time (T_t), and Time (t) which is given below [11]:

$$CPF = \frac{1}{ROP} \times \left[\left(\frac{BC}{t}\right) + RR \times \left(1 + \frac{T_t}{t}\right)\right] \dots\dots.2.1$$

FPD is calculated by multiplying the average ROP by 24 as in equation 2.2

$$FPD = ROP_{avg} \times 24 \dots\dots.2.2$$

MSE is accomplished through Weight on Bit (WOB), ROP, size of the bit A_b, the rotational speed (N) as well as the torque needed to turn the bit (T) as expressed in equation 2.3 and as developed by Teale [12].

$$MSE = \frac{WOB}{A_b} + \frac{60 \times 2\pi \times N \times T}{A_b \times ROP} \dots\dots\dots 2.3$$

Evaluating all the PQs together will give an effective result of drilling efficiency. Cochener [13] reported that drilling efficiency can be determined by cover time, distance, performance, productivity, and financial parameters including:

• Footage drilled per hour
• Days to depth (drilling days)
• Footage drilled per rig
• Wells drilled per rig
• Success rates (or dry holes)
• Reserves added per well
• Reserves added per rig
• Production per well
• Dollars per foot
• Energy consumption

When testing the PQ together, it is found that an increase in the cost of downhole equipment life may result in a decrease in drill efficiency, even if the above-mentioned components (such as MSE) are improved through ROP. Increases must be seen in the average ROP for the drilling efficiency to be positively affected. On the other hand, some unwanted vibrations and unplanned events can lead to an average ROP reduction that negatively affects drilling efficiency. ROP is the key factor for evaluating the drilling this.

Wilmot et al. [11] defined the rate of penetration as progress per unit time, when the drill bit drills at the bottom and front. Average ROP is measured at average drill intervals. Cochener [13] described the most influential factor of ROP as the physical properties of the rock (lithology) at different depths. Rock lithology directly affects ROP through MSE. Other factors affecting ROP include mud condition, WOB, bit type, and rotary speed. Intuitively, there is an inverse relationship between ROP and MSE. Germiquet and Minnitt [14] also demonstrated a comparison of rock strength and ROP for different rock types or stratigraphic units. These showed an inverse relationship between penetration rate and rock strength that is indicated in Figure 2.2.
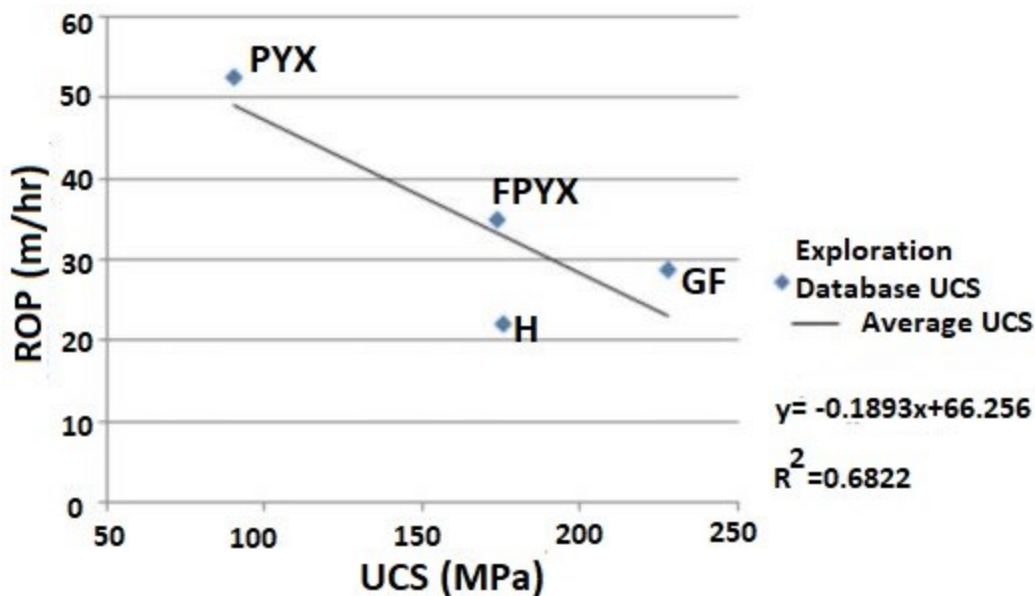
Figure 2.2: ROP compared to UCS for different rock types: pyroxenite(PYX),feldspathic pyroxenite (FPYX), granofels (GF), hybrid norite (H) *[14]*

The relationship between ROP, MSE, and power (P) has been intuitively investigated through graphs during drilling activity described by Pessier et al. [15]. This is called a power graph. The graph can illustrate how PQ's drilling efficiency and ROP are influenced. Figure 2.3 indicates the varying effect of the RPM and WOB to the drill bit through Power Graph.
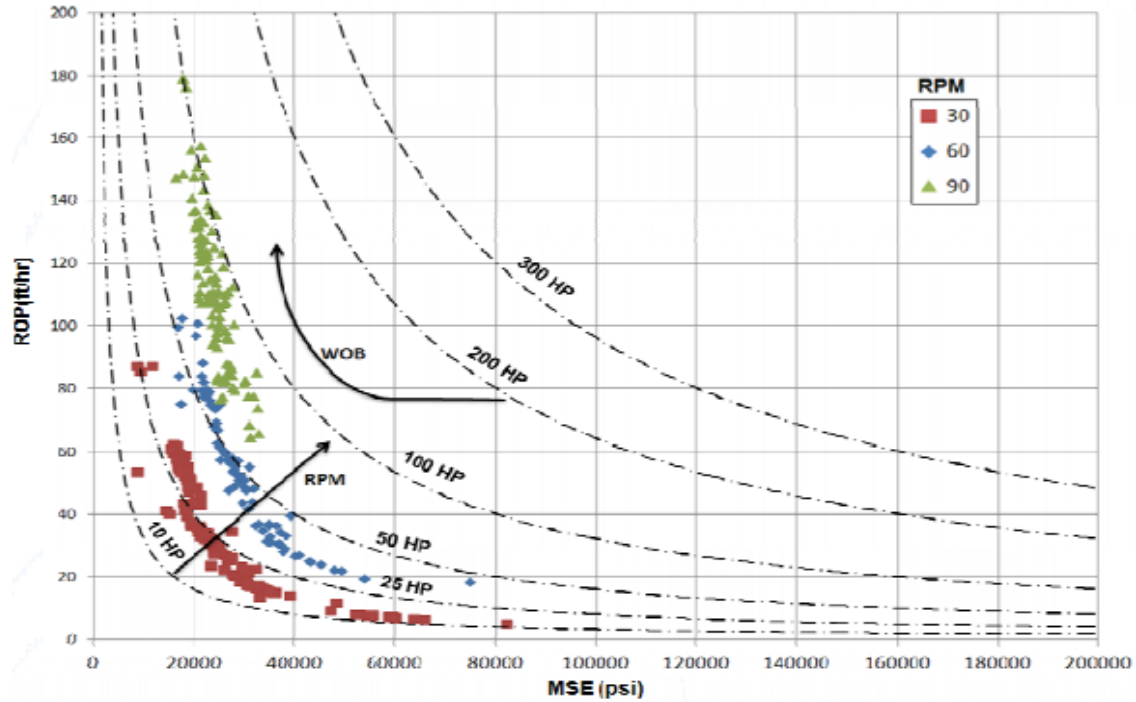
Figure 2.3:Power Graph of the combined effect of WOB and RPM *[15]*

Figure 2.4 shows the dependence of ROP on MSE at different depths for U.S. land rigs.
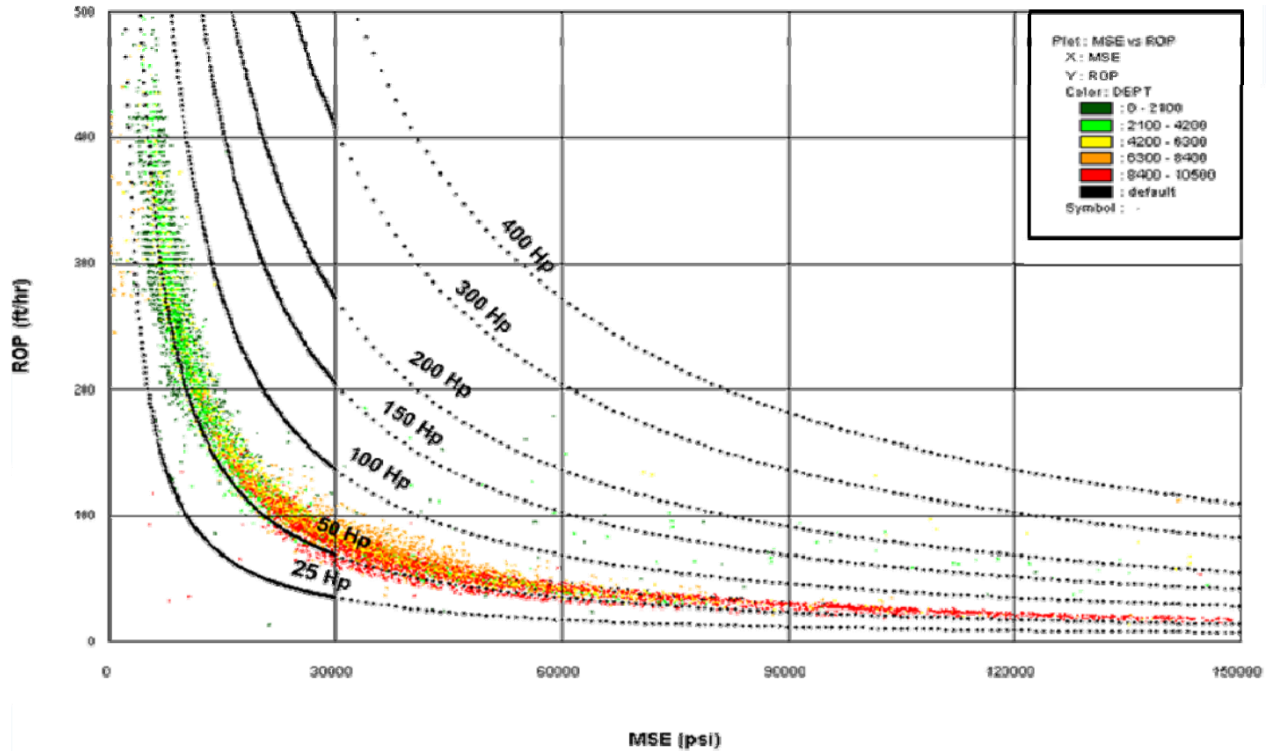
Figure 2.4:Power graph of the ROP vs MSE for the US land Rig *[15]*

2.3. Factors Affecting the Rate of Penetration

The most important factor influencing drilling efficiency is the improvement of ROP which has been studied by various researchers for decades. It is described in various researches that factors affecting ROP are varying Surface Drilling Parameters, Bottom Hole Pressure (BHP) and Bottom Hole Cleaning (BHC) [5], [16], [17].

2.3.1. Bottom Hole Cleaning

Maurer [5] evaluated the effect of Bottom Hole Cleaning (BHC) on ROP. In this study, ROP varied directly with the RPM and the square of WOB. It also changed inversely with the square of the bit diameter and the square of the strength of the rock being drilled. Maurer [5] suggested the condition where all of the rock debris removed between tooth impacts as indicated the perfect cleaning. The BHC influenced with the area of interaction between the bit and the rock.

Figure *2.5* indicates the relationship between rate of penetration, Weight on Bit, Rotary Speed and Bottom Hole Cleaning.
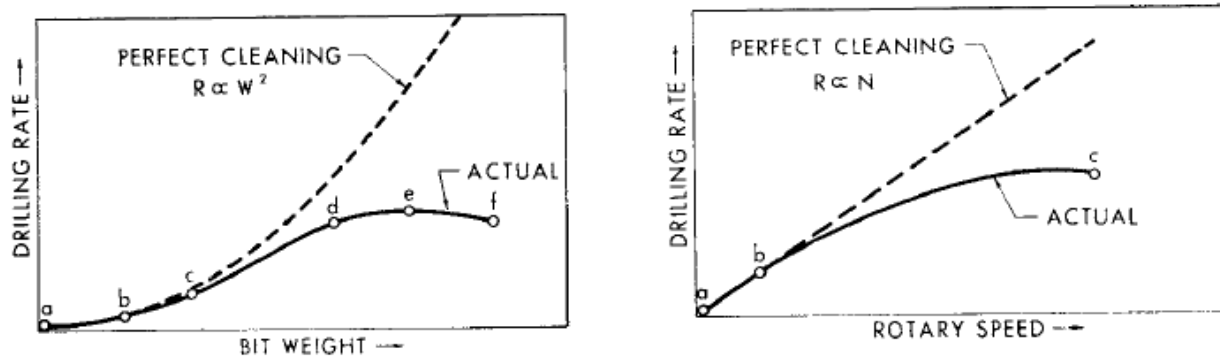
Figure 2.5: Maurer's [5] study on the relation between rate of penetration and Bottom Hole Cleaning

2.3.2. Surface Drilling Parameters

At the end of the 1930s, Brantly et al. [16] analyzed data from 500 wells drilled in several states across the United States. In this study, it was found that four factors, personnel and equipment, WOB, rotary speed and circulation fluid volume were considered to be effective for ROP control. A total of 123.7 percent increase in penetration rate was observed, relative importance of three factors: personnel and equipment, 55.5 percent; Rotational speed, 39.6 percent; the volume of drilling fluid 28.6 percent that shown in Figure 2.6. With the increase in the WOB, the penetration rates were increased by 50-70 percent through formations as shown in Figure 2.6.d.
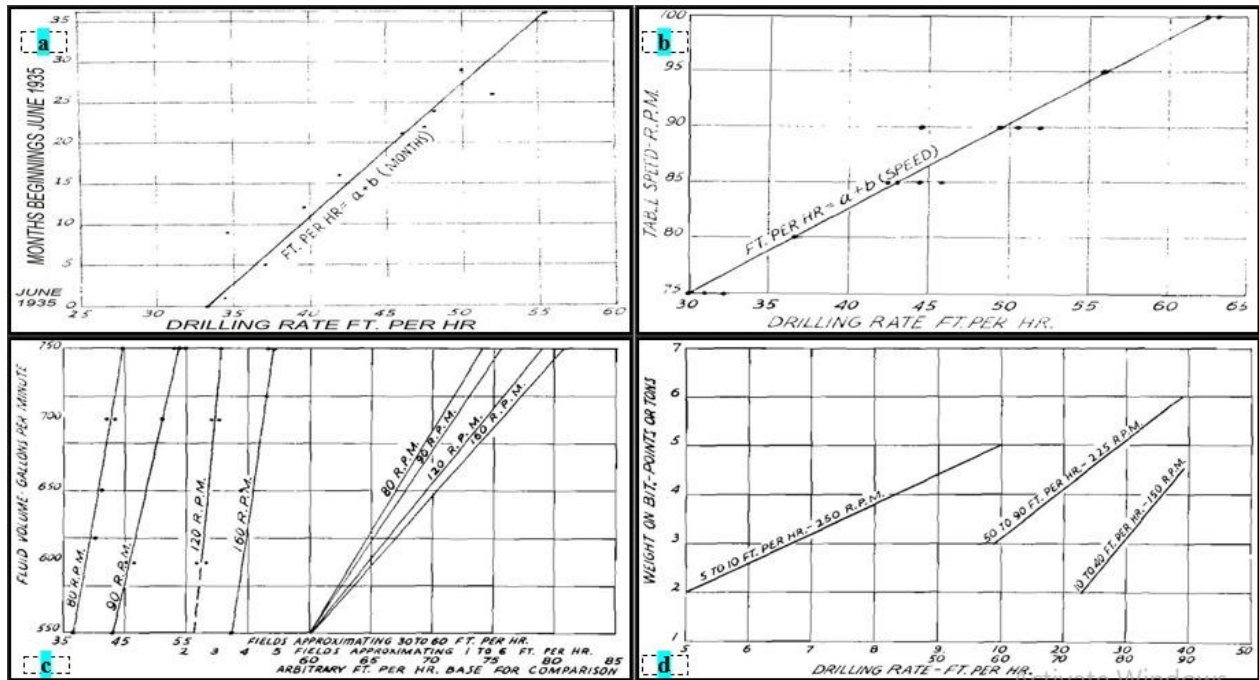
Figure 2.6: Penetration rate increase due to increased: a: Personnel and Equipment; b. Rotating Speeds; c. Fluid Volume; d. Weight on Bit. *[16]*

2.3.3. Bottom Hole Pressure

The decrease in penetration rate due to the increase in the strength of the rock is driven by the difference between the mud pressure and the pressure of the pore liquid in the formation that is shown in Figure 2.7 .Garnier and Van Lingen [17] reported Obernkirchener Sandstone and Vaurian Limestone were drilled, changes in BHP using water as a drilling fluid instead of drilling mud had no significant effect on ROP
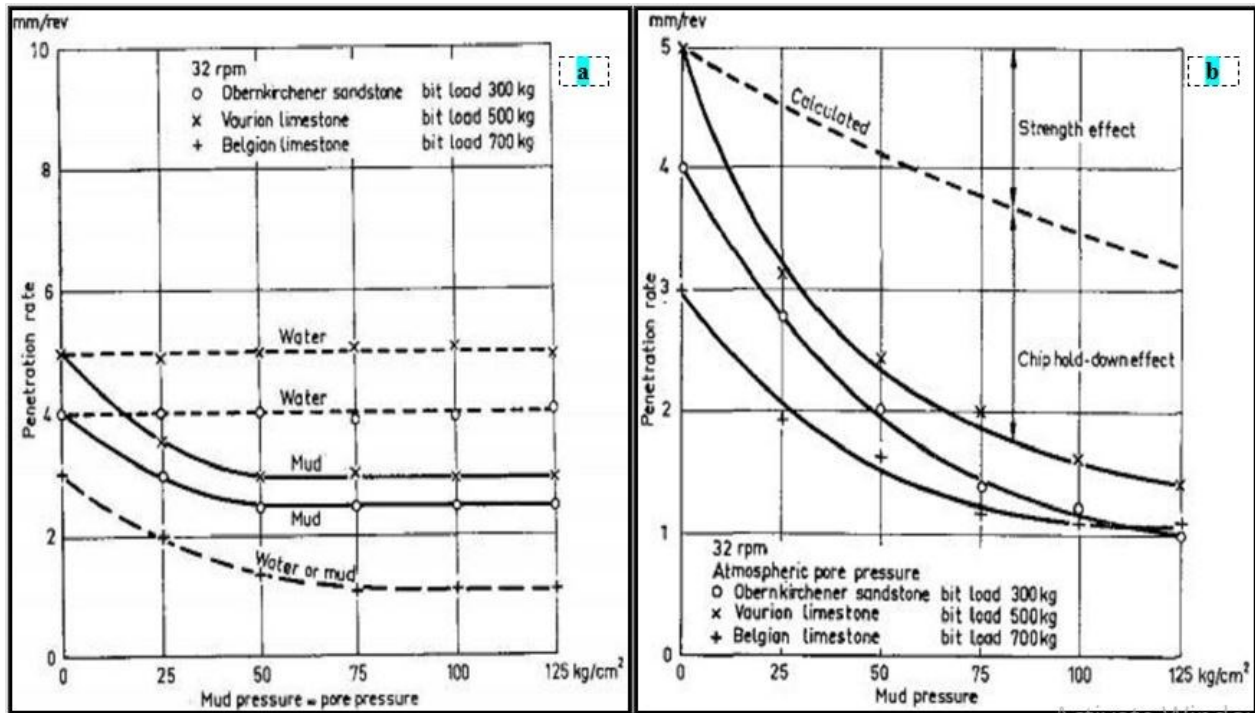
Figure 2.7: Experimental results for the effect of BHP on ROP: a. ROP as function of mud pressure; b. ROP as function of mud pressure at atmospheric pore pressure condition [17]

By increasing the BHP without fluid circulation, Garner *[18]* examined the performance of a diamond cutting bit at the penetration of the shale and limestone, resulting in a significant reduction in the amount of cutting.

2.4.   Penetration Mechanism of Coring bits

The diamond core drill bit is designed to remove a cylinder of material that looks like a hole. The core drill bit has an elongated cylindrical body with the first end and the opposite end. At one end portion there is a drive platform for facilitating the attachment of the bit to a drill assembly or other motor-driven drive mechanism. A cutting head is included at the other end of the body. The cutting head forms a group of cuttings mounted on the annular face of the second end of the body. Each section has an outer part, a middle part, and an inner part where diamond particles are scattered throughout. Each section includes a greater concentration of diamond particles than the middle section of the inner part and the cut portions of the outer part [3]. The metals of the matrix around the diamond are silver, copper, molybdenum, and tungsten. Annular holes are formed in concrete,

asphalt, rock, and related materials for a variety of reasons. Figure *2.8* shows the schematic view of the diamond coring bit and different sizes of the coring bits for hard rock coring.
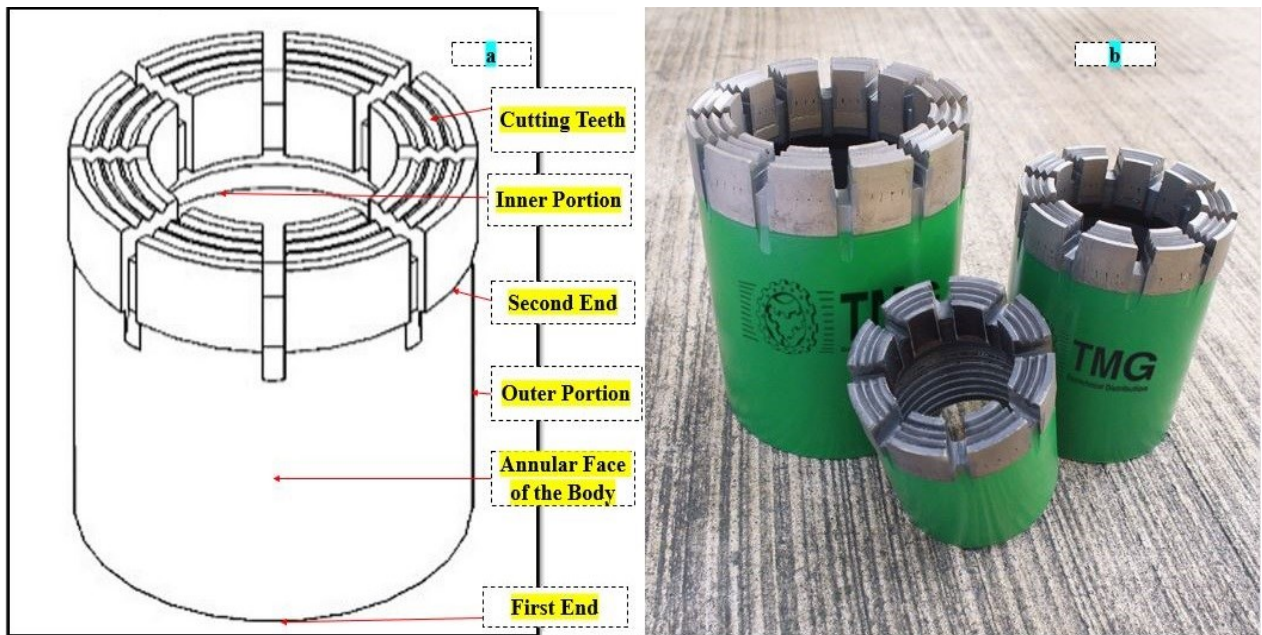
Figure 2.8: a. Schematic view of the Diamond Coring bit *[19]*; b. Different sizes for hard rock coring bits *[20]*

Drill bits have waterways with different numbers of teeth such as six, eight, ten etc. where most of the water flow during drilling rests between the rock and the drill bit. Each tooth has a hole pointing inwards or outwards to further increase the chances of cutting from the cutting area that is shown Figure *2.9*.a. When drilling, the upper part of the drill bit is facing downwards and cutting the rock. Figure *2.9*.b depicts a tooth from the drill bit [21], [22].
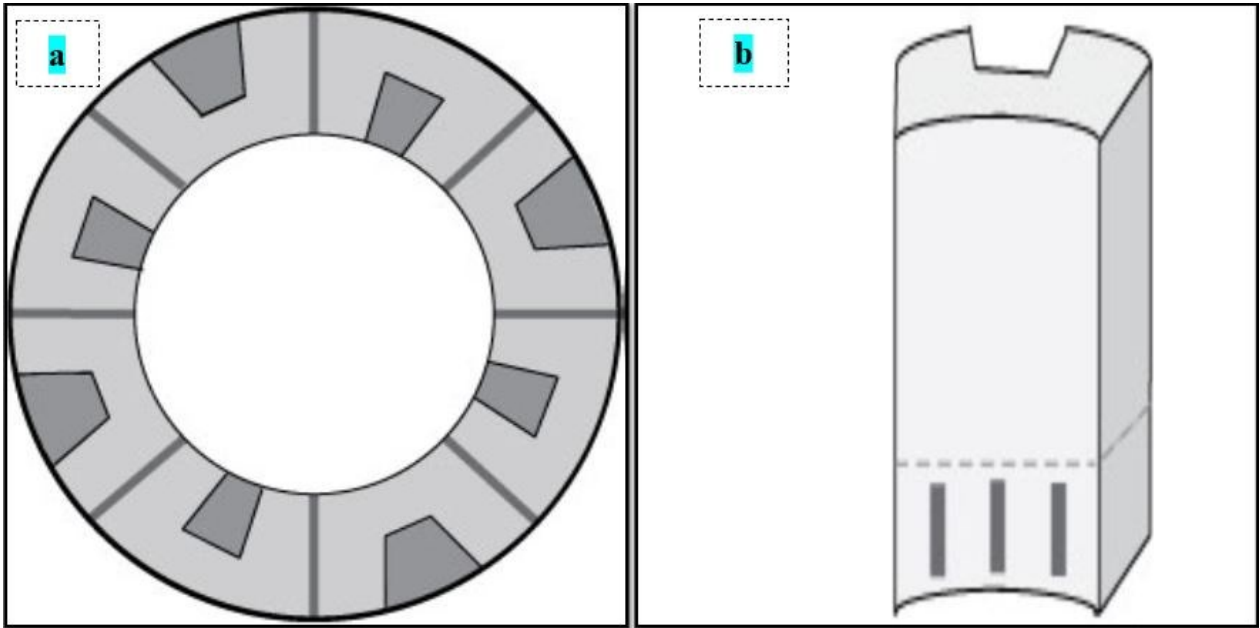
Figure 2.9:a) A picture of the drill bit from top view; b) A picture of one tooth from the drill bit. The dashed line indicates a change in material *[22]*.

The process of core drilling consists of three parts which include drilling, recovery of the core, and resumption of drilling. The drill stem is rotated clockwise with a drill bit attached to the bottom when drilling. The WOB manages the pressure on the drill bit which determines the penetration rate, ROP. The principle of the core drilling is illustrated in Figure *2.10*. The drill string is formed with an outer and inner tube.

Water flow is used between the tubes to cool the drill bits and to wash the cuts from the drilling. A small amount of water can act as a lubricant when carried between the drill bit and the rock. Core samples are collected inside the inner tube. The rock cuttings and drilling fluids are removed by the outer tube to the surface of the bit. A certain successive drilling break is given and core samples (about a meter long) are brought to the surface [23].
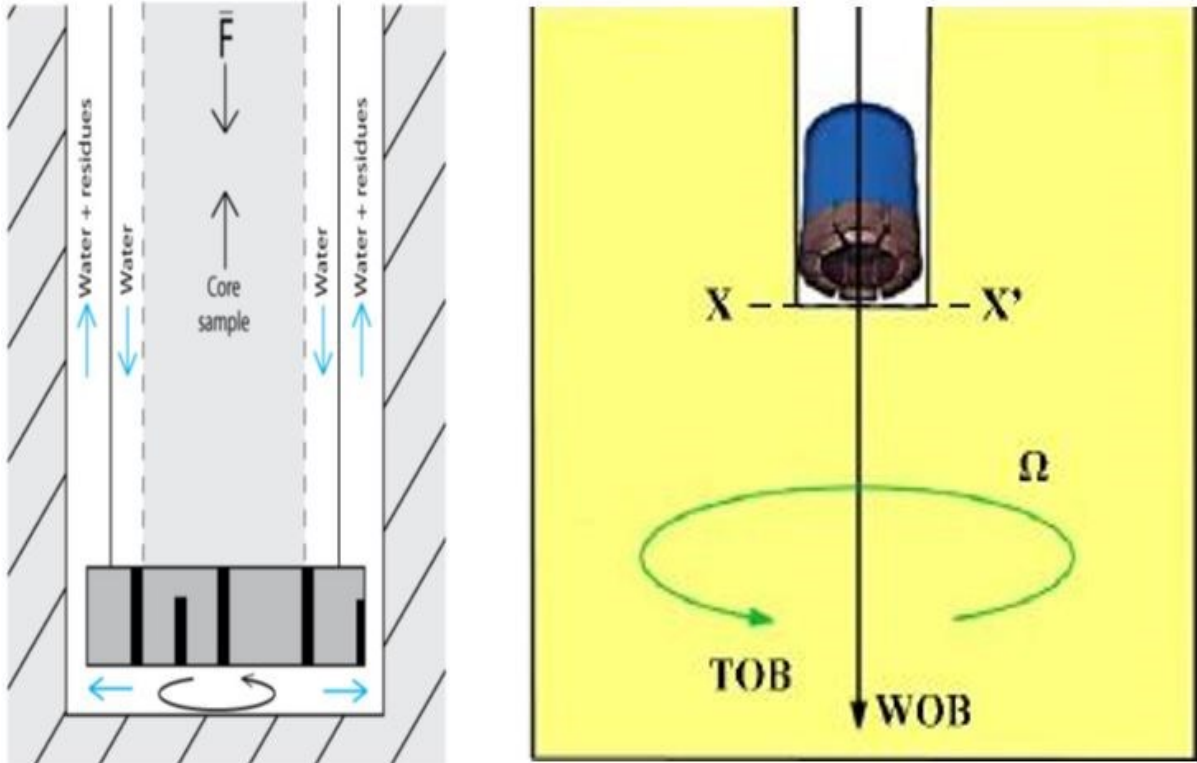
Figure 2.10: Schematic view for the principle of the coring drilling *[23]*, *[24]*

Based on the penetration rate and how the water flows, a model of the behavior of the boreholes is done that showed in Figure *2.11*.a. This indicates the schematic model for the bit/rock interface during penetration. The diamond is not pressed too deeply into the drill bit as there is a low penetration rate which leads to a larger gap between the drill bit and the rock. This occurs at the very top of the rock surface [24] .Figure *2.11*.b shows the contact of the diamond with the rock. When the rock is not touching the matrix, the larger gap also leads to lower wear of the matrix. Due to the large space between the rock and the drill bit the matrix is not worn so a large gap leads to the higher ridges. Water flows easily between the rock and the drill bit with large gaps, which leads to better transport of the rock cutter.

The flow of water can be turbulent and the drill bit matrix is eroded by cutting rocks in the water. During higher penetration rates the diamond is pushed more deeply into the rock which reduces the height of the gap as seen in Figure 2.11.c. The height of the reduction interval leads to a small space between the matrix and the rock which obstructs the flow of water and the surface of the drill bit worn by the debris causes the matrix to wear harmful wear from cutting the rock in the water.

17

If the WOB remains constant and only the rotational speed increases, then a lifting force may be raised. This has the same effect as reducing the WOB, i.e. longer intervals [25].
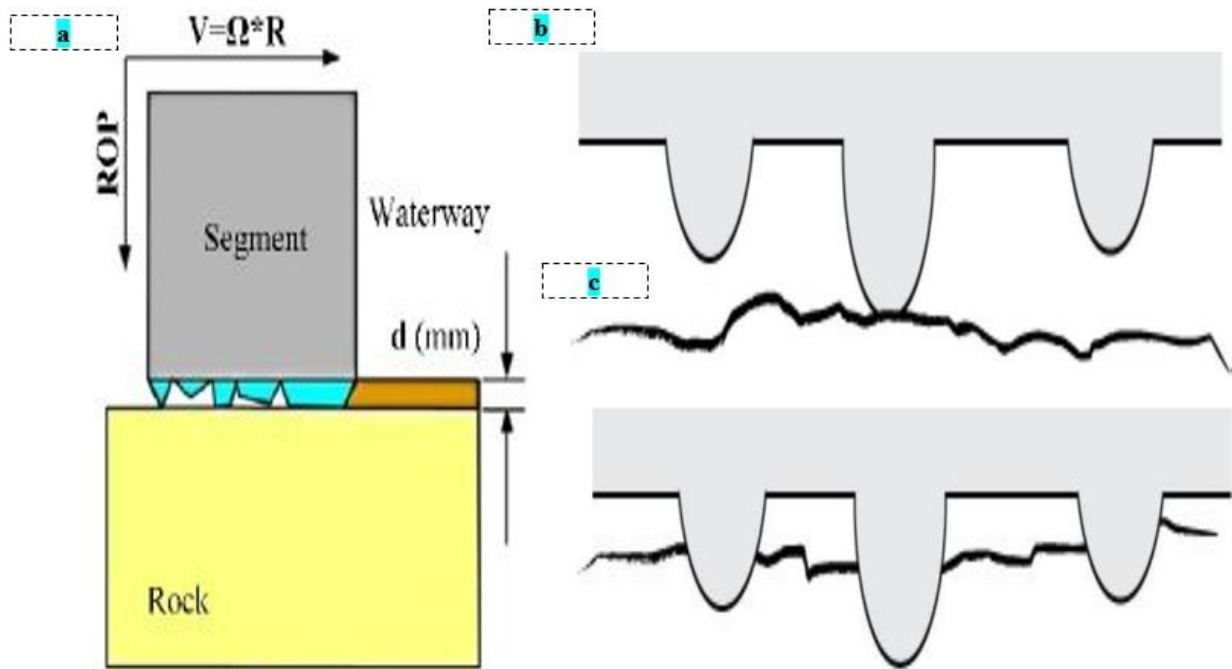
Figure 2.11:Schematic view of the penetration process; a. A Schematic model for bit/rock interface *[25]*; b. At a low ROP leads to a large gap *[22]*; c. At a higher ROP the diamonds are pressed into the rock *[22]*

2.5. Bit Vibration and Bit-rock Interaction

In drilling engineering, drill hole vibrations are divided into four terms: axial, lateral, torsional, and eccentered vibrations [26], [27] . These are illustrated in Figure *2.12*.

2.5.1. Axial Vibrations

Axial vibrations are defined as resonant axial motion which causes bit bounce. The bit repeatedly lifts off from the bottom and impacts the formation resulting in vibrations. These usually occur because of large differences in bit-weight. Axial vibrations usually occur in near-vertical holes, either using tri-cone bits, drilling out of the shoe track, in hard formations, or in stringers. It can also be the result of a premature bit, BHA component failure, and reduced ROP.

2.5.2. Torsional Vibrations

Torsional vibrations are defined as an alternate slowing and acceleration of BHA rotation. Sometimes after a certain period, the bit stops the rotation resulting in the drill string to periodically torque up and spin free. This usually occurs in high angle wells when aggressive Polycrystalline Diamond Compact (PDC) bits are used and where the BHA to wellbore friction is high. The fluctuations of torque and rpm are hints of the surface. This process can lead to over-torqued and damaged connection washouts. The increased bit speed and side-effect forces can remove cutters from PDC bits and roller cone bits. ROP can be adversely affected.

2.5.3. Lateral Vibrations

Lateral vibration is defined as an eccentric rotation of the bit. Instead of rotating around its geometric center, the bit rotates eccentrically as a result of contact with the wellbore. Surface detection is nearly impossible but downhole detection is easier due to the presence of high downhole lateral shocks consistent. High shock encouraged by bit rotation can cause premature BHA component failure, bit failure, and reduce ROP.

2.5.4. Eccentered Vibrations

Eccentered vibrations are the eccentric rotation of the BHA around the wellbore. Eccentered vibration combines the torsional vibration of stick-slip with side to side bending vibration creating eccentered vibration or BHA whirl. A combination of the thigh downhole lateral and torsional shocks is generating eccentered vibration. This high shock can easily cause a bit and BHA material to fail.
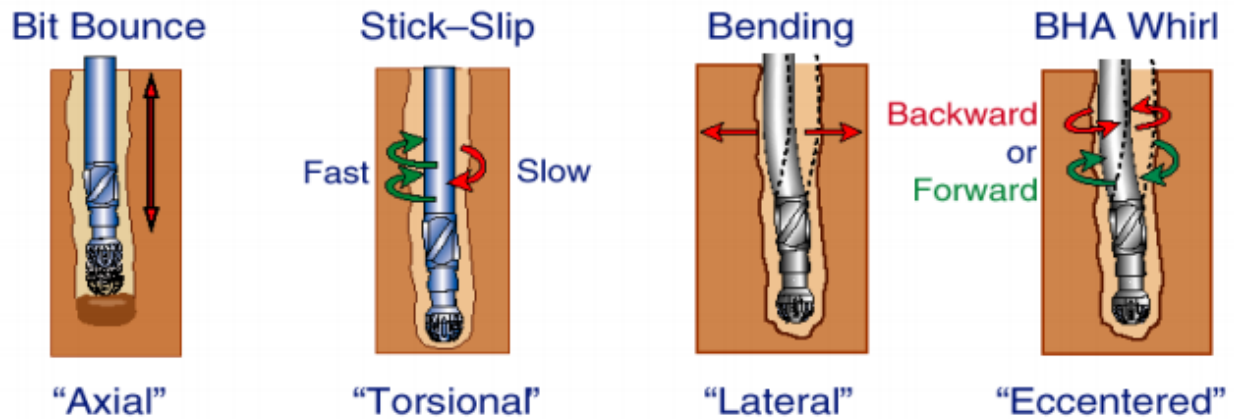
Figure 2.12:Drill string dynamic vibrations categories *[26]*

Drilling performance is strongly affected by bit vibrations and bit-rock interaction. It has been widely investigated using roller cone and PDC bits. Empirical models have been developed to study the application of roller cone bits with correspondence ROP under the drilling conditions. Rock type, DOC, and bit wear conditions from single-cutter PDC bits to the drag force are proposed to correlate [28], [29], [30]. Some researchers have indicated bit-rock interactions by measuring and evaluating the methods of drill string vibration that these drill string vibrations are stimulated by bit-rock interaction [31]. A number of the studies of combined axial and torsional vibrations defined the root cause of self-excited vibrations as a suspension in the axial position of the bit during bit-rock interaction. These bit vibrations were experimentally calculated as stimulation with the down-hole sensor sub; used to relate bit vibrations to drilling conditions with the interpretation of acceleration data such as rock type and WOB [32], [33], [34]. In laboratory experiments, the axial bit vibration was produced from the pVARD equipment and was recorded by a laser sensor, which showed that the vibration contributed greatly to improving drilling performance, and the peaks at the frequency of the axial bit vibration were found to be around the angular velocity and its properties [31], [35], [36].

2.6. pVARD Technology

DTL patented the VARD [37] and then turned it to pVARD tool for increasing the ROP, drilling efficiency and reducing the MSE under the drilling conditions. DTL has two pVARD tools of the first and second generation in small lab scale and in field scale. Both the small lab scale and the field scale pVARD tool were manufactured to evaluate the mechanisms by which passive vibration affects drilling efficiency. Both tools allow the interior of the tool to be rearranged during operation to adjust spring rate and damping. Recently, a large lab scale pVARD has been designed for the third generation based on the existing two scale tools for laboratory drilling simulators. The all scale prototype pVARD tools have been designed by using rock-bit interaction with axial vibration, providing full rotation speed and torque to the drill bit. This tool is formed with three sections: a compliant section of Belleville springs that utilizes encouraged axial vibrations, a dampening section of elastic materials (i.e. rubber), and a torque transmitting unit. It is assembled with five parts including the inner shaft, the outer shell, and stacked rubber and springs [35]. The designs of the different scale tools are covered in the following sections.

2.6.1. Small lab Scale pVARD Tool

A laboratory scale pVARD tool (Figure 2.14) was designed and manufactured for use on the small drilling simulator (Figure 2.13). Details of this tool were previously described by Rana et al. [35] and Broke [38] .

Figure 2.13: Small Drilling Simulator of DTL

To operate this tool with the small drilling simulator, it was designed to work with loads up to 250 kg, torques up to 600 Nm and flowing pressures of 1,000 psi. Since the equipment is to be used in a laboratory environment, a minimum of five safety factor was maintained to ensure the safety of the device during operation.
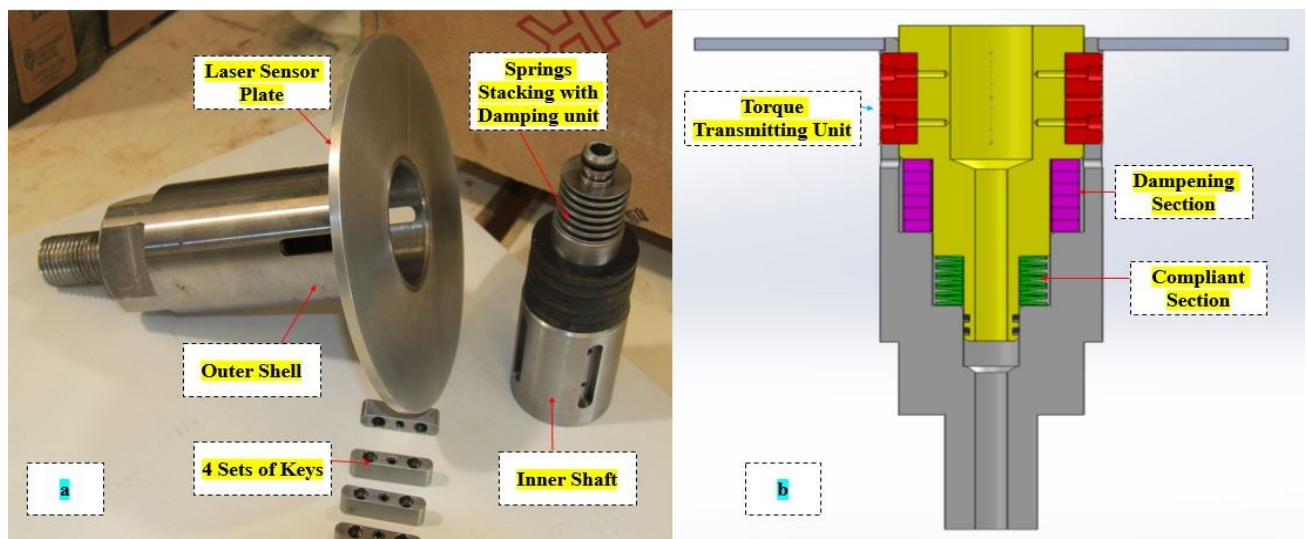
Figure 2.14:SDS-pVARD tool a. Generic view *[35]* ; b. Schematic view *[38]*

2.6.2. Field Scale pVARD Tool

This pVARD tool was designed and manufactured for the field trial that is shown in Figure *2.15*. To operate this tool, the Ingersoll Rand T3W drill rig is used so as to produce 111.2 kN of downward thrust, 10846.5 N-m of torque, and a pullback capacity of 177.9 kN. Details of this tool were described by Zhong [39] Broke [40] . The weight of the 200 m drill string is added to the downward thrust. The outer diameter of the tool was limited to 0.1016 m using a 0.1524 m bit with a bottom hole assembly. The tool also had a fluid passage in the middle of at least 0.03175 m to allow drilling fluid flow.
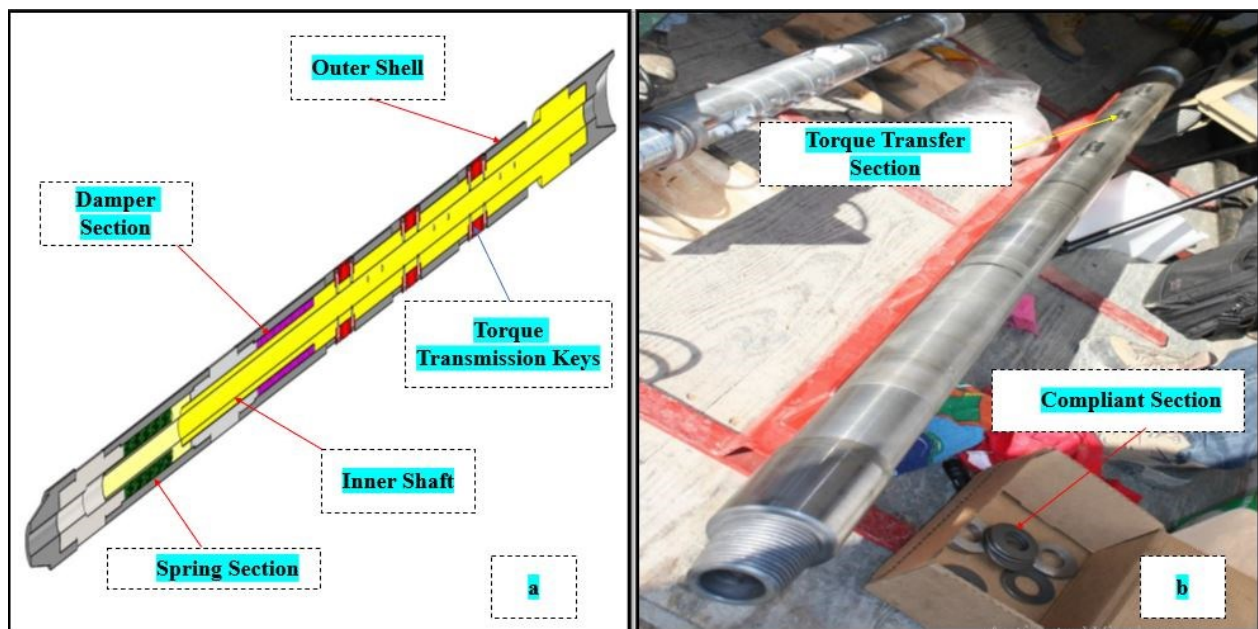
Figure 2.15:Field scale pVARD tool; a. Schematic view; b. Generic view *[40]*

2.6.3. Large lab Scale pVARD Tool

This pVARD prototype is designed on the basis of the extensive -range drilling parameters of up to 100 kN of applied Weight on Bit (WOB), 1200 N-m of torque, and up to 1000 rpm of rotational speed for the large drilling simulator which is illustrated in Figure 2.16. The minimum Factor of Safety (FOS) are simulated as five which assumed to be satisfactory for this design that is described in Chapter-6. The details design of this tool is given in Appendix A-D.
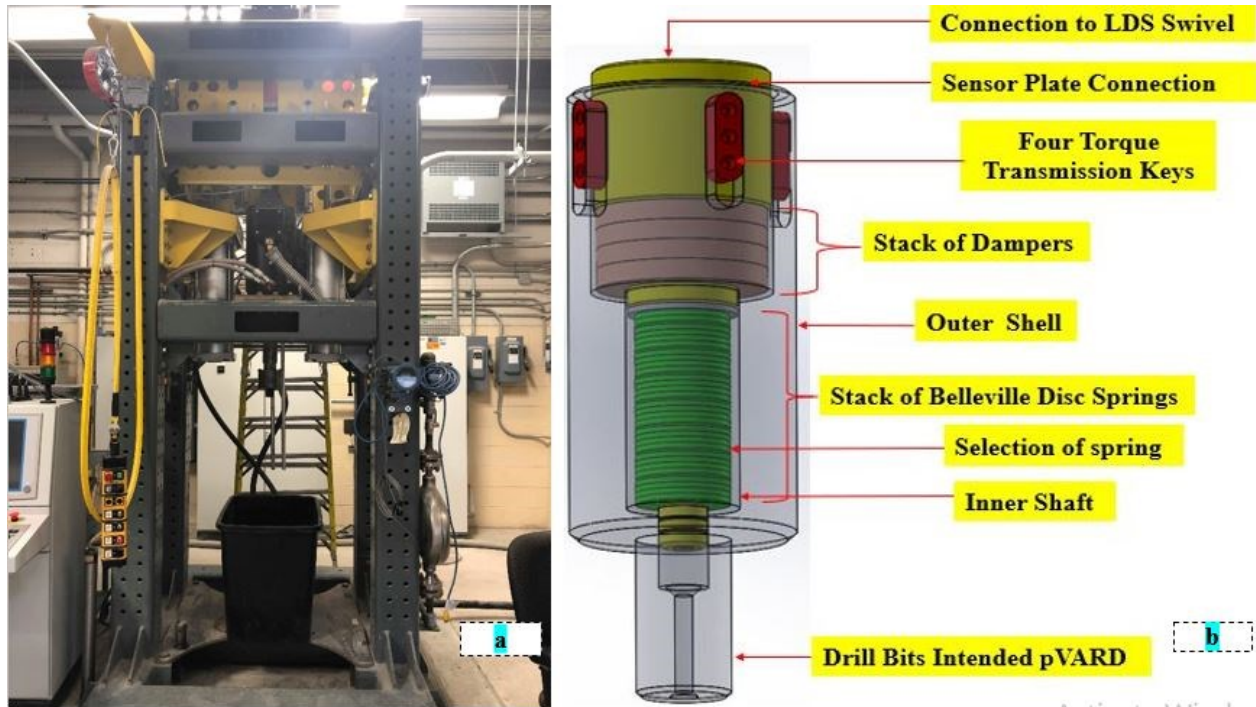
Figure 2.16:a. Large Drilling Simulator; b. Schematic view of the LDS-pVARD

The four different Belleville spring configurations have been selected from the manufacturer for using the LDS-pVARD. The specifications of these springs are shown below in
Table *2.1*

Table 2.1: LDS-pVARD Springs specifications

Spring Specifications	Spring Type and Model Number			
Model	9712K31 (Strongest)	9712K95 (Strong)	9712K29 (Medium)	9712K94 (Soft)
Internal Diameter (in)	1	1	1	1
Outside Diameter (in)	2	2	2	2
Thickness (in)	0.142	0.097	0.084	0.065
Height (in)	0.177	0.145	0.136	0.13
Deflection @ working load (in)	0.017	0.024	0.026	0.032
Working Load (lbs)	2410	1180	855	590
Flat load (Ibs)	4824	2140	1488	860
Material	High-Carbon Steel	High-Carbon Steel	High-Carbon Steel	High-Carbon Steel

Chapter 3:   Background Study of Vibration on ROP

3.1.   Effect of vibration on ROP

Researchers have extensively explored all types of vibrations to explore how to use vibrational energy to eliminate damage while drilling and increase drilling efficiency. The use of vibrations to increase ROP has been studied for more than half a century primarily by the Russian researchers. Eskin et al. [41] reported preliminary research on the effects of vibration in ROP which considered as the preliminary research on the effects of vibration in ROP. Burkap [42] conducted an experiment on drilling in red granite in laboratory conditions using axial vibrations between 67 and 83 Hz with the drill bit rotating from 37 to 254 rpm. These experiments proved the feasibility of the positive effect of ROP while reducing rotary speed and WOB by the application of axial vibrations.

During 1979 the all Union Drilling Institute (VNI) in Moscow performed drilling experiments on Urals "Koelga" Marble having 79 MPa UCS using 33 mm cutter bits with a constant speed of 42 rpm and an excessive dynamic force that was noted by Baidyuk [43]. In this experiment, WOB's pulse loading had a positive effect on ROP. The loading frequency varied between 1 to 24 times that of the rotational speed.
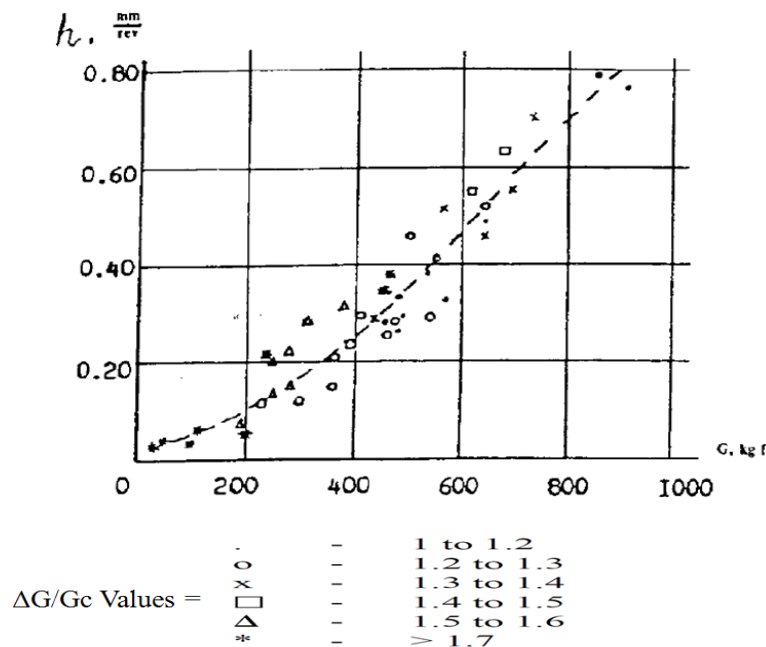
Figure 3.1: Experimental drilling results after applying additional vibration load *[43]*

The above graph Figure *3.1* shows the experimental results where penetration per revolution (h) on the y-axis versus the weight of the bit on the x-axis. The different points show various ratios of additional vibration load of amplitude (ΔG) over WOB (Gc).

Among Russian researchers including Izosimov et al. [44] Sintsov et al. [45] developed a number of special mechanical vibrators to increase drill string vibrations which raised power to enhance drilling rates and drilling efficiency. Western researchers also conducted investigations in the 1950s with an industry body called Drilling Research Investigation Limited (DRIL) for possible improvement in ROP, from which Pennington [46] published some results about the possible improvement in ROP by utilizing vibration and percussion drilling techniques. The researchers asserted that drilling using vibration and percussion drilling techniques could be greatly accelerated although they also noticed a decrease in ROP with increasing pressure and depth of the downhole.

3.2.   VARD Analysis

Recent studies have shown that the effects of vibrations on penetration rates have potential benefits for ROP. The concept of using downhole vibrations to enhance ROP was studied by Li et al. [47] In the lab scale setup of vibration assisted drilling, vibrations were created using an electromechanical axial shaker mounted on top of the drill stand. A 2-inch diamond coring bit was used to drill a 20 MPa sample of synthetic rock made using commercial quick setting concrete. The experiments carried out a fixed frequency of 60 Hz and a range of amplitudes. ROP – WOB curves were generated keeping fixed rpms [48] .
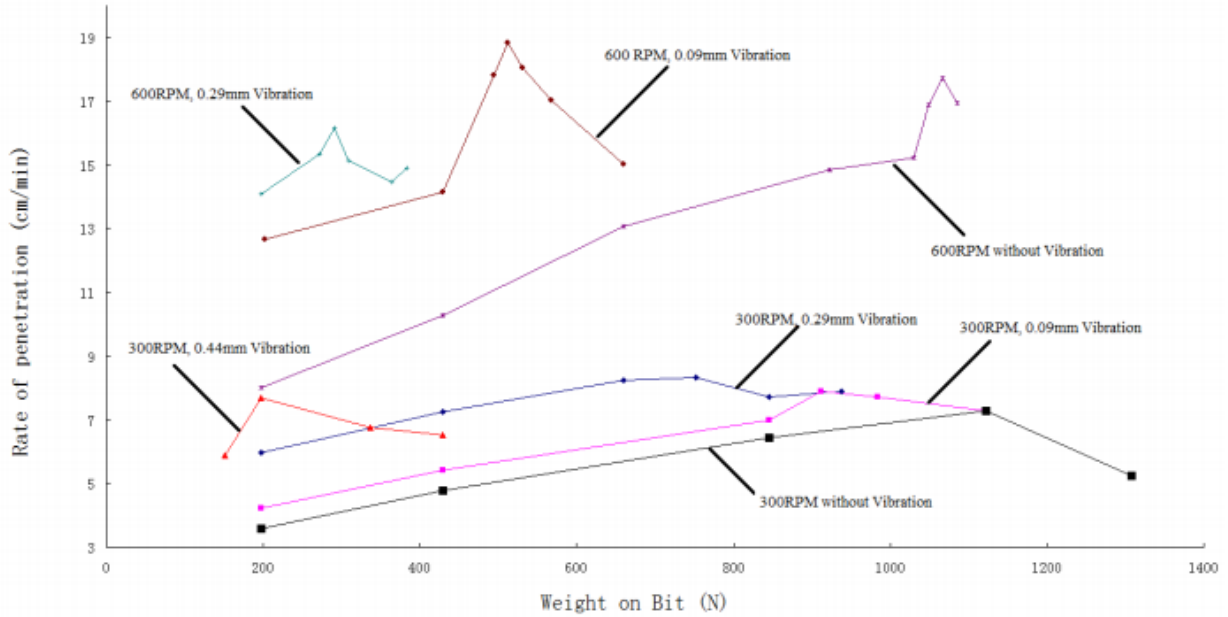
Figure 3.2: Li's *[47]* , *[48]* experimental results of vibration assisted rotary drilling

These sets of experiments proved that vibration assisted drilling leads to an increase in ROP. As it can be seen in Figure *3.2* the ROP increases with an increase in amplitudes excepting the case of 600 rpm, but the ROP achieved with vibration is still more than the ROP achieved without vibration. The ROP enhancement is seen in Figure *3.3*. It is concluded that the expansion amplitude of the vibration leads to an increase in ROP until the founder point is reached and the relationship between amplitude and ROP becomes non-linear.

ROP/Amplitude at 197.6N bit weight, 300 RPM
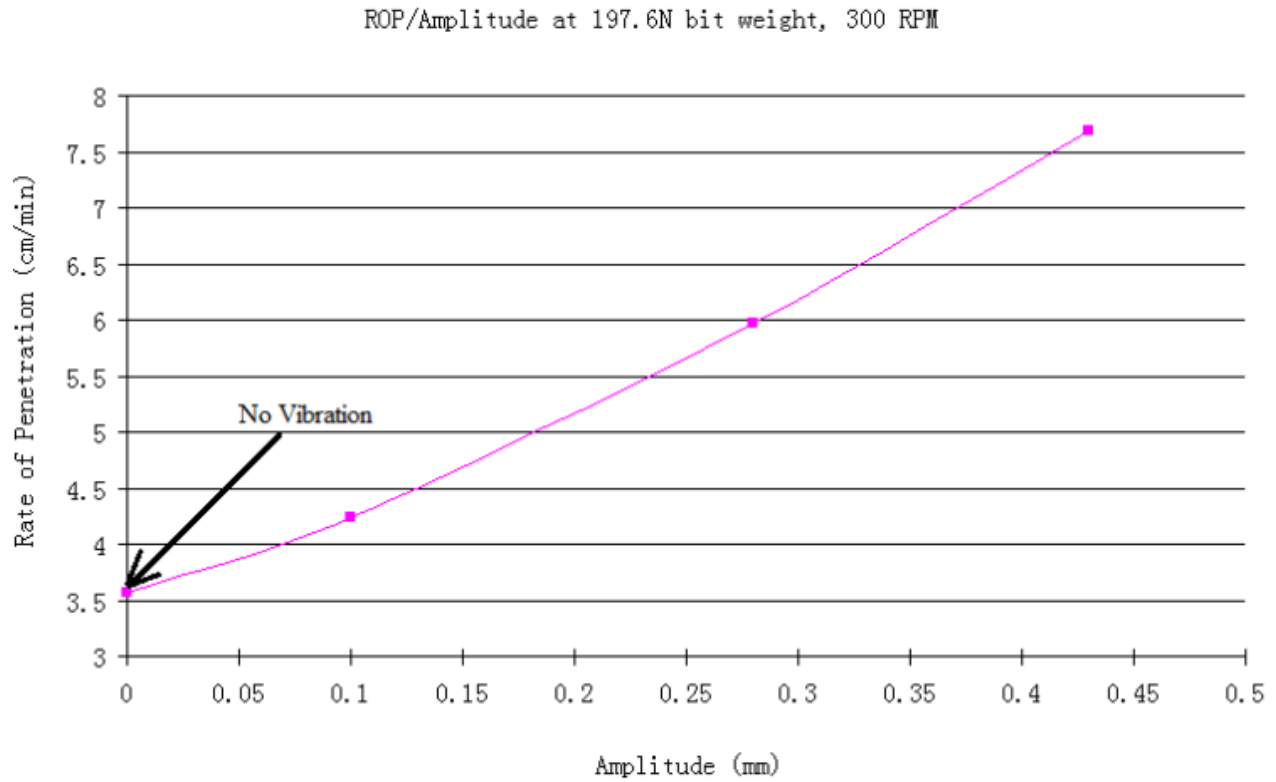
Figure 3.3:Li's *[47]* consequences on the ROP with constant WOB and RPM

Li et al. [47] observed similar results (Figure *3.4*) with drilling experiments using a full face diamond impregnated bit and concluded that the Vibration Assisted Rotary Drilling technology (VARD) could significantly enhance the ROP.
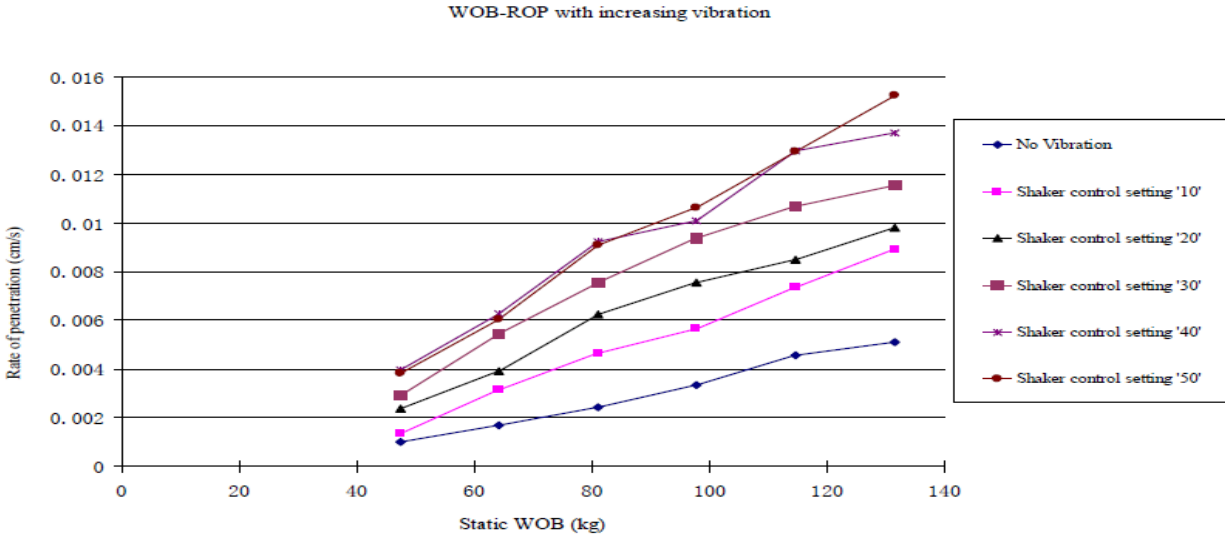
Figure 3.4:Experimental results with the full face bit *[47]*

Based on Li's [48] work, Babatunde et al. [49] varied the vibration frequency with amplitude and utilized the diamond drag bit as well as a PDC bit with two cutters to drill through synthetic concrete. Three levels of vibration amplitude (low, medium, and high) and three levels of frequency (45, 55 and 65 Hz) were used for both experiments. Figure 3.5 shows that the ROP increase was achieved at a constant vibration amplitude with different frequencies for both experiments compare to conventional. The increase in WOB for diamond full-face drag bits at 45 frequency resulted in a moderate increase in ROP values compared to other frequencies Figure 3.5.a, but the mostly lower ROP value for PDC bits Figure 3.5.b.
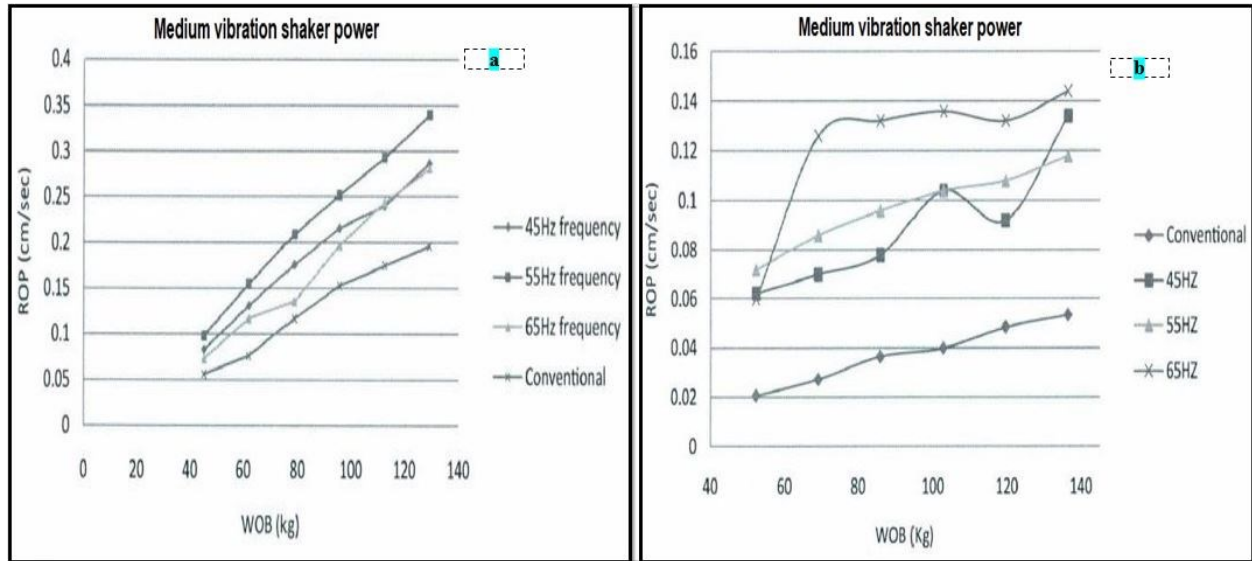
Figure 3.5:WOB vs. ROP under vibration; a. for a diamond drag bit; b. for a PDC bit *[50]*

Babatunde [49] remarked that VARD provides a significant improvement in ROP compared to conventional rotary drilling whereas a drag bit produced more than a PDC bit. It also recommended that bit life was not affected notably enough to assuage overall drilling efficiency.

Abtahi [51] examined to find the optimum drilling conditions at lower WOB considering both ROP and wear including the effect of vibration using diamond impregnated coring bits that showed the increase of ROP with applied vibration that is showed in Figure 3.6.
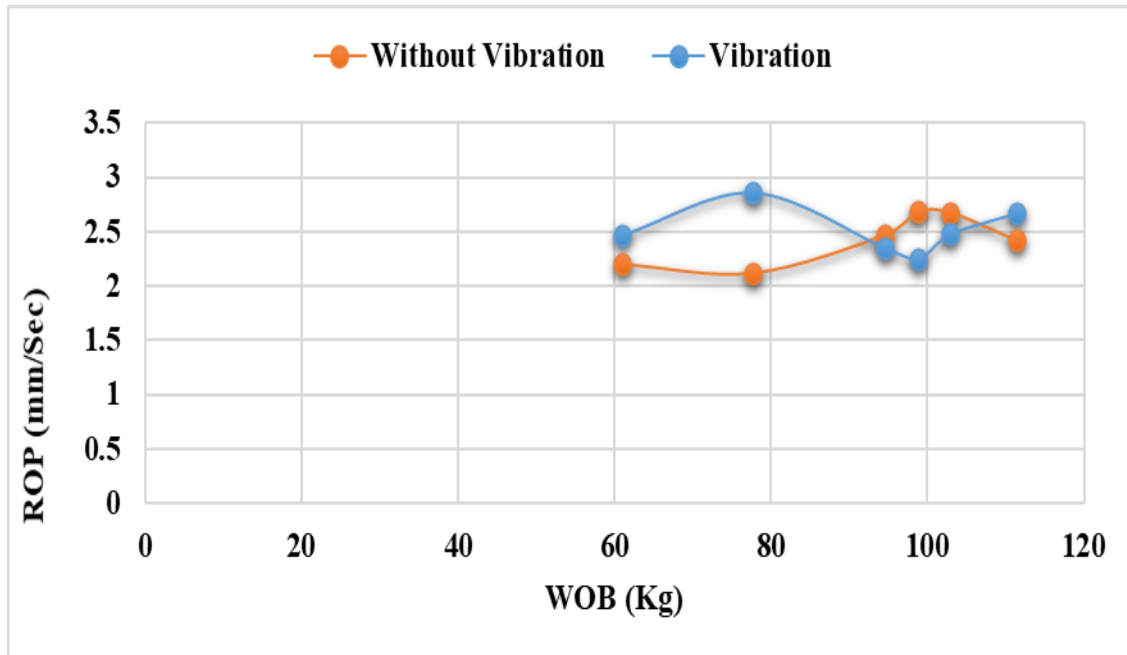
Figure 3.6:Experimental results of the coring with and without vibrations level *[51]*

In all experiments, profile shapes appeared after some laboratory drilling condition in the sequence of: unused bit; b. flat end; c. rounded edge; d. V-Grooved (Figure *3.7*).The highest ROP results were gained with V grooved, decreasing in the order: unused, flat end, and rounded edge. The vibration had a greater effect on bit wear than profile shape. The profile with sharper-edged wore out very quickly [51].
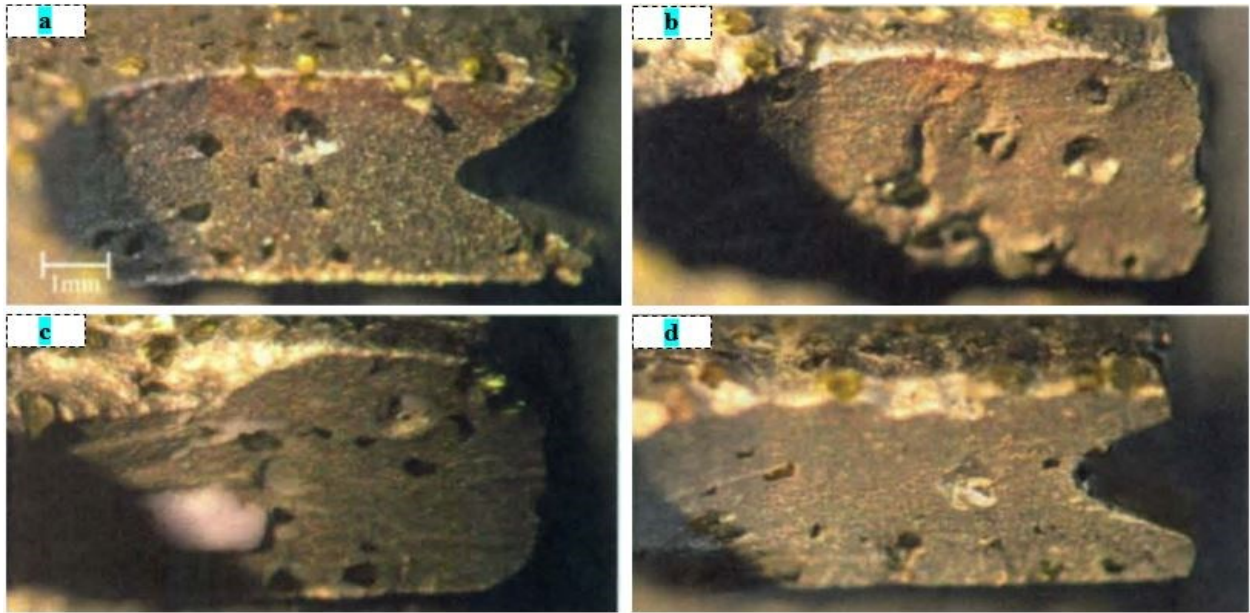
Figure 3.7:Profile shapes appeared after some drilling: a. unused bit; b. flat end; c. rounded edge; d. V-Grooved *[51]*

Khorshidian et al. [52] studied the influence of vibrations on the penetration mechanism with a single PDC cutter on Carthage Limestone using the Distinct Element Method (DEM). The DEM parameters were equalized to the real UCS test results of the Carthage Limestone. The simulations indicated that axial vibrations had two possible effects on cutter penetration. Initially, there was an improvement when the cutter had a significant effect on the rock as the result of cratering. After crossing the optimal points, the vibration was increasing thereby requiring more MSE which turned up a negative impact. It is concluded that the improvement of the penetration system of the PDC cutter due to the vertical oscillation in both cases reduces the force required to move the cutter horizontally and the effect loading causes the formation of larger chips. The Figure *3.8* indicates the cutting generation in front of the PDC cutter with normal chipping and the combination of chipping and cratering.
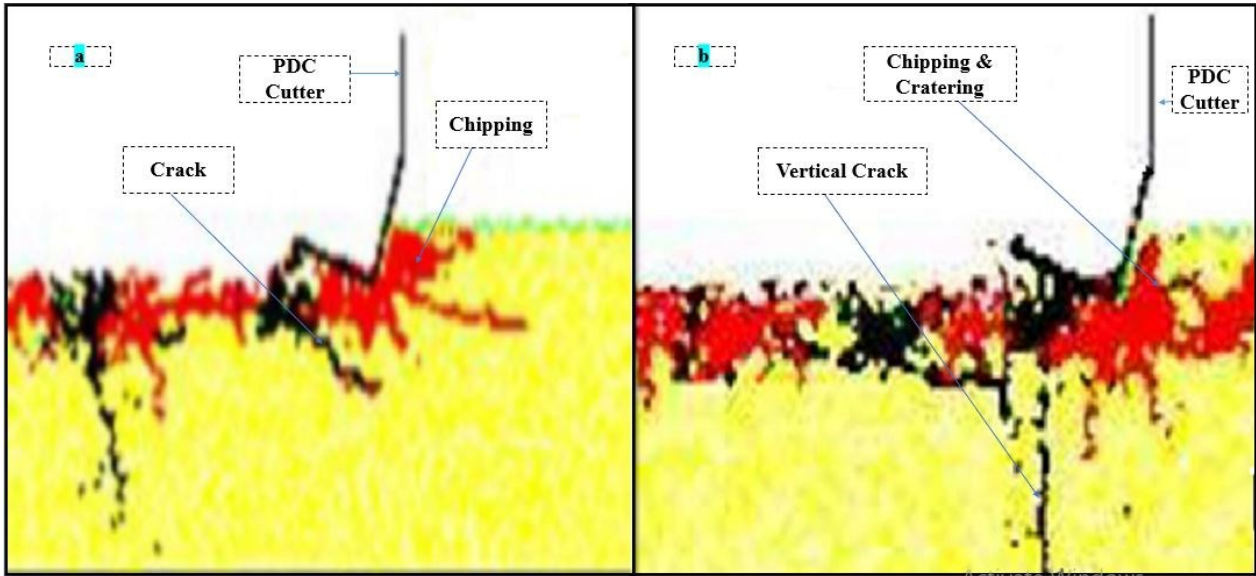
Figure 3.8:DEM models for cutter penetration; a .Normal chipping; b. Combination of chipping and cratering *[52]*

Wang et al. [53] analyzed the applied vibration of the CFD simulation. This simulation performed with the effect of the Downhole Oscillating Device (DOD) and a one-degree of freedom spring, mass damper on BHA that is in Figure *3.9*.
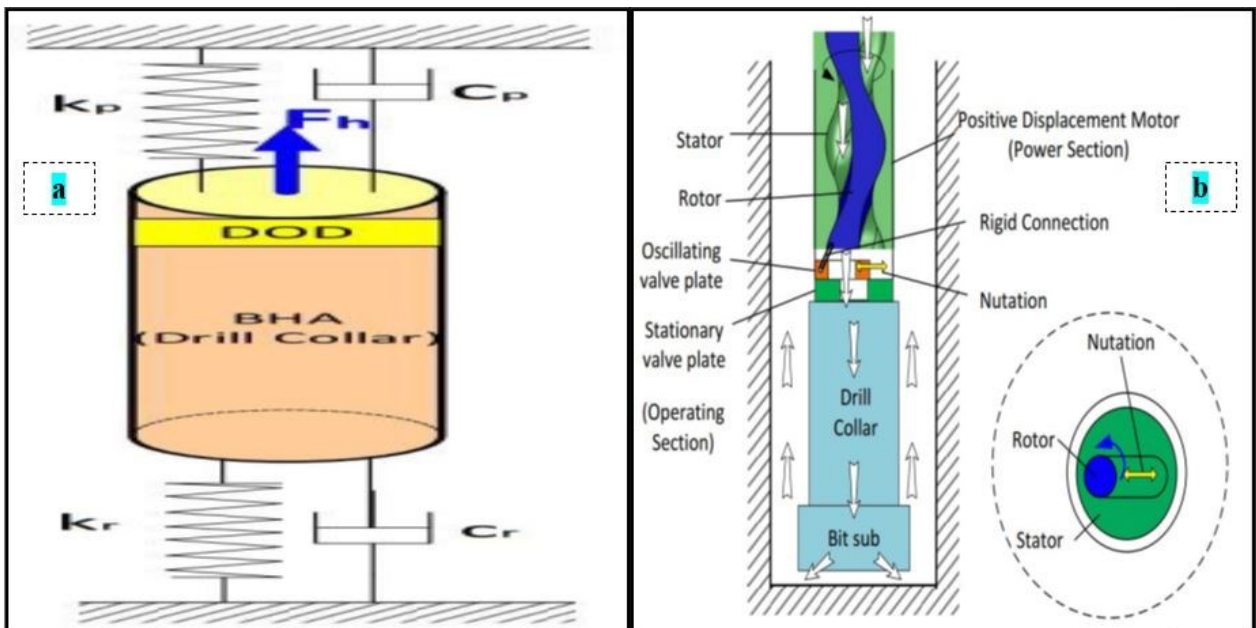
Figure 3.9:Schematic view of the a. BHA Dynamic System; b. DOD Configuration *[53]*

It also simulated the BHA, WOB, and displacement both with DOD and without DOD using these models. Time series plots of the WOB and displacement over time are shown in Figure *3.10* with drilling both on a flat surface with and without DOD.
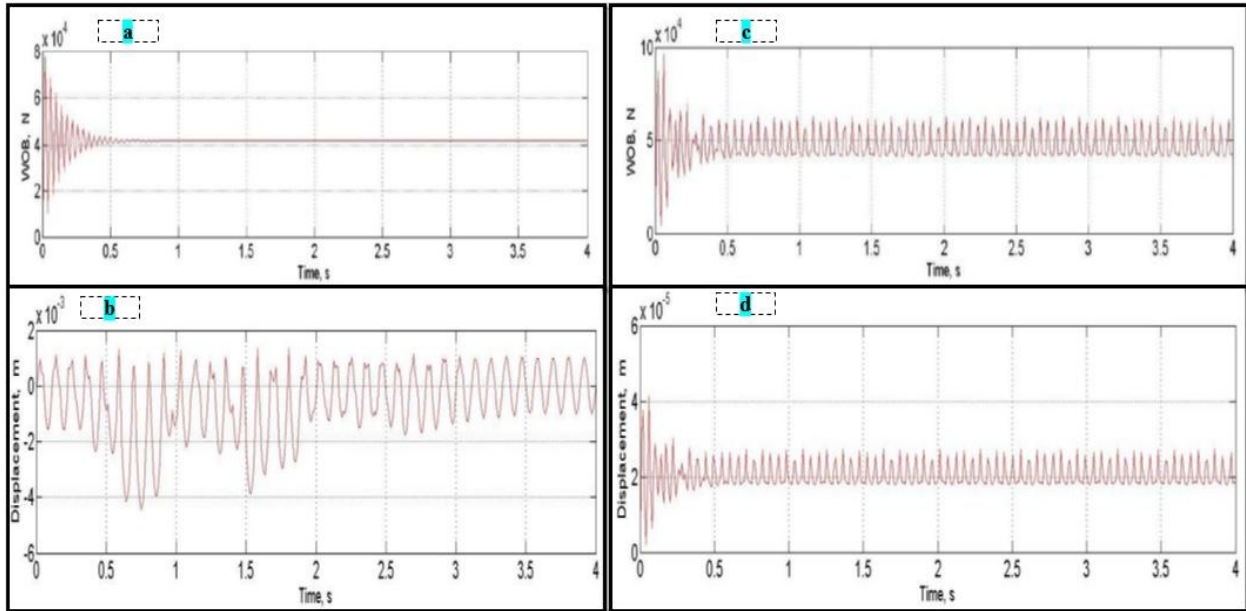
Figure 3.10:BHA Weight on Bit and Displacement profile, a. WOB and b. Displacement without-DOD; c. WOB and d. Displacement with DOD *[53]*

Lastly, Wang et al. [53] associated the average ROP with the pressure pulsation amplitude of the DOD (Figure *3.11*.a) where pulsation amplitude was increased by 60% due to about 3% ROP. It further noted that the properties of drilling fluids affect the expansion amplitude of DOD by high density and high viscosity fluids resulting in an increase of about 8% ROP (Figure *3.11*.b).
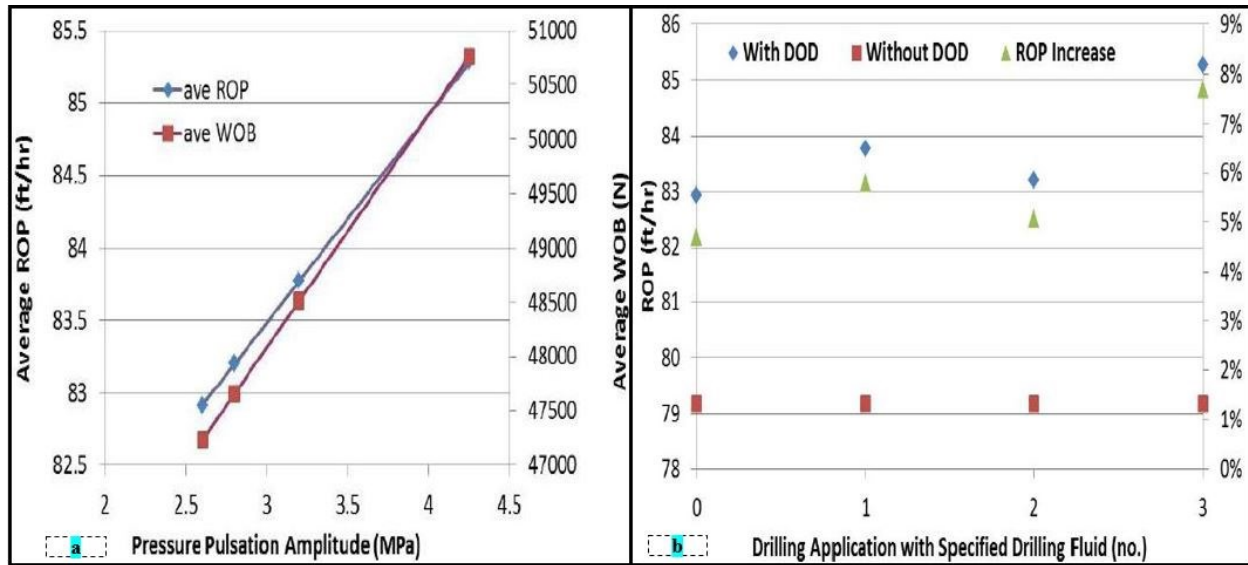
Figure 3.11:a. ROP and WOB verse pressure pulsation amplitude from the DOD; b. ROP and percentage increase verse different drilling fluids *[53]*

The applied vibration has been largely reviewed up to this particular point. Also, of interest is the idea of utilizing self-activated vibration or damping specific vibration which leads to the concept of a passive vibration tool that gives the bit some axial freedom or compliance. This type of device was tested by Khademi [54] in DTL that consisted of a set of rubber mounts placed between the drilling sample and the support frame of the laboratory drill rig. In this uplifting system, the rock sample was placed under the bit for natural vibration. Afterward, it changed the mount with different compliances that altered the rock sample vibration [54] .

Khademi [54] notified a "sweet spot" for the compliance of this system that related to ROP and MSE (Figure *3.12*). It was observed that increasing compliance leads to an increase in ROP until the optimal point was exceeded and ROP dropped.
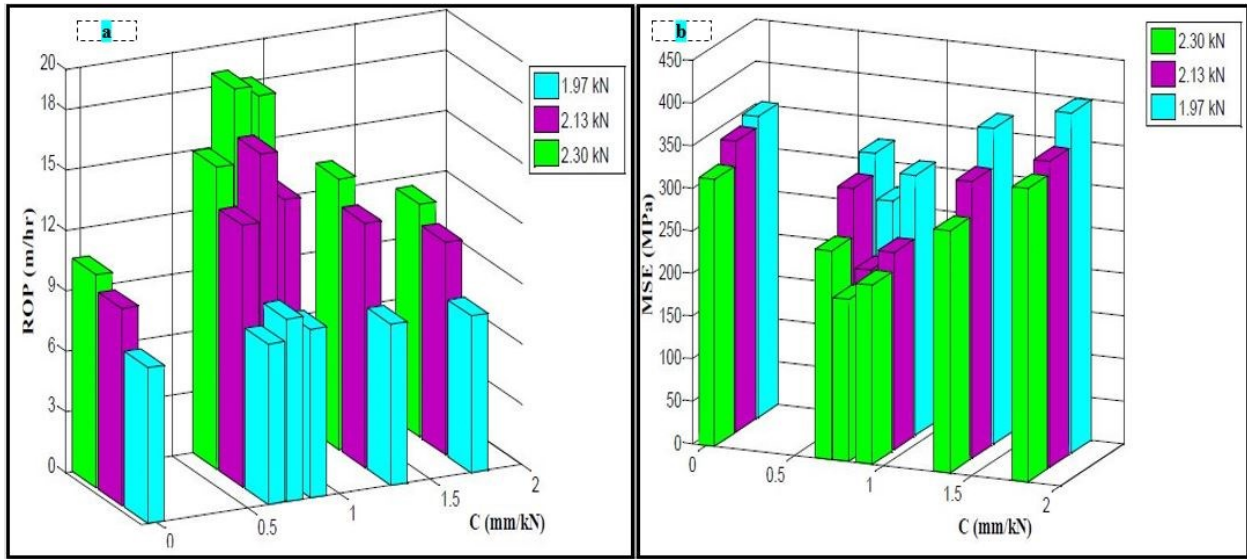
Figure 3.12:For selected levels of WOB; a. ROP verse compliance; b. MSE versus compliance
[54]

Although ROP is divided by RPM referred to as DOC, the increase in ROP was related to the increase in DOC by Khademi [54] as shown in Figure 3.13.
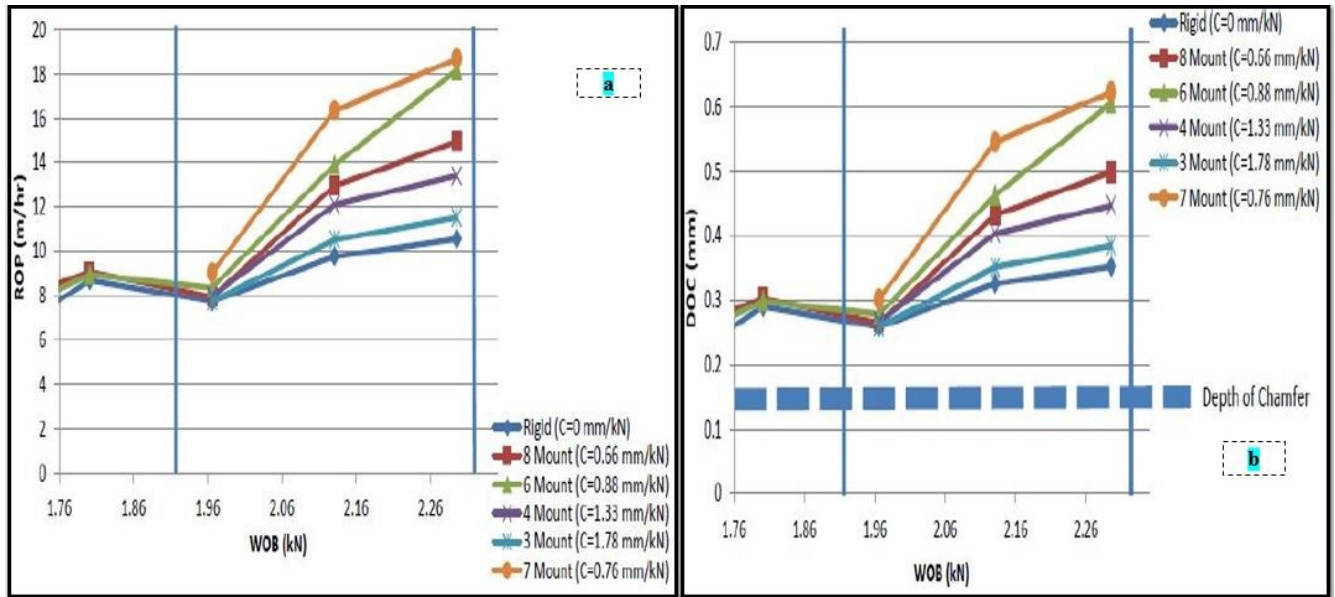
Figure 3.13:For various compliance; a. average ROP vs. WOB; b. DOC vs. WOB [54]

36

3.3. pVARD Analysis

Based on all other promising results from VARD, the Drilling Technology Laboratory of the Memorial University of Newfoundland patented a new tool that provided higher penetration rates and more economic value in drilling. The name of this tool is passive vibration Assisted Rotation Drilling (pVARD). The tool was formed with the Belleville springs and damper stack. Rana et al. [35] performed experiments using this porotype lab scale pVARD and described in detail.

Rana et al. [35] carried out 80 tests combining four levels of compliance, five ranges of WOB, and four different flow rates. DOTs were done with analogue fine-grained concrete and its UCS was ~50 MPa. It was found that without using the pVARD tool applied WOB was proportional to ROP. But it was shown that using pVARD with multiple configurations at different flow rates and at different levels of WOB, ROP was increased in some instances. There should have an optimal compliance design for the proposed specific drilling parameters as pointed out by Khademi [54] .WOB vs ROP graphs of the lab scale pVARD tool are shown in Figure *3.14*.
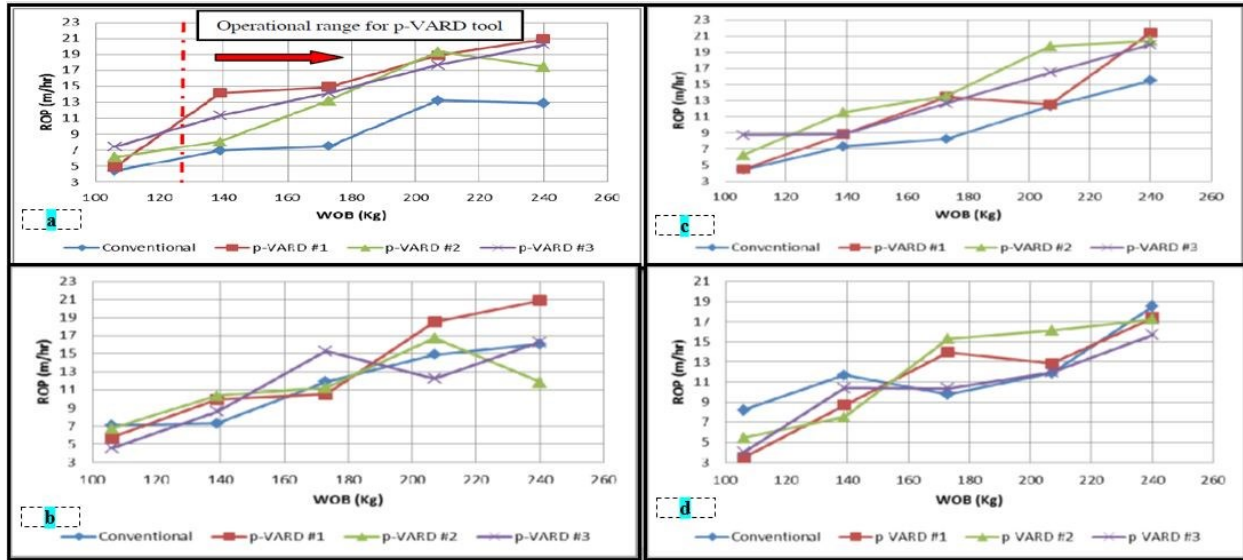
Figure 3.14:Laboratory test ROP versus WOB under four different compliance settings; a. 16 lpm flow rate; b. 44 lpm flow rate; c. 72 lpm flow rate; d. 100 lpm flow rate *[35]*

Rana et al. [35] also reported that 136 field trials were done on the red shale formation in Conception Bay South where mechanical properties were similar to the laboratory tests. In this

field trial, higher ROP was observed in some of the configurations compared to conventional drilling (Figure *3.15*).
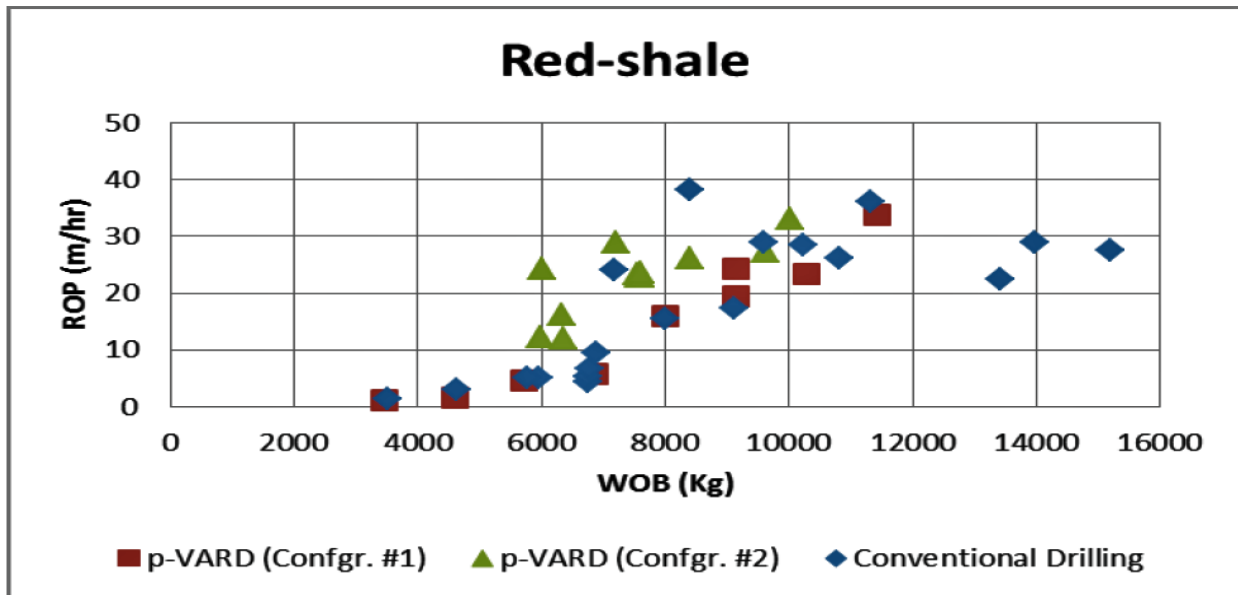
Figure 3.15:ROP vs WOB for three different compliance settings on Red shale in field trial *[35]*

From this analysis it is concluded that when using the pVARD tool, ROP only increased for a specific operational range. Finally, Rana et al. [35] showed that flow rate has an operative effective effect on the pVARD tool performance where lower flow rate was required to remove cuttings as well as axial vibrations generated by tools assisted in cutting removal.

Xiao et al. [55] performed DOTs on synthetic concrete with a UCS around 40 and with a small scale pVARD tool under laboratory conditions. But it was found that using pVARD with multiple configurations at fixed water flow rates and at different levels of WOB, ROP was increased in most scenarios (Figure *3.16*) [55] .
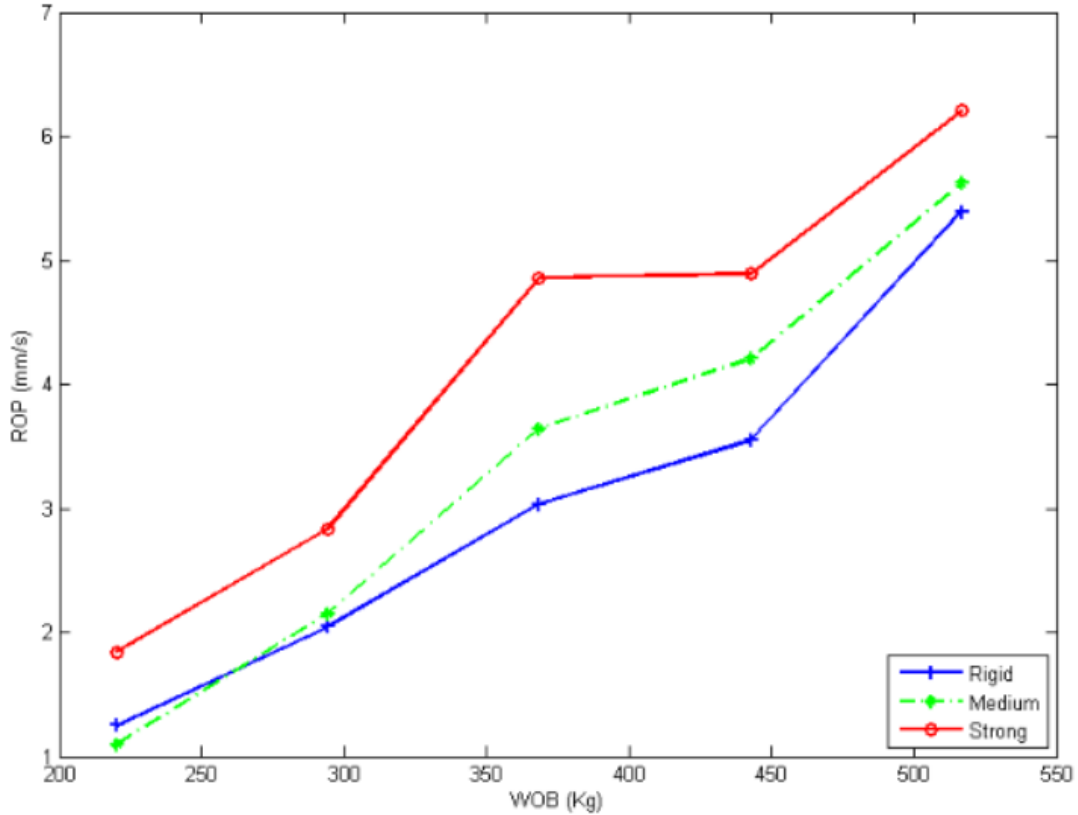
Figure 3.16:ROP versus WOB for three different compliance settings under laboratory condition
[55]

Zhong et al. [56] looked at the increasing of ROP using pVARD tool. The simulations were done with PFC2D and calibrated using laboratory tests with the lab scale pVARD tool. The simulations were done with PFC2D and calibrated using laboratory tests with the lab-scale small pVARD tool. This model was fixed up with the bit axial motion with spring stiffness and damping coefficient (Figure *3.17*.a). The results were characterized by mechanical specific energy (MSE), depth of cut (DOC), and material removal rate (MRR).
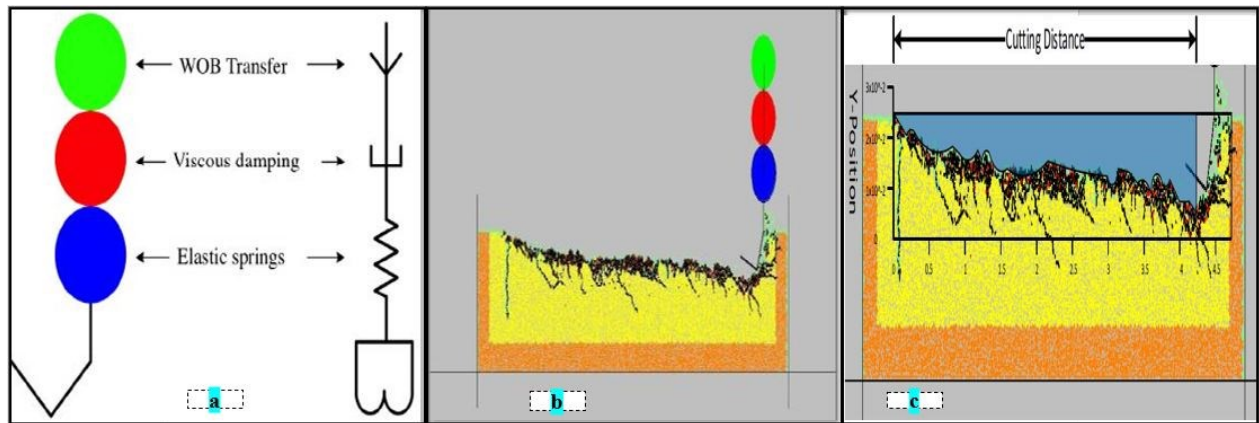
Figure 3.17:PFC2D simulation; a. Setup for pVARD; b. Cutting process by single cutter; c. DOC and MRR measured by cutting area *[56]*

The drill-off was conducted in fine-grained concrete with a UCS of 46 MPa using a 35mm, 2 cutter PDC bit on the laboratory scale drill rig. Afterward, the DOTs results were compared to the PFC2D simulation outputs (Figure *3.17*.b). The single cutter area is shown in Figure *3.17*.c to measure the DOC and MRR.
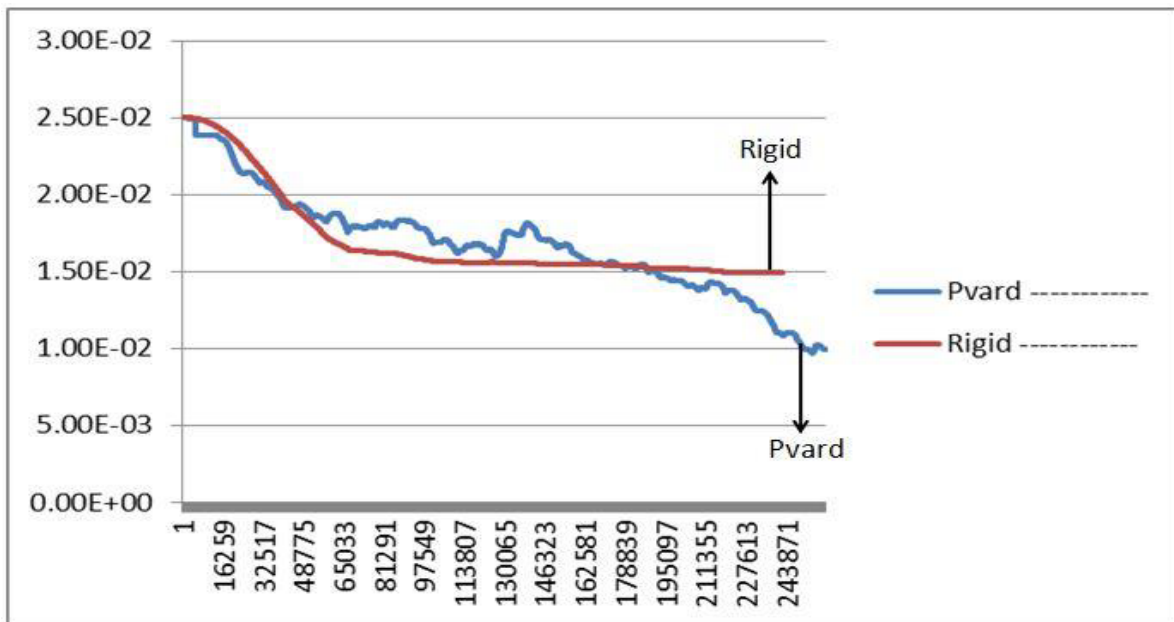
Figure 3.18: PFC2D simulations by Zhong et al. *[56]* for Y-axis bit position (mm) vs time (10 sec)

It is observed that the simulation results agreed with the experimental data except for the MSE. For the simulations, the fluid flow rate was not considered therefore there were some errors in the simulated MSE results. The simulation results were shown to be bit vibration using pVARD with rigid configuration (*Figure 3.18*). Conclusively, Zhong et al. [56] obtained that the layout of the drilling experiment could be simulated by using discrete element modeling.

Gillis and Butt [38] explored the effects of the pVARD tool on MSE and compared the effects displayed on the lab trail with those seen during the field trails that were previously performed in DTL. MSE vs WOB graphs were produced by using lab and field scale pVARD tools along with conventional drilling are shown in Figure *3.19* and Figure *3.20*.
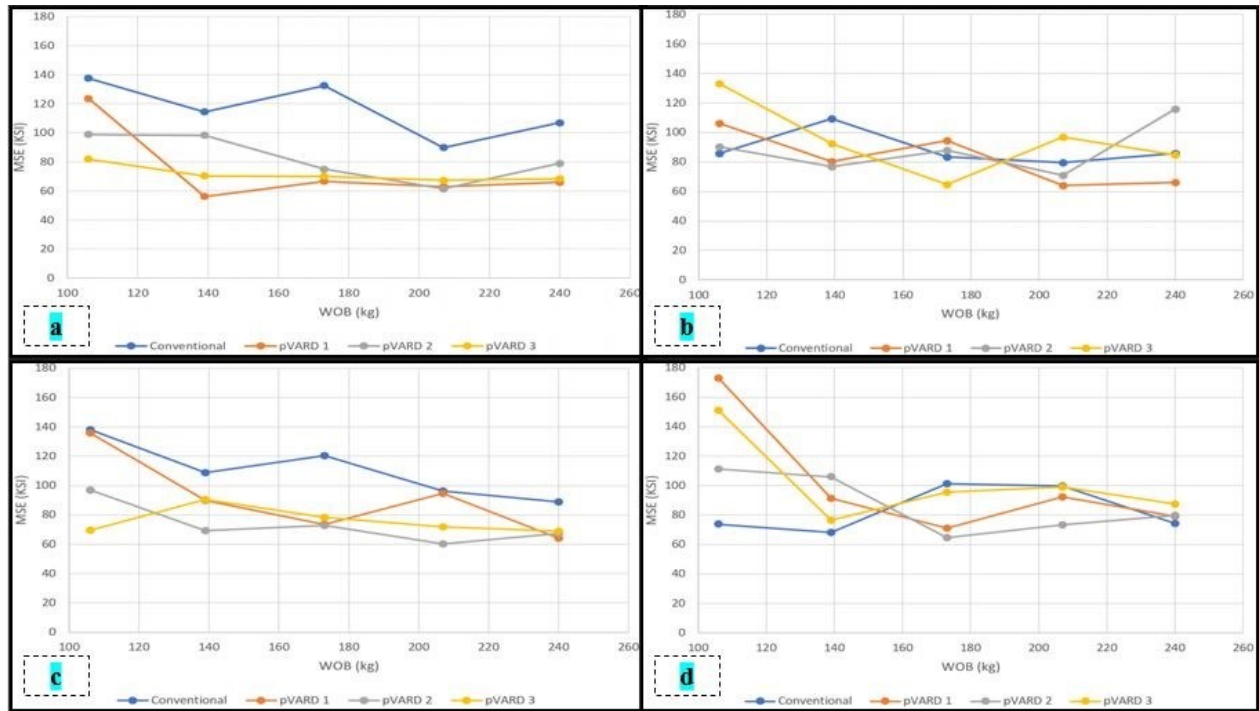
Figure 3.19:MSE versus WOB for lab scale at various compliance settings; a. 16 lpm flow rate ; b. 44 lpm flow rate; c. 72 lpm flow rate; d. 100 lpm flow rate *[38]*
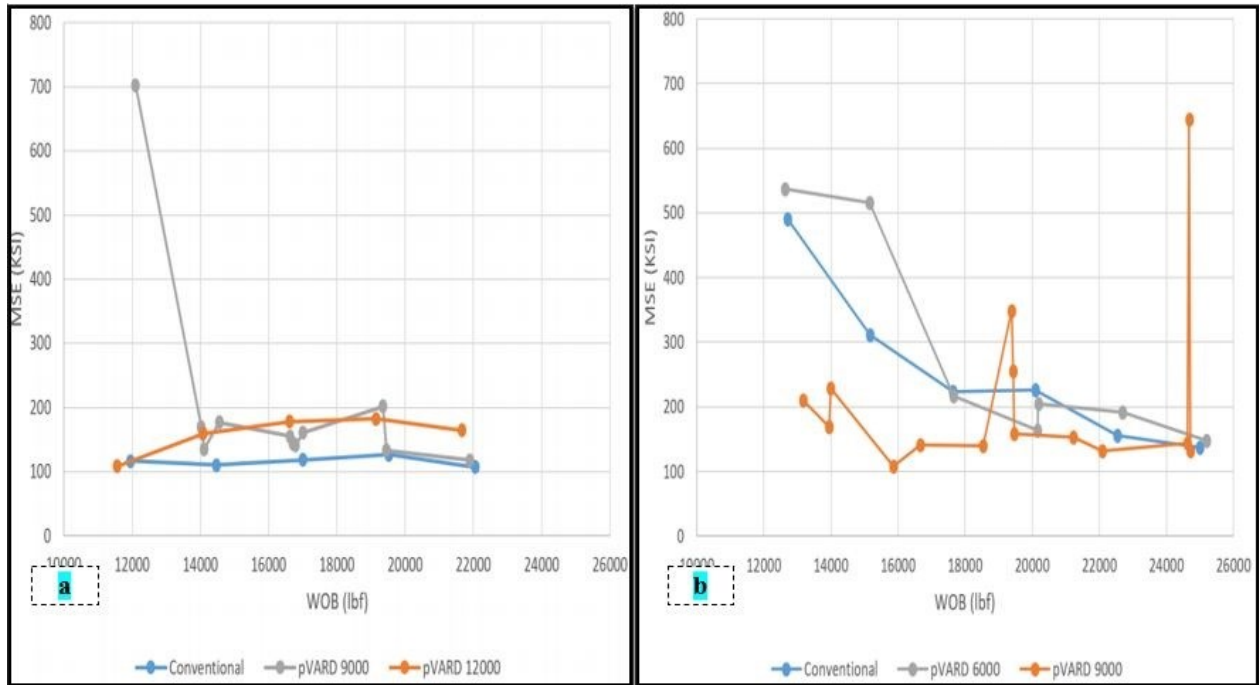
Figure 3.20: MSE versus WOB field trail; a. Gray shale formation: b. Red shale formation *[38]*

The laboratory-scale pVARD tool observed the best results as more variety of operational ranges could be tested than field tests. Gillis and Butt [38] reported that the effect of the pVARD tool on MSE varies with different drilling parameters.

Chapter 4: Research Methodology

This section contains methodology, test setup and apparatus, materials and sample preparation techniques, and test procedure for research experiments and tests. The research procedure including physical, simulation, mechanical, and drilling measurements that are described sequentially.

4.1. Granite Rock Strength Characterization

4.1.1. Methodology

This research involved several laboratory experiments which investigated granite rock strength through mechanical strength measurement. These were conducted in several stages: (i) sample preparation, (ii) measurement on standard NQ cores samples, (iii) conducting the tests using loading frame and (iv) completion of the strength characterization.

4.1.2. Strength tests

Tests were conducted to determine the strength of granite rock. It included (i) standard Unconfined Compressive Strength (UCS) and (ii) Indirect Tensile (Brazilian) Strength (ITS) test using a commercial loading frame (i.e. geomechanical load frame), whose maximum loading capability is around 490 kN.

4.1.3. Test procedure

For strength tests: in accordance with ASTM Standards D7012-2014e1 for the Unconfined Compressive Strength (UCS), and D3967-2016 for the Indirect Tensile Strength (ITS), the oriented strength for granite rock was determined.

4.2. Numerical and Experimental Study on Belleville Springs for LDS-pVARD for Drilling Performance

Simulation and laboratory experiments were used when selecting optimal Belleville Springs of the LDS-pVARD tool for optimal drilling performance. These were conducted in several stages: (i) springs selection, (ii) selection of the number of spring configurations, (iii) completion of the simulation analysis, (iv) conducting the compression tests using loading frame, (v) comparison of the simulation with compression tests.

4.2.1. LDS pVARD Design

The third-generation Large Drilling Simulator (LDS) pVARD prototype is designed for wider-range drilling parameters of up to 100 kN of applied Weight on Bit (WOB), 1200 N-m of torque, and up to 1000 rpm of rotational speed.

4.2.2. Finite Element Analysis

The Finite Element Analysis (FEA) has done for the torque transmitting section of the LDS-pVARD. The simulation results provided in this section are interpreted in terms of the minimum Factor of Safety (FOS), which is related to the maximum stress concentration. The keys have a minimum FOS of 5 which assumed to be satisfactory for this design.

4.2.3. Spring Selection

The LDS- pVARD is designed for 1" ID and 2" OD of Belleville springs which is selected from manufacturer. For the compression test 10 and 18 series in a single parallel configuration of the 9712k31 were selected.

4.2.4. Simulation Analysis

The numerical study was done by simulation. This simulation was programmed based on the Almen and Laszlo [57] equation.

4.2.5. Mechanical compression tests

The experiments were conducted with geo-mechanical loading frame using the compression tool. The spring compression details were determined using Hooke's law [58] which derives the relationship between the compressive load and the deflection.

4.2.6. Comparison of simulation with compression tests

A comparative analysis of both (i) the simulation and (ii) the mechanical compression test was performed on 9712k31 spring type.

4.3. Hysteresis effect analysis on the LDS-pVARD springs

4.3.1. Methodology

This research involved several laboratory experiments to investigate hysteresis effect analysis on LDS-pVARD spring. These were conducted in several stages: (i) sample selection, (ii) selection of the number of spring configurations, (iii) selection of the lubrication, (iv) conducting the tests using loading frame, (v) determination of the displacement cycling characterization and (vi) completion of the hysteresis effect analysis.

4.3.2. Spring Selection

The LDS- pVARD is designed for 1" ID and 2" OD Belleville springs which are selected from the manufacturer. For the compression test, 10 and 18 series springs in a single parallel configuration of the 9712k31 were selected.

4.3.3. Lubrication Selection

A commercial type of Grade 2 grease was selected as the lubrications for this research.

4.3.4. Hysteresis analysis

In this research, the tests were conducted to evaluate the hysteresis effect of LDS pVARD springs. These tests include (i) displacement cycling tests of the springs using geomechanical loading frame with the compression tool: a. without lubrication b. with lubrication (ii) mechanical test data plotted on the stress/strain curve and determined the hysteresis and (iii) comparing hysteresis effects among the various number of parallel spring stacking, without lubrication and with lubrication.

4.4. Study of the Enhancement of ROP Using pVARD

4.4.1. Methodology

This research explored improving drilling performance through increasing the drilling Rate of Penetration (ROP) by using the passive Vibration Assisted Rotary Drilling (pVARD) tool in the laboratory conditions. pVARD was designed to induce controllable axial oscillations that could increase ROP with different compliant configurations that generate various magnitudes of the axial

oscillations. The experiments were conducted on granite sample using coring bit and involving constant water flow rate. They also involved the atmospheric and drilling system configuration that were summarized in Table 4.1.

Table 4.1: Drilling parameters and drilling system configurations

Rock Type	Pressure	Temperature	PRM	Water Flow Rate	Drilling System
Granite	Atmospheric	Room Temperature	Constant	Constant	Rigid
					SinSoft (pVARD-high compliance)
					SinStiff (pVARD-medium compliance)
					DouStiff (pVARD-low compliance)

4.4.2. Test Procedure

The small drilling simulator was used for the drilling experiments using pVARD vs. rigid. A granite sample was selected and drilled in the laboratory using the laboratory scale pVARD vs. rigid in atmospheric conditions through the following steps:

A granite sample (304.8 mm x 304.8 mm x 203.2 mm) was placed into the drilling pressure cell. Applying a pre-determined water flow rate (selected from the several flow rates provided by the water pump) provided optimal cleaning and cutting removal for the best drilling performance as a function of flow rate. When the drilling was conducted under atmospheric pressure, no back pressure was applied, and the chock valve was fully open. The required static WOB for a drilling performance curve was applied. The drilling process through Drill off Test (DOT) conditioned either by time or by depth intervals; an average 2 cm of depth interval was the drilling depth interval of this project. The variable parameters were WOBs, water flow rate, RPM, and the drilling system of the pVARD and rigid.

4.4.3. Drilling Performance

The drilling performance was analyzed based on Maurer [5] model. The criterion selected the highest ROP as a function of several associate parameters of (i) flow rate, (ii) WOB (iii) RPM, (iv) drilling system of pVARD and rigid. The results show the positive influence of pVARD on drilling performance against rigid drilling.

Chapter 5:   Granite Strength Evaluation

5.1.   Introduction

In this section, tests were conducted to determine the strength of granite. These tests included (i) standard Unconfined Compressive Strength (UCS) test and (ii) Indirect Tensile (Brazilian) Strength (ITS) using commercial Geomechanics frame, whose maximum loading capability is around 490 kN.

5.1.1. Methods of strength measurements

The determination of intact rock strength in the laboratory is performed by the following tests: point load index, unconfined compression, triaxial compression, indirect tensile (Brazilian), and direct tensile [59]. Rock strength was measured by the unconfined compression and indirect tensile (Brazilian) test.

5.1.2. Standard of Strength measurements

In accordance with ASTM Standards D7012-2014e1 [60] for the Unconfined Compressive Strength (UCS), and ASTM D3967 -2016 for the Indirect Tensile Strength (ITS) [61], the rock strength for granite samples was determined.

5.2.   Description of Granite Rocks

Granite is the most common type of granular crystalline intrusive igneous rock in Earth's continental crust. The color of granite is white, pink, or gray depending on the minerals present in it and it contains three essential minerals: feldspar (50% or more), quartz (25-40%), and mica (3-10%) which give each unique type of rock its own color, texture, and structural properties in different proportions [62].

5.3.   Procedure of specimen preparation

For the UCS, samples were prepared by following ASTM D7012-2014e1 (Figure *5.3*) [60]. For these experiments, a standard 2-inch cylindrical coring bit was used to core the sample by using SDS (Figure *5.1*).

Figure 5.1: Coring for Granite Strength Test: a. SDS with coring bit; b. Granite Coring with bit ;
c. Drill hole

Saw was used to cut, and grinder used to ensure parallel ends (Figure *5.2*). ASTM D4543-2008
was followed for ensuring appropriate sample preparation for UCS [63].

Figure 5.2: a. Core cutting saw; b. Grinder; c. Ensuring parallel edges of the core sample by grinder

Figure 5.3: Granite samples for UCS test according to D7012-2014e1

ITS test samples were prepared according to ASTM D3967 - 2016, (Figure 5.4) [59]. Coring, Cutting, and ensuring parallel edges were also done (Figure 5.1,Figure 5.2).
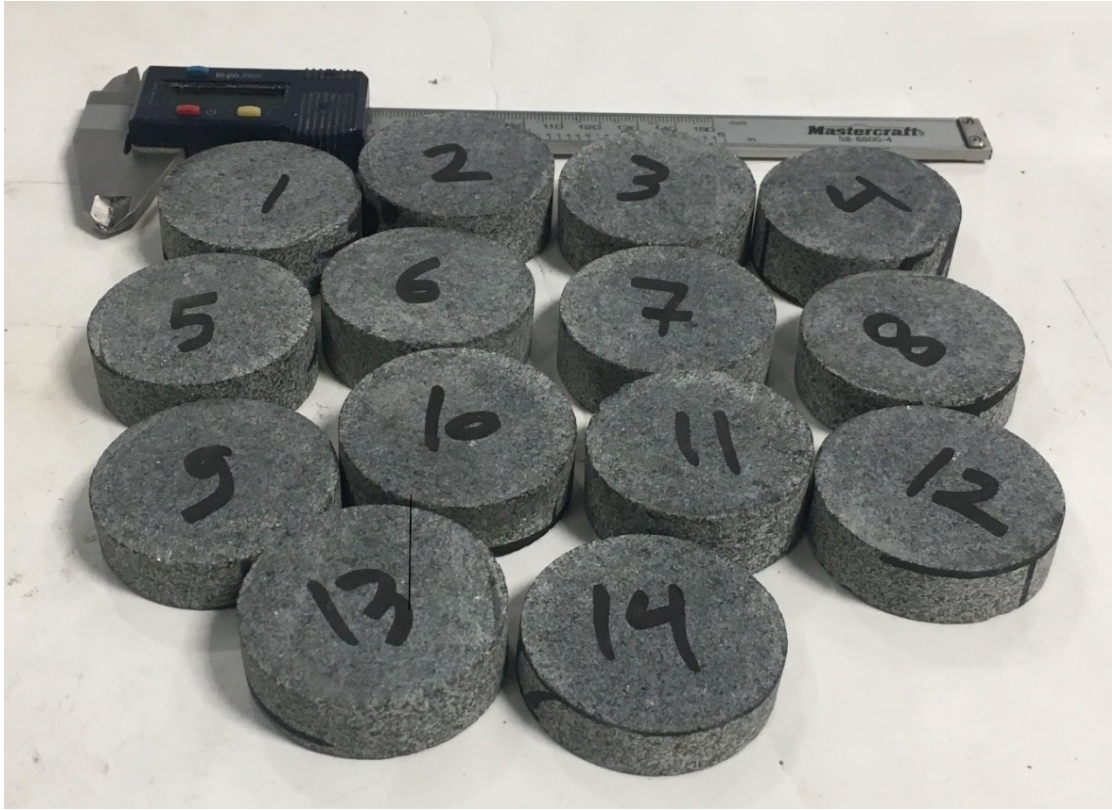
Figure 5.4:Granite samples for ITS tests according to D3967 - 16

5.4. Experimental Apparatus

Displacement Transducer, Geomechanics Loading Frame, Electronic Balance and Vernier Caliper.

5.5. Design of the Experiment

The number of samples required to obtain a certain level of statistical results can be randomly determined according to E122 [64]. The details of the pre-testing matrix for the UCS and ITS experiments are given in Table 5.1 and Table 5.2.

Table 5.1: Pre-testing matrix details of the UCS test for granite sample

Sample no	Diameter, mm	Length, mm	Weight, Kg	Area, mm2	Density, Kg/m3
1	44.41	104.54	0.473	1549	2922.2
2	44.47	98.08	0.445	1553.2	2918.5
3	44.47	103.39	0.469	1553.2	2918.7
4	47.09	116.43	0.592	1741.6	2919.5
5	44.49	103.25	0.469	1554.6	2920.7
6	44.43	103.42	0.468	1550.4	2918.1

7	44.82	95.87	0.436	1577.7	2879.3
8	44.49	98.81	0.447	1554.6	2911.3
9	47.07	109.95	0.556	1740.1	2906.0
10	44.44	101.46	0.461	1551.1	2932.5

Table 5.2:Pre-testing matrix details of the ITS test for granite sample

Sample no	Diameter, mm	Thickness, mm	Weight, Kg	Area, mm2	Density, Kg/m3
1	47.1	15.1	0.077	1742.3	2915.3
2	47.06	17.6	0.089	1739.4	2907.3
3	47.11	16.1	0.082	1743.1	2907.7
4	47.03	17.25	0.085	1737.2	2826.5
5	47.06	14.91	0.077	1739.4	2969.1
6	47.04	16.02	0.08	1737.9	2873.4
7	46.98	15.2	0.075	1733.5	2918.5
8	47.02	14.26	0.072	1736.4	2895.6
9	47.18	12.27	0.062	1748.3	2899.6
10	47.06	16.56	0.081	1739.4	2808.6
11	44.18	16.82	0.074	1533.0	2862.1
12	47.05	14.02	0.071	1738.6	2921.0
13	47.11	15.18	0.076	1743.1	2861.0
14	47.04	11.26	0.057	1737.9	2902.6

5.6. Strength measurements

5.6.1. Unconfined Compressive Strength

The Unconfined Compressive Strength (UCS) is the maximum axial compressive stress that a right-cylindrical sample of material can withstand under unconfined conditions—the confining stress is zero [65]. The Unconfined Compressive Strength (UCS) tests were performed in accordance with ASTM D7012-14. UCS tests were performed by using the Geomechanics Loading Frame (Figure *5.5*).
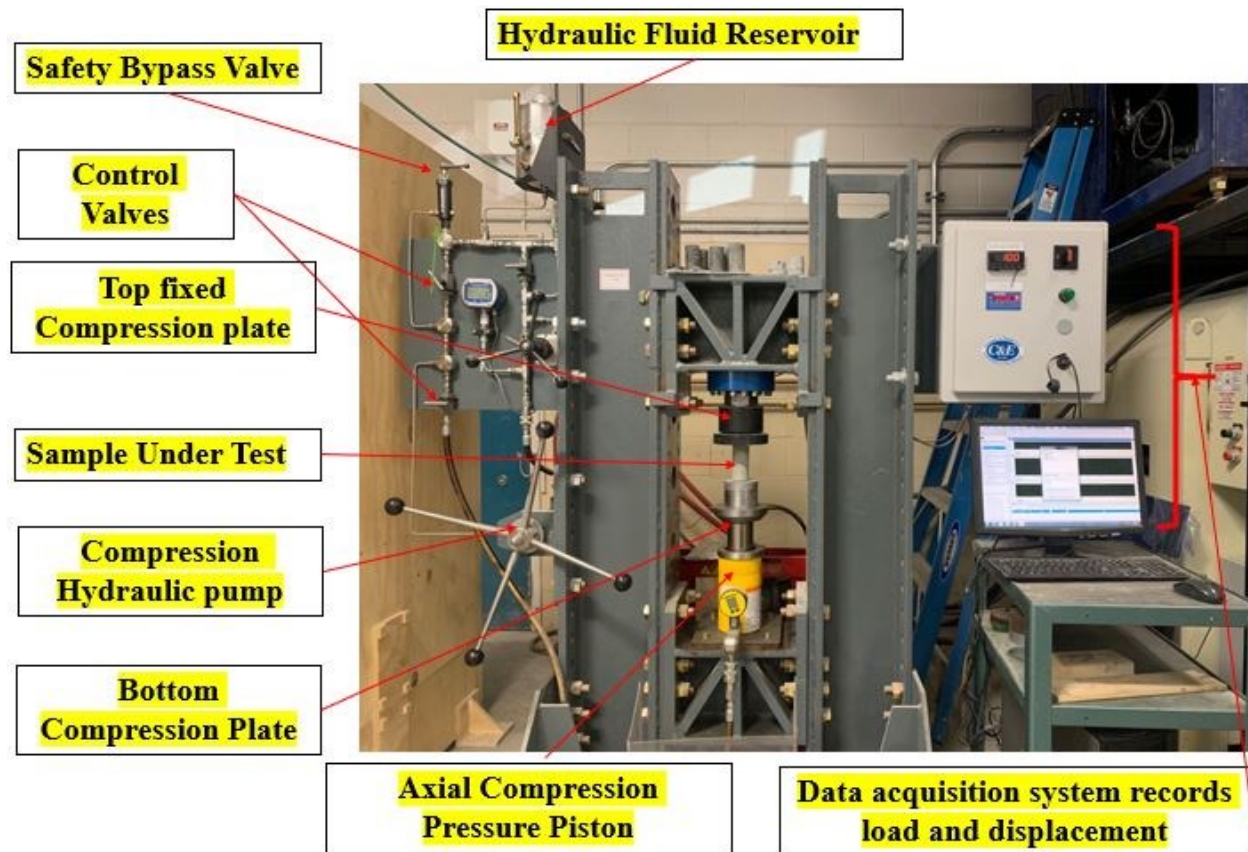
Figure 5.5: Geomechanics Loading Frame

UCS were measured by following steps: Place the lower platen on the base or actuator rod of the loading device. Swab the test specimen and the upper & lower platens. Start the axial load until failure (Figure 5.6). Then, calculate the compressive strength in the test specimen from the maximum compressive load on the specimen and the initial computed cross-sectional area as follows in equation 5.1:

$$\sigma_{UCS} = \frac{P_{max}}{A} \ldots \ldots \ldots \ldots \ldots \ldots .5.1$$

Where:

σ_{ucs} = *Compressive strength (MPa)*

P_{max} = *Maximum load, (kN)*

A = *Cross sectional area, (mm²)*

Figure 5.6: Granite samples after conducting the UCS test

5.6.2. Indirect Tensile Strength

It is indirect tensile because the loading direction is not tension but compression. This type of test requires the disk shape sample [66] . The Indirect Tensile Strength (ITS) tests were performed in accordance with ASTM D3967 - 16. ITS tests were performed by the using Geomechanics Loading Frame (Figure 5.5). Determined the IT strength through the following steps:

Place every disk between flat-end pistons; Start loading the frame while recording the increase of load until the sample failure (Figure 5.7); using equation 5.2 for calculating the IT strength

$$\sigma_t = \frac{2P}{\pi LD} \ldots \ldots \ldots \ldots \ldots \ldots \ldots ..5.2$$

Where:

σ_t = *Splitting tensile strength, MPa*

P = Maximum applied load indicated by the testing machine, N

L = Thickness of the specimen, mm

D = Diameter of the specimen, mm
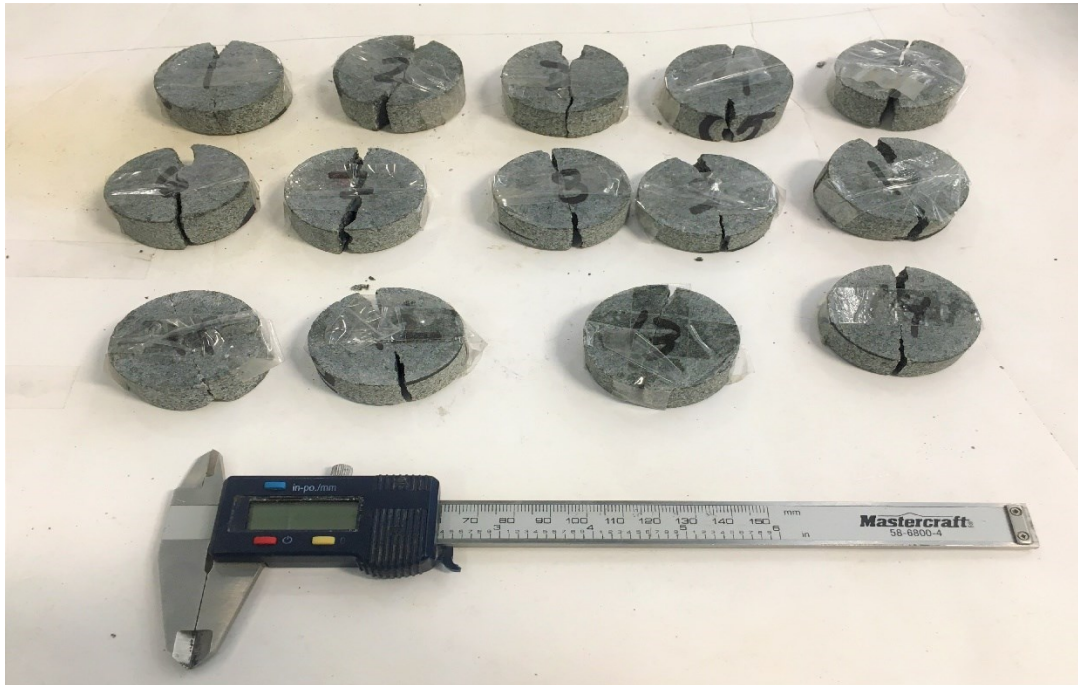
Figure 5.7:Granite samples after conducting the ITS test

5.7. Result and Discussion

UCS and ITS experimental analysis were conducted, and the results are discussed in the following subsections.

5.7.1. UCS Data and Results Matrix

Table 5.3 contains all the processed data from the Unconfined Compressive Strength (UCS) tests. The table indicates that sample no. 4, 6 and 7 are creep samples. The three creep samples have been separated for further research. The load-displacement and stress-strain interpolation process are in the Appendix E.

Table 5.3: UCS experimental Data analysis matrix of the granite samples

Sample no	Maximum Load, kN	UCS (MPa)
1	249.3	161.0
2	271.8	175.0
3	269.2	173.3
4	273.8	Creep
5	274.6	176.7

6	271.6	Creep
7	274.6	Creep
8	266.8	171.6
9	274.3	157.6
10	253.7	163.6

Figure 5.8 demonstrates the processed data of the relationship between load vs displacement for the UCS tests in Table 5.4. This graph shows the maximum loading value of the experiments which calculated from the UCS values.
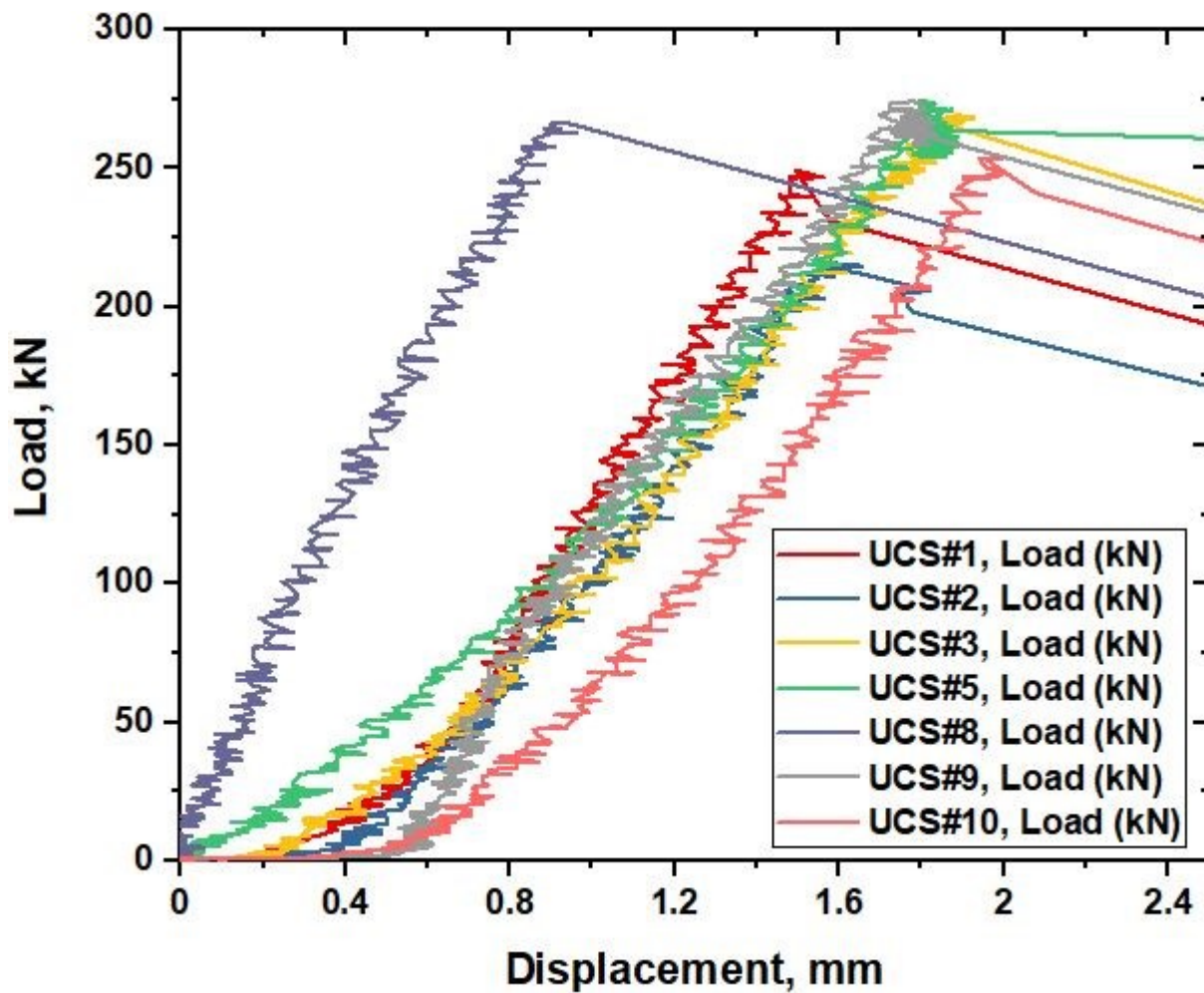
Figure 5.8: Load-Displacement relationship for UCS tests

Table 5.4: UCS matrix results of the granite samples

Sample No	Maximum Load, kN	UCS(MPa)	Young Modulus (GPa)
1	249.3	161.0	15.6
2	271.8	175.0	11.5
3	269.1	173.3	12.0
5	274.6	176.7	11.2
8	266.8	171.6	17.4
9	274.3	157.6	12.8
10	253.7	163.6	12.7

Figure 5.9 contains the UCS details from the stress vs strain graph and the results of the current work. UCS is indicated on the stress vs strain graph. The value of the UCS in Figure 5.9 and the calculated UCS value in Table 5.4 are the same.

In addition, Young's Modulus is calculated by the slope of the linear portion of the Stress vs Strain graph for the UCS tests that are shown in Table 5.4. The interpolation process of the slop is shown in Appendix E. Young's Modulus is a mechanical property that measures the stiffness of a solid material. The Modulus defines the relationship between stress and strain for a material in the linear elasticity regime of a uniaxial deformation. The slope of the linear portion of the Stress vs Strain graph is Young's Modulus as follows in equation 5.3 [67] .

$$E = \frac{\sigma}{\epsilon} \dots\dots\dots\dots\dots\dots\dots\dots.5.3$$

Where:

E= Young's Modulus (GPa)

σ= Normal Stress (MPa)

ε= Normal Strain (Dimensionless)
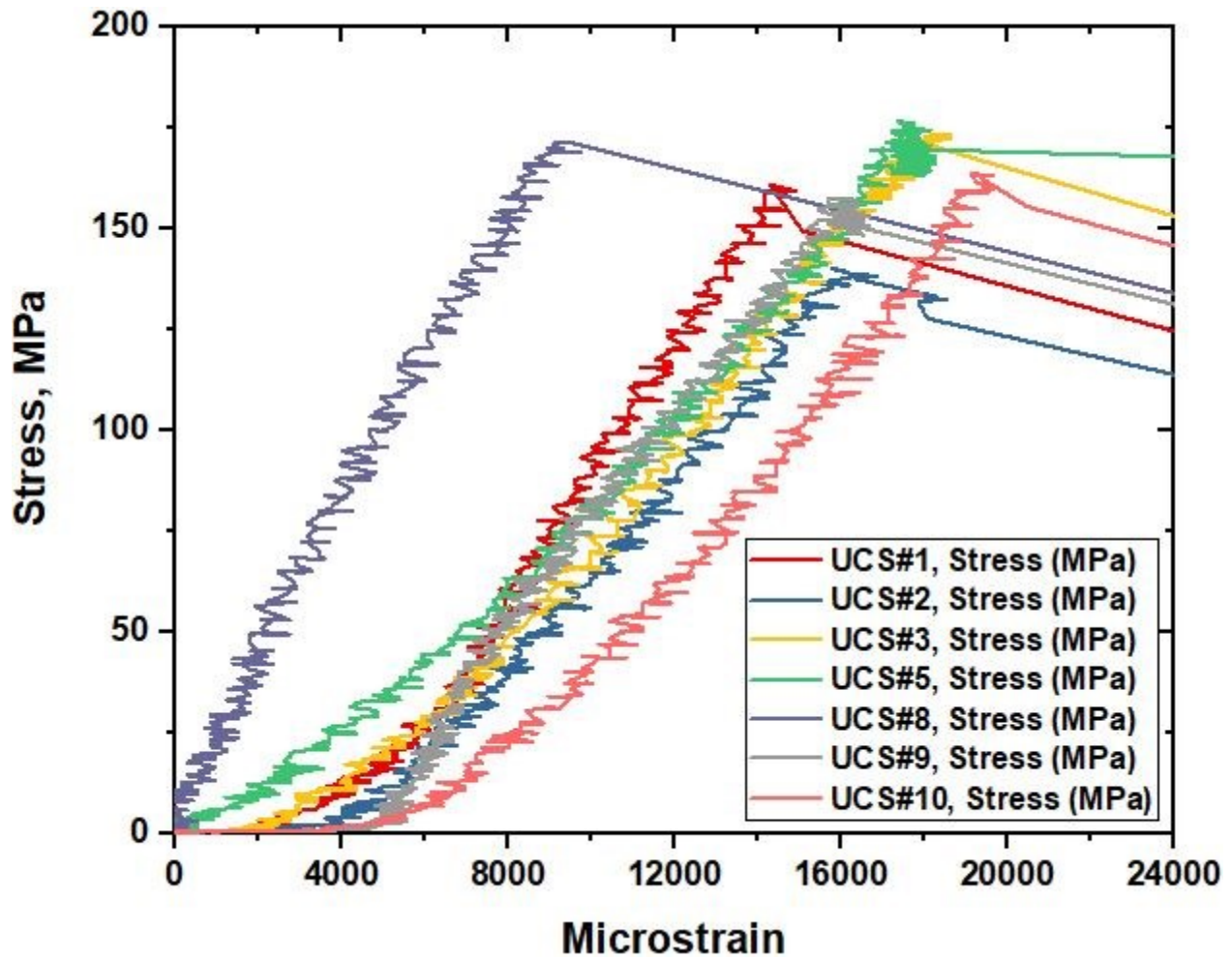
Figure 5.9: Stress-Strain graph for UCS tests

5.7.2. ITS Data and Results Matrix

Figure 5.10 illustrates the processed data of the load vs. time relationship for ITS tests in Table 5.5. This graph shows the maximum loading value of the experiments which obtained from ITS values. The ITS for each sample was calculated using Equation 5.2 after obtaining the maximum loading of the test from Figure 5.10 and other characteristics such as the thickness and length of the sample from *Table 5.2*. The load vs time detail results are reported in the Appendix F.
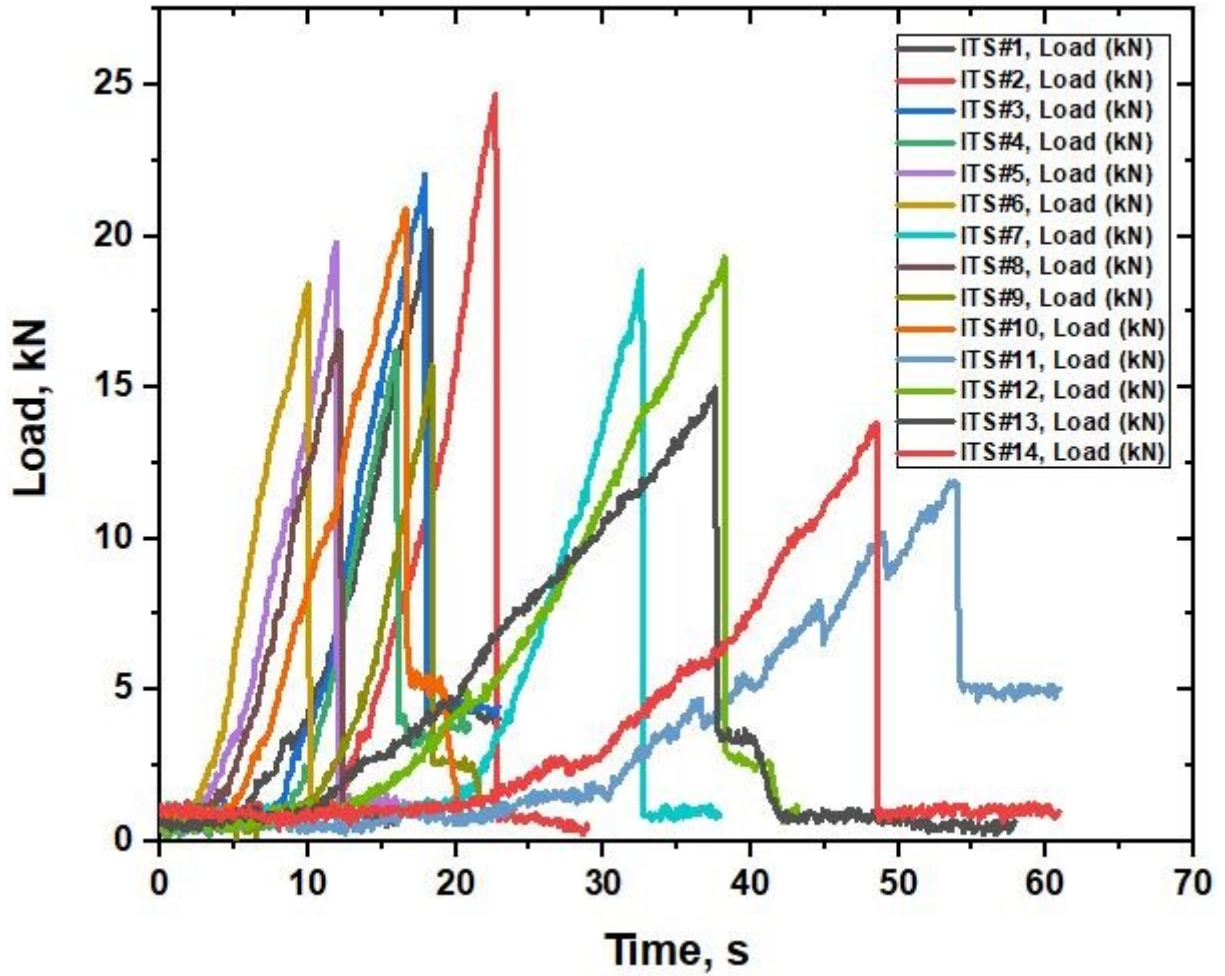
Figure 5.10: Load vs Time graph for ITS tests

Table 5.5: ITS matrix results of the granite samples

Sample no	Maximum Load, kN	ITS (MPa)
1	20.2	18.1
2	24.7	19.0
3	22.0	18.5
4	16.2	12.7
5	19.8	18.0
6	18.4	15.6
7	18.8	16.8
8	16.9	16.0
9	15.7	17.3
10	20.9	17.1
11	11.9	10.2
12	19.3	18.6

| 13 | 15.0 | 13.3 |
| 14 | 13.8 | 16.6 |

5.7.3. Precision

According to ASTM D7012 − 14 e1 and ASTM D3967 – 16 ,the probability is approximately 95 % that two test results obtained in the same laboratory on the same material will not differ by more than the repeatability limit for UCS and ITS respectively. The precision statistics are calculated from the equation *5.4*.

$$r = 2\left(\sqrt{2}\right)S_r \dots\dots\dots\dots\dots\dots\dots\dots\dots 5.4$$

Where:
r = The repeatability limit
S_r = repeatability standard deviation.

The precision statistics for the UCS and ITS tests of the granite are demonstrated in Table 5.6.

Table 5.6: The strength test results statistics

Parameters	UCS	ITS
Average/Mean value (MPa)	168.4	16.3
Standard Deviation	7.5	2.6
Repeatability Limit	21.3	7.2

5.8. Conclusion

The standard methods are introduced to estimate the uniaxial compressive strength and Indirect Tensile Strength of the granite rock. The work of this thesis covers the strength measurements including estimating the UCS and ITS of the granite rock by mechanical method. From the analysis, it is determined the average UCS of the granite is 168.4 MPa and average ITS is 16.3 MPa. The UCS and ITS tests result provide the correlation of the granite strength evaluation which is consistent with each other results obtained using the rule of thumb. Although strength correlations between UCS with ITS were widely used by numerous researchers, the main purpose for such correlations was to provide alternatives to estimate rock strengths by different methods. Moreover,

it is also useful in developing a baseline procedure for granite rock strength evaluation that can be used as a base for further research.

Chapter 6: Numerical and Experimental Study on Belleville Springs as Vibrational Element of Passive Vibration Assisted Rotary Drilling (pVARD) Tool for Drilling Performance Applications

This chapter is based on the conference paper "Numerical and Experimental Study on Belleville Springs as Vibrational Element of Passive Vibration Assisted Rotary Drilling (pVARD) Tool for Drilling Performance Applications" authored by Md. Shaheen Shah, Dipesh Maharjana, Abdelsalam Abugharara, Syed Imtiaz and Stephen Butt, and published in the Proceedings of the Canadian Society for Mechanical Engineering International Congress 2020, Charlottetown, PE, Canada.

6.1. Co-authorship Statement

The contributions of this collaborative work are described in the following six parts. 1) Identification of research topic is collaborative between all co-authors. 2) Md. Shaheen Shah, Dr. Abdelsalam Abugharara and Dipesh Maharjana have contributed to the simulation analysis. 3) Design of experiments are contributed by Md. Shaheen Shah, Dr. Abdelsalam Abugharara and the main supervisor Dr. Stephen Butt. 4) Md. Shaheen Shah and Dr. Abdelsalam Abugharara is responsible of conducting compression experiments. 5) Data analysis and discussion of results is a collaborative work contributed by all co-authors, 6) Manuscript preparation is mainly contributed by Md. Shaheen Shah, with revision assistance provided by all other coauthors.

6.2. Abstract

A novel small-scale laboratory drilling tool, passive Vibration Assisted Rotary Drilling (pVARD) was previously designed and tested through intensive laboratory experiments in the Drilling Technology Laboratory at Memorial University of Newfoundland, Canada. The initial laboratory small-scale pVARD prototype showed promising results in enhancing drilling performance. The current Large Drilling Simulator (LDS) pVARD prototype is designed for wider-range drilling parameters of up to 100 kN of applied Weight on Bit (WOB), 1200 N-m of torque, and up to 1000 rpm of rotational speed. For optimal pVARD configurations and best drilling results, a pVARD operational detail is an important step. The study of this paper concentrates on mechanically designing the pVARD compatible to the LDS, selecting optimal Belleville Springs, conducting experimental and simulation studies to optimize Belleville Springs stacking and pVARD

configurations. The mechanical and simulation studies include conducting dynamic and static compression tests as well as a numerical study using simulation on various scenarios of Belleville Spring stacking. The initial mechanical compression tests, numerical study, and subsequent planned intensive drilling experiments can collectively provide important information in optimizing the pVARD fundamentals and can provide pVARD pre-setting and configurations based on the rock types to be drilled and the drilling parameters to be applied for the optimal drilling performance. The results of spring compression tests with the results of drilling performance (planned) can be analyzed based on drilling with and without pVARD. The results can also include the analysis of vibrations produced in both drilling systems recorded by an associated laser sensor.

Keywords-pVARD; Compression tests; Belleville Springs; Simulation; mechanical design; working load; drilling performance.

6.3. Introduction

A series of drilling experiments were carried out by the Drilling Technology Laboratory (DTL) using a small scale passive Vibration Assisted Rotation Drilling (pVARD) tool with a fully instrumented Small Drilling Simulator (SDS) fully described by Khorshidian et al. [52] and Rana et al. [35]. The results of the previous studies (i.e. laboratory and numerical) using a small scale pVARD tool was productive and showed drilling performance enhancement through increasing the drilling Rate of Penetration (ROP). However, to further evaluate the operation mechanism of pVARD and how it can be optimally used to maximize drilling performance, a laboratory large scale pVARD is designed and tested and eventually utilized for laboratory drilling experiments using a fully instrumented Large Drilling Simulator (LDS) (Figure *6.1*).
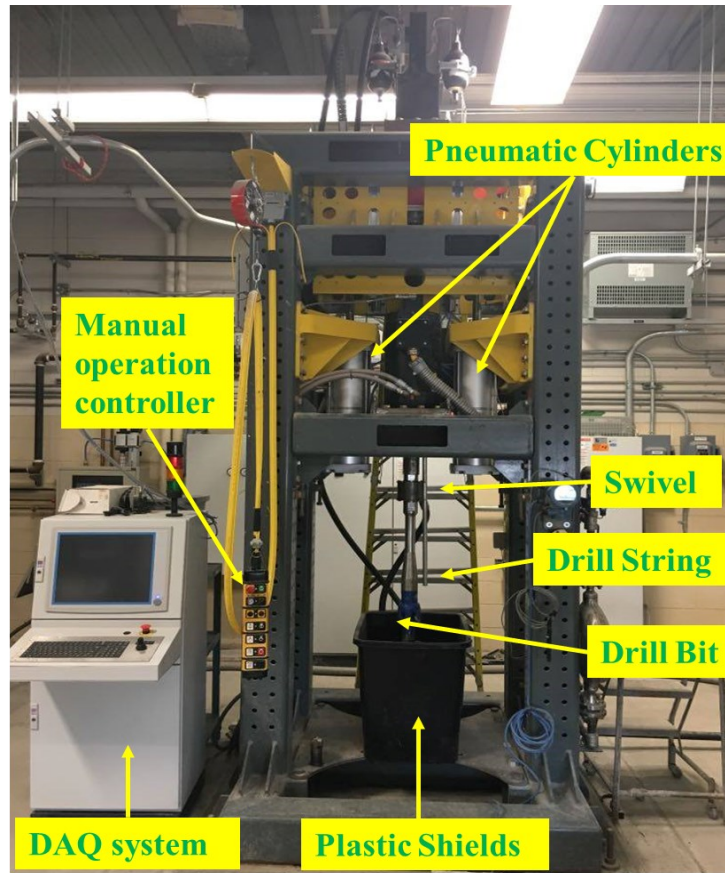
Figure 6.1:Laboratory Setup of the Large Drilling Simulator

The LDS-pVARD is manufactured to be attached to the drill bit during the experiment. This tool has been constructed using rock-bit interaction and induces axial vibration, providing full rotation speed and torque to the drill bit. This tool is comprised of three sections: (i) a compliant part of Belleville springs, which utilize induced axial vibrations, (ii) a dampening section of elastic materials (i.e. rubber), and (iii) a torque transmitting unit (Figure *6.2*). Figure *6.2* also demonstrates the assembled pVARD including the inner shaft, the outer shell, and stacked rubber and springs. The inner blank shaft and the outer shell provides relative motion between the converse ends of the tool. Keys are used to transmit full torque to the drill bit. The compliance can be adjusted to different configurations in this tool by utilizing various spring stacking [35].
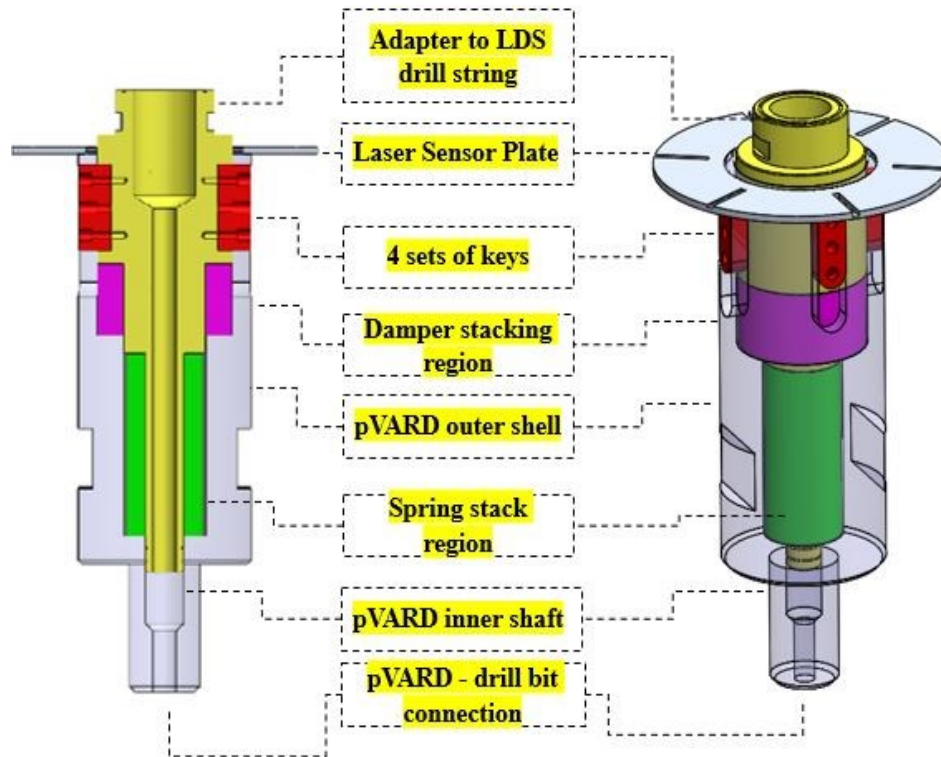
Figure 6.2:Longitudinal section (left), complete assembly (right) of pVARD

The dynamic simulation results of the LDS pVARD have been showed that adding a pVARD makes the drill string axially oscillate and compliant. These results are at lower system's natural frequency in the range of 100rpm to 600 rpm. Positive effects of the pVARD have been reported in this paper with specific conditions [68]. To determine the mechanism and the operational range of how the compliance of the pVARD works on the new drilling tool and how it can improve the rate of penetration in drilling by applying passive vibration, the authors invented a new testing method based on preceding vibration equipment that tests rubber and spring. Spring is the prime part of the pVARD tool and for this study the Belleville springs or coned disc springs are selected and tested in various stacking.

Belleville springs are generally exercised in different mechanical modes which can support various load statically or dynamically along its axis. This spring can be compressed and can generate different non-linear load–displacement curves by various standards. Although Julien Belleville patented the principle of the disc spring in 1867, it was published in 1936 [69], [70]. Although several works have been done for Belleville Spring to better understand load-deflation graphs,

66

Almen-Laszlo [57] first proposed it through a mathematical formula with some assumptions: the cross-section is assumed to be a small angular deviation, the spring cross-section does not pervert but only rotates at a neutral point, and the loads are centrally distributed. To improve the accuracy of this equation, several researchers have proposed theoretical models and approximate equations by revising the above-mentioned assumptions. Zhiming et al. [71] proposed and considered the finite rotation and greater discontinuity problems of the shell of a beam and an angular branch. Rosa et al., 2001 has reported theoretical and numerical analysis on disc springs with linear variable thickness to extend the range of constant loads [72]. When considering the effects of the calculation of friction for disc springs Curti et al. [73] proposed an analytical solution. Ozaki et al. [74] evaluated the outcomes of friction boundaries on the static and dynamic characteristic of the Belleville disc springs. However, in practice, the effect of the Belleville disk spring's friction factor cannot be measured, therefore some research is underway. In this study on Belleville disc springs the friction factor is ignored but its effect is identified through numerical and experimental comparative analysis.

This study is stage I in optimizing pVARD by performing numerous (numerical and experimental) compression tests involving different spring configurations that can lead to producing a spring compression details to be use in evaluating drilling performance against rigid drilling in stage II.

6.4. pVARD Components

This section summarizes the basic characteristics of different components of LDS-pVARD tool. There are five major component groups including 1) Inner shaft, 2) Outer shell, 3) Keys, 4) Sensor plate, 5) Belleville Springs and Rubbers (Figure *6.2*). These parts are explained in more detail in the following sections:

6.4.1. Inner Shaft

The top of the inner shaft has a 13mm through hole for circulating fluid and is designed to connect to the existing swivel of the LDS. There are four major turnings in the inner shaft which serves their unique purposes with a swivel connection, keys connection, rubber stacking and spring

stacking. Moreover, the shaft section of the spring stacking also makes up a 1" space which is used for the O-rings (Figure *6.2*).

6.4.2. Outer shell

The outer shell of the pVARD is designed in such a way that it attaches to the inner shaft with the help of 4 keys while providing the movement of 32 mm towards the axis. The bottom of this shell is designed to connect to the rest of the drill string of the LDS. The top of the outer shell is turned 5 mm to place the sensor plate. In the inside, the outer shell has the landing faces for compression of springs and rubbers together with the sliding face for the O-rings (Figure *6.2*).

6.4.3. Keys

There are 4 keys that transmit torque between the inner and outer shaft. The keys have three holes. Two of these holes are in the top and bottom and do not have threads in them. These holes are there to connect the keys to the inner shaft. The middle hole has thread in it and its purpose is to pop out the keys from the inner shaft while disassembling. All three holes are designed for the M5 × 1 screws (Figure *6.2*).

6.4.4. Sensor plate

The laser sensor array reflector is a 5 mm thick aluminum plate with 6 uniformly spaced grooves as shown in Figure *6.2*. Five grooves have a cross-section of 5 mm (width) × 3.5 mm (depth) and the sixth groove has a cross-section of 5 mm (width) × 1.5 mm (depth). The unique depth of sixth groove is to identify the completion of one rotation during the analysis of the laser sensor data used to measure several parameters such as the level of axial vibrations, rotational speed, etc.

6.4.5. Belleville Springs and Rubbers

The LDS- pVARD is designed for 1" ID and 2" OD of Belleville springs. The rationale behind the selection of this Belleville spring dimension is the availability of 4 different springs with unique compliances that share the same dimensions (ID and OD). This makes it applicable to change the compliance of the tool itself not only by changing the spring configuration but also by using a

completely different spring type, thus adjusting the range of the pVARD working range. The height of the spring stack is designed to be 5", in an experimental scenario where total spring height is less than 5", the remaining space must be filled with rigid spacers.

Likewise, each rubber ring is designed with 2.35" ID, 3.70" OD, and 0.25" thick as shown in Figure *6.2*. Four sets of these rubbers are stacked in series when assembling the tool. Since these rubbers are not used as perfect dampers, they possess certain amount of spring elements along with the damper element. For accurate estimation of the tool compliance, the damping coefficient and the spring coefficient of the rubbers must be experimentally calibrated and integrated into the numerical modeling of the tool.

6.5. Finite Element Analysis

This section presents the results of the Finite Element Analysis (FEA) of the torque transmitting section of the LDS-pVARD. For the simplicity of the simulation, all the complex features like thread, chamfers, through holes (in the inner shaft), etc. of the components are suppressed. Table *6.1* summarizes the configurations of the simulation.

Table 6.1: Summary of configuration settings for FEA

Particular	Description
Components	Keys, inner shaft & outer shell
Material	AISI 4140 Steel
$Tensile\ Strength\ (\sigma_t)$	655 MPa
$Yield\ Strength\ (Y_s)$	415 MPa
$Young's\ Modulus\ (E)$	200 GPa
Meshing	Curvature-based mesh
Mesh quality	High
Minimum element size	2 mm
Maximum element size	10 mm
Torque	1200 Nm

6.5.1. Results of Simulation
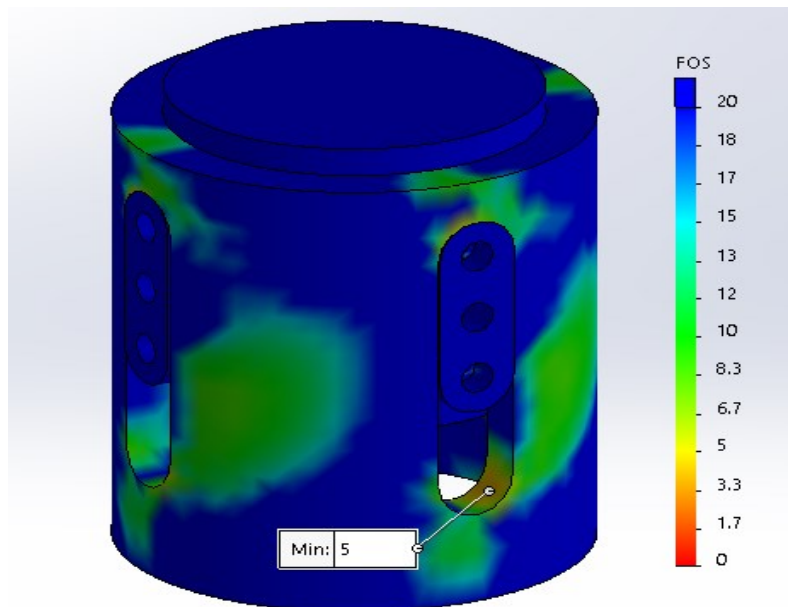
Figure 6.3: Minimum FOS in the Outer shell

The simulation results provided in this section are interpreted in terms of the minimum Factor of Safety (FOS), which is related to the maximum stress concentration. The results of the FEA analysis show that the keys can safely transmit the torque of 1200 Nm with an FOS of more than 10. As shown in Figure *6.3*, the highest concentration in the keys occurs at the through holes of the screws. Similarly, the outer shell has a minimum FOS of 5 at the far end of the slots where the keys are engaged and the maximum stress concentration in the inner shaft occurs at the top and bottom contact points. The keys have an average FOS of 16, where both FOS are assumed to be satisfactory for this design.

6.6. Experimental Apparatus

6.6.1. Mechanical compression tests

A mechanical compression test is conducted to measure the specimen's (Belleville springs) properties by applying compressive loading in the opposite direction, as opposed to squeezing or flattening. The tested specimen is usually placed between two plates, with the load being distributed across the entire surface of the two opposite faces of the sample. Then, the plates are advances towards one another by a standard test machine to flatten the sample. Typically, a compressed sample is shortened by the applied force and extended axially.

The compression test, which is the opposite of the more general tension test [75] , is performed to determine the behavior or the response of the material by sensing a compressive load and measuring the basic variables such as strain, stress, and deformation. During the experiment, different properties of the specimen are recorded, calculated, and plotted as a stress-strain diagram that is used to measure the properties of elastic limit, proportional limit, yield point, yield strength, and compressive strength for some materials [73], [76], [77], [78].
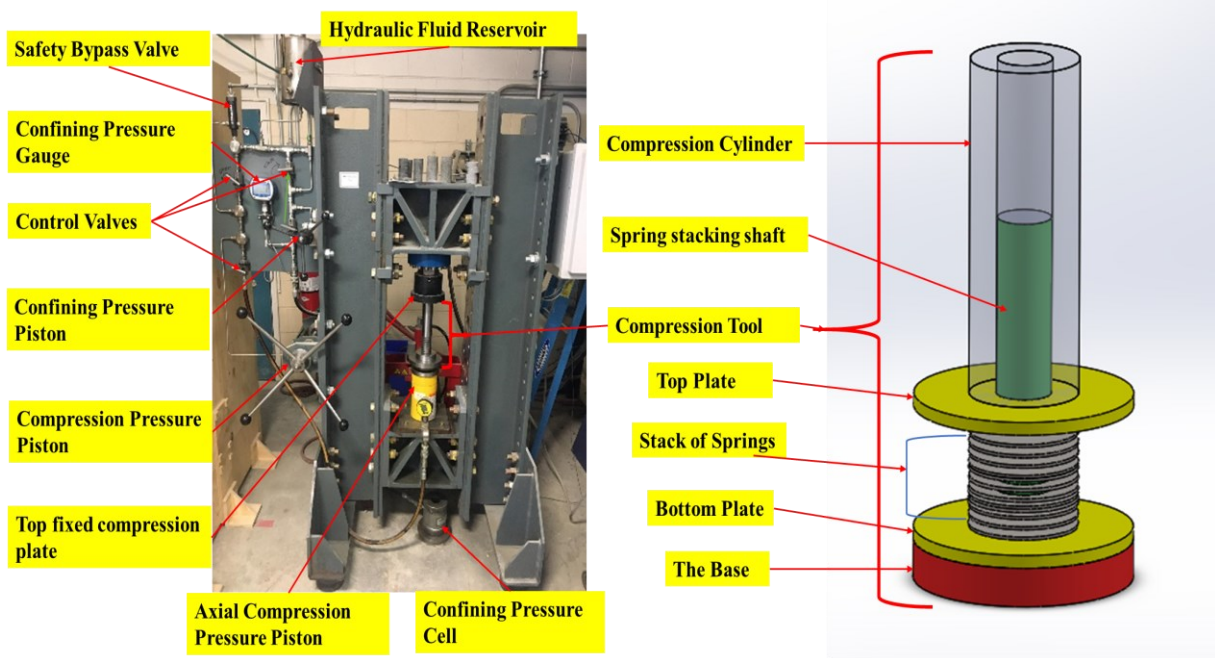
Figure 6.4:Geomechanics loading frame and pVARD spring compression tool

The three main compression tests were conducted on two different stacking of Belleville springs that include 10 and 18 sets of the model 9712k31. There are 18 numbers associated with the Belleville coned disc springs. The loading range of this test is selected with the average 22 kN. The spring compression details are determined using Hooke's law [58] which derives the relationship between the compressive load and the deflection with stiffness. In this experiment, the load frame is set up at different loading rates and resulted in displacement. Stiffness is obtained from Hooke's formula [58].

$$F = -Kx \text{ ... ... .6.1}$$

Here, F is the restoring force, x is the displacement from equilibrium or deformation, and k is a constant related to the difficulty in deforming the system called displacement. The minus sign indicates that the restoring force is in the direction opposite to the displacement.

6.6.2. Simulation

The numerical study has been done by simulation. This simulation is programmed based on the Almen and Laszlo [57] equation [77], [79]. This equation derives the relationship between spring force "F" and spring deflection of a coned disc spring having thickness of "t", inner radius of "D_i", outer radius of "D_e", disc height of "h", inside disc height of "$h_0 (h - t)$", dimension ratio of "δ" and shape coefficient of "K_1" which is described in equation 6.2.

$$F = \frac{4.E}{(1-\mu^2)} * \frac{t^3.s}{K_1.D_e^2}\left[\left(\frac{h_o}{t} - \frac{s}{t}\right).\left(\frac{h_o}{t} - \frac{s}{2t}\right) + 1\right] \text{ ... ... .6.2}$$

$$K_1 = \frac{1}{\pi}.\left[\frac{(\frac{\delta-1}{\delta})^2}{\left(\frac{\delta+1}{\delta-1} - \frac{2}{ln\delta}\right)}\right]$$

$$\delta = \frac{D_e}{D_i}$$

The coned disc springs used in this analysis have the following material properties: (i)Young's modulus E= 210 GPa and (ii) Poisson's ratio μ =0.3. This calculation is designed for a Belleville spring without any machine assistance. Furthermore, the calculation does not take into account the

effect of friction. The purpose of this analysis is compatible for large loading forces, characteristics of nonlinear (degressive) work, measuring spring constant (stiffness), less space requirements, simple mounting and dismantling, less production costs, etc. For this analysis, there are some parameters of spring specification data involving the outer/inside diameter, minimum/maximum working load, working stroke, disc height, and material thickness, which all can be provided by the manufacturer. The simulation produces the maximum permissible loading with maximum spring deflection. By obtaining this data spring stiffness is calculated by using Hooke's formula equation 6.1. In addition, more analysis can be performed by Microsoft Excel using the same spring specification without any simulation. The conclusive comments have come after completing data processing from the simulation and Microsoft Excel [77], [79].

6.7. Experimental procedure and methodology

The Experiments were conducted using the compression tool set described in Figure *6.4* (right).

6.7.1. Results and discussion

The numerical and experimental analysis were conducted, and the results are discussed sequentially. With the help of the simulation, the characteristics of 1-10 & 1-18 configurations of the 9712k31 springs were analyzed. A load vs. displacement relationship is drawn using the simulation results of 1-10 configurations of the 9712k31 as shown in Figure 6.5. In this figure the resulted trend is liner.
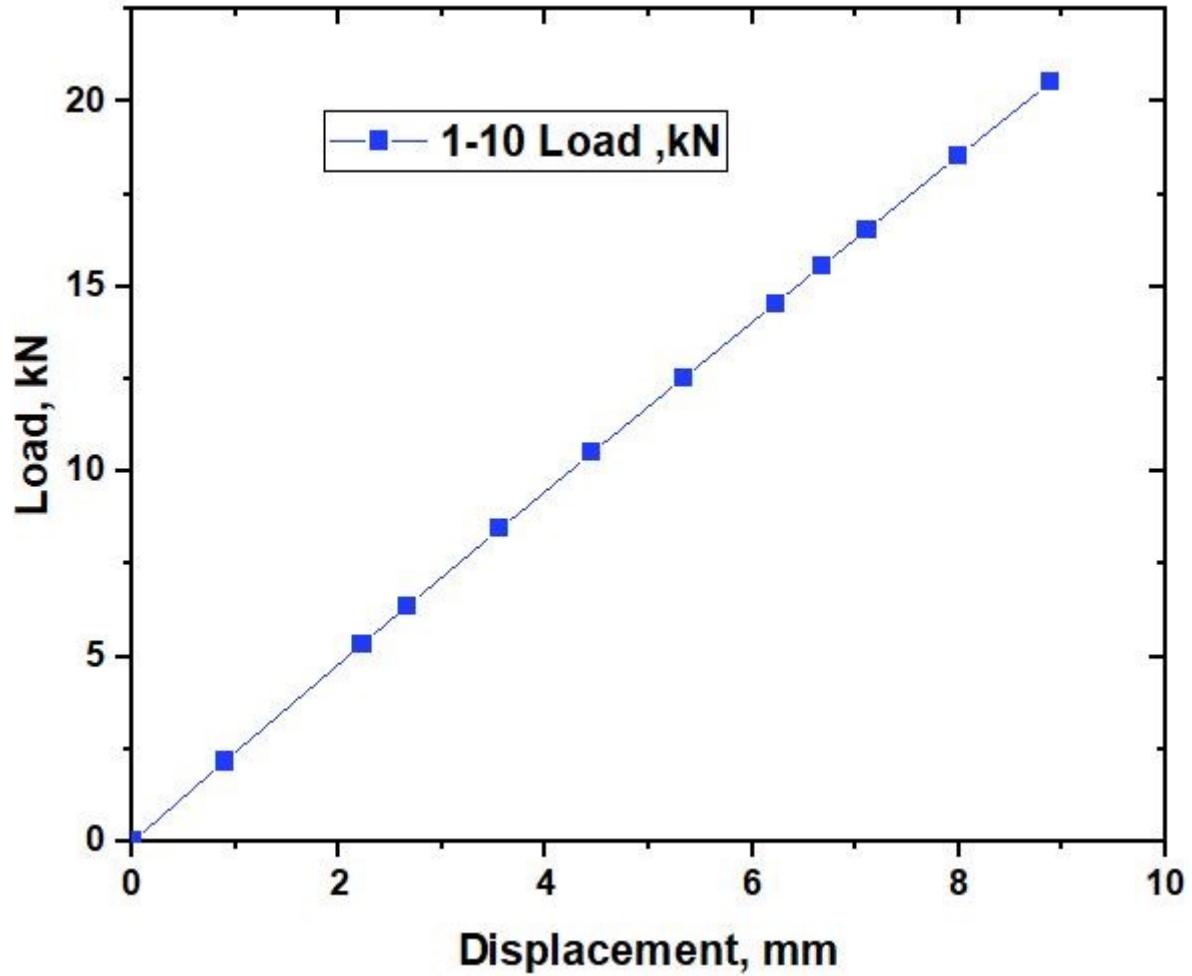
Figure 6.5: Simulated result of "1-10, 9712k31" spring configuration

Also, a load vs. displacement relationship is drawn using the simulation results of 1-18 configurations of the "9712k31" spring is shown in Figure *6.6.* In this figure the resulted trend is liner applying the same force, however the complete flattening occurs at longer displacement.
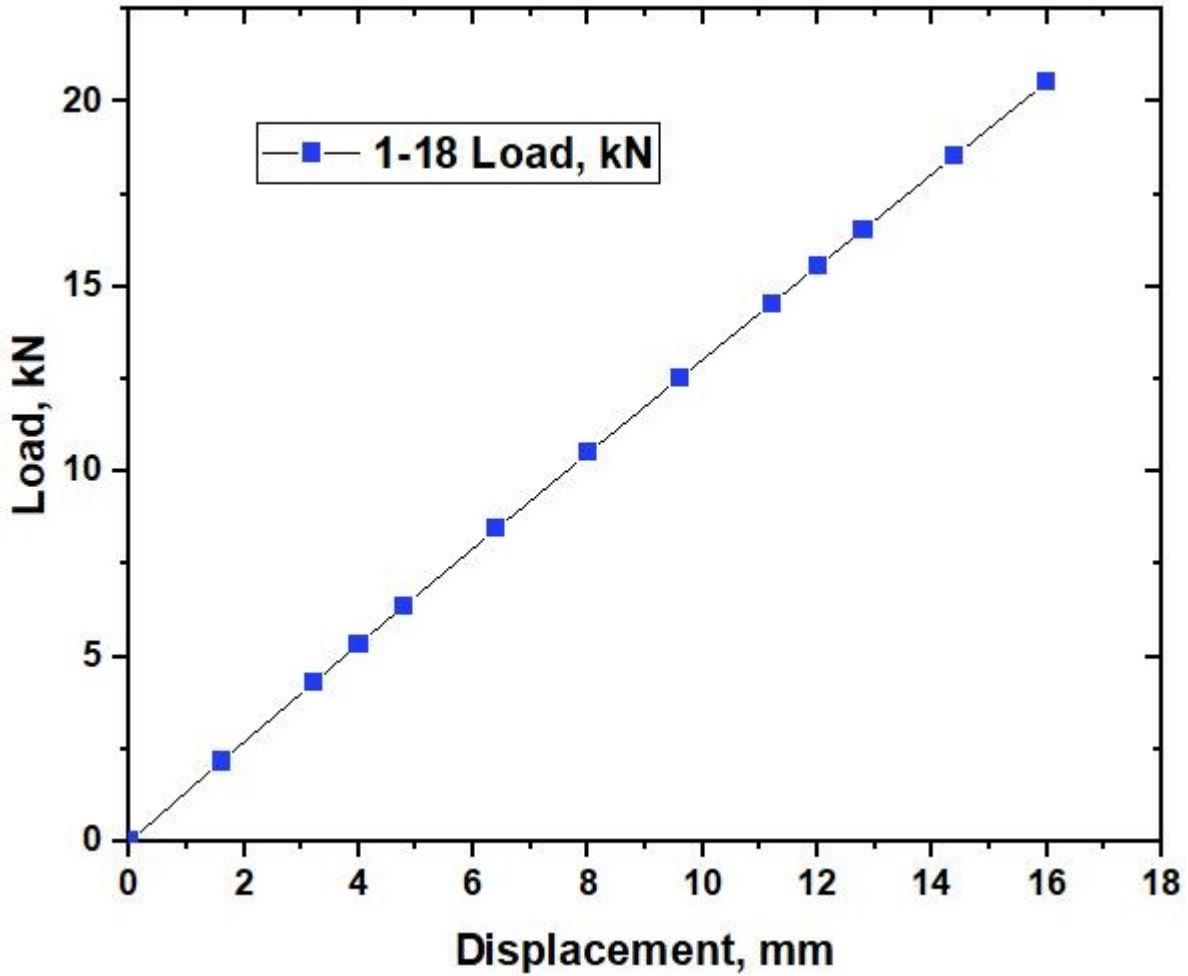
Figure 6.6:Simulated result of "1-18, 9712k31" spring configuration

In compression test was repeated three times (a, b, c) on both spring configurations of the [10 series in a single parallel configuration of the 9712k31] and the [18 series in a single parallel configuration of the 9712k31]. The results of these repeated tests are displayed in Figure *6.7* and Figure *6.8*, respectively. All results show liner relationships.
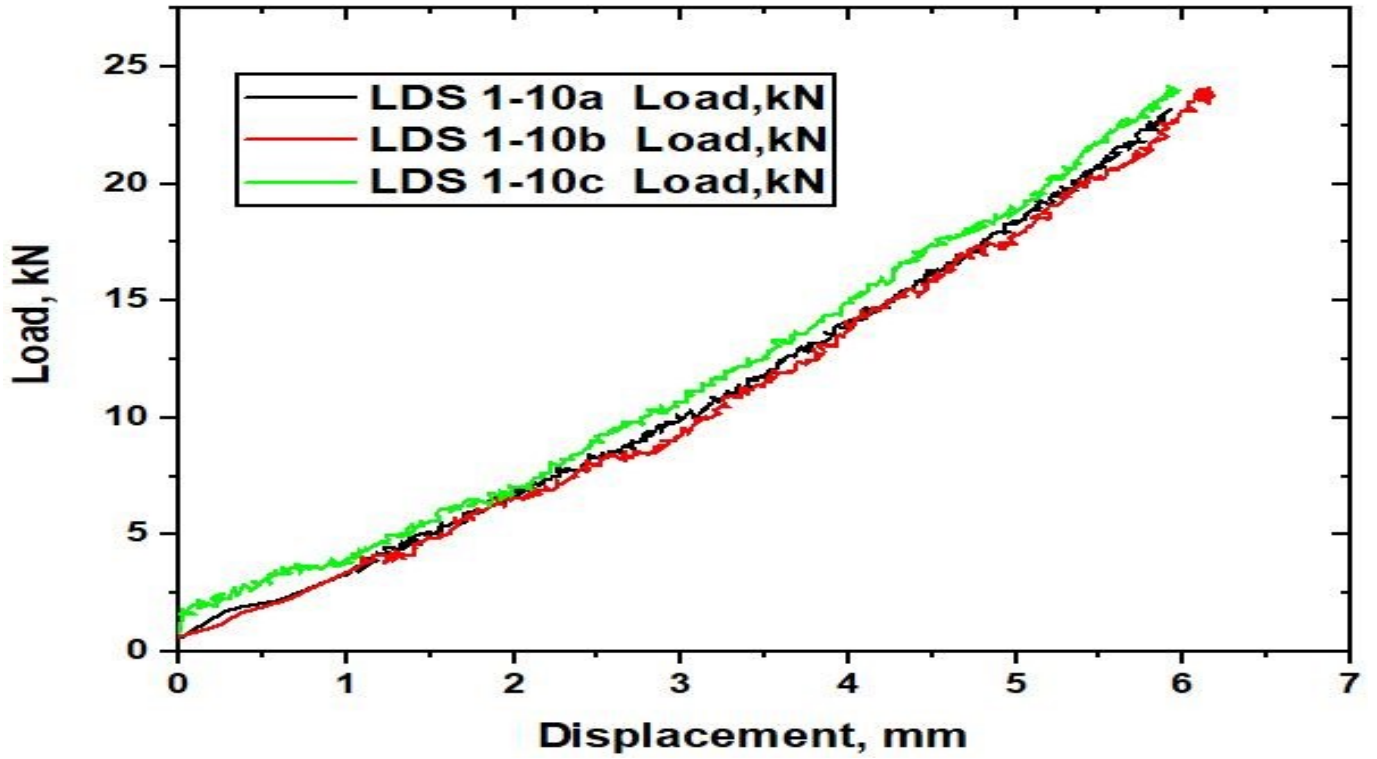
Figure 6.7:Three compression test results of the "1-10; 9712k31" spring configuration.
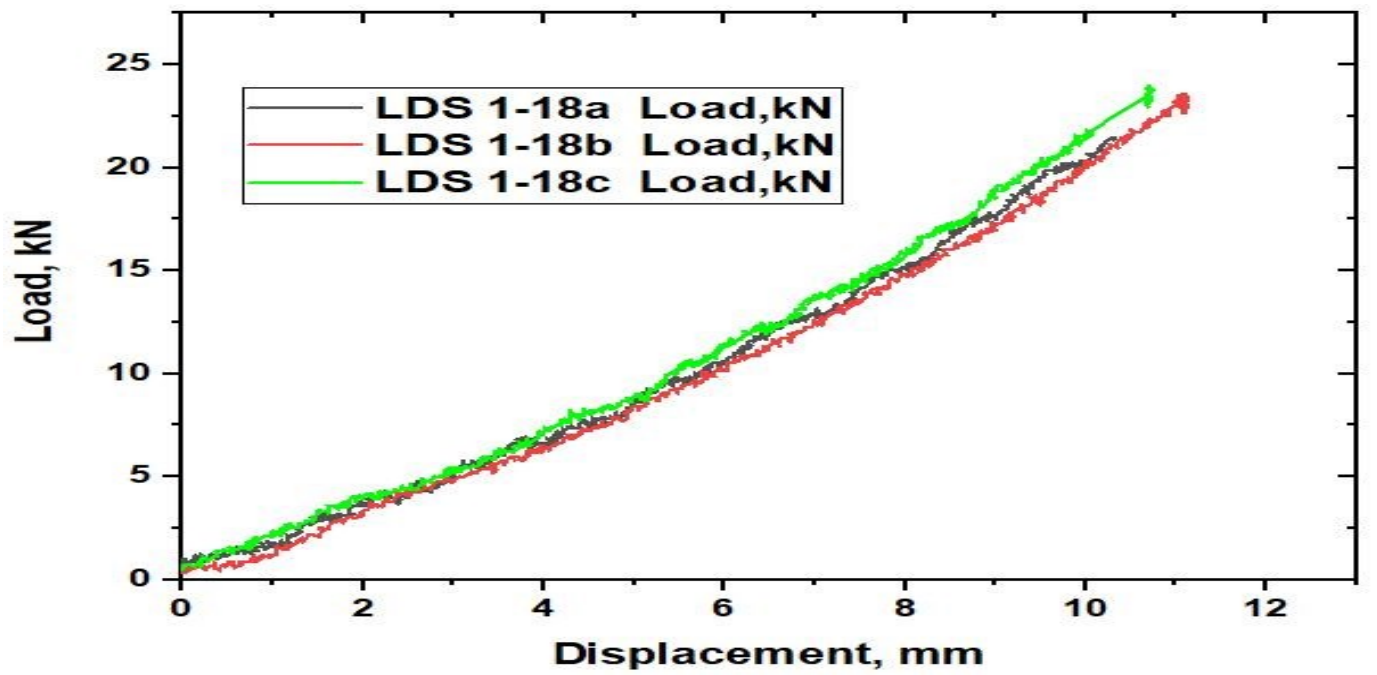
Figure 6.8:Three compression test results of the "1-18 ,9712k31" spring configuration.

A comparative analysis of both (i) simulation and (ii) the mechanical compression test performed on 9712k31 spring type is displayed in Figure *6.9* and Figure *6.10*. The simulation does not consider the friction factor but there is a friction factor considered in the compression test. Due to the increase of the contact area between the compressed springs with the increasing load, the friction increases and the resistance of spring flattening increases, which influences the curve of the mechanical tests to deviate upwards. This can be observed in Figure *6.9* and Figure *6.10*.
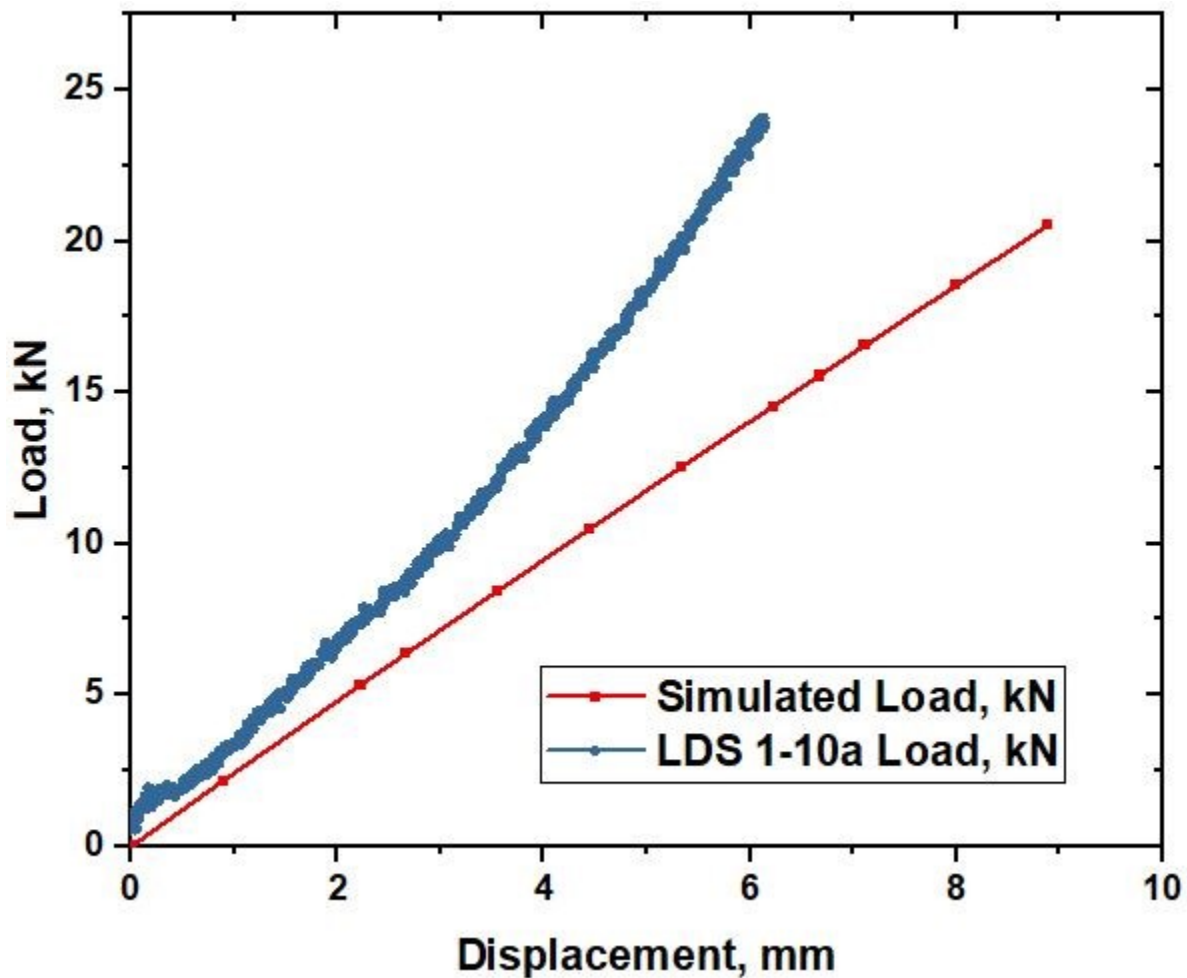
Figure 6.9:Comparison of the simulation with compression test result of the "1-10,9712k31" spring.
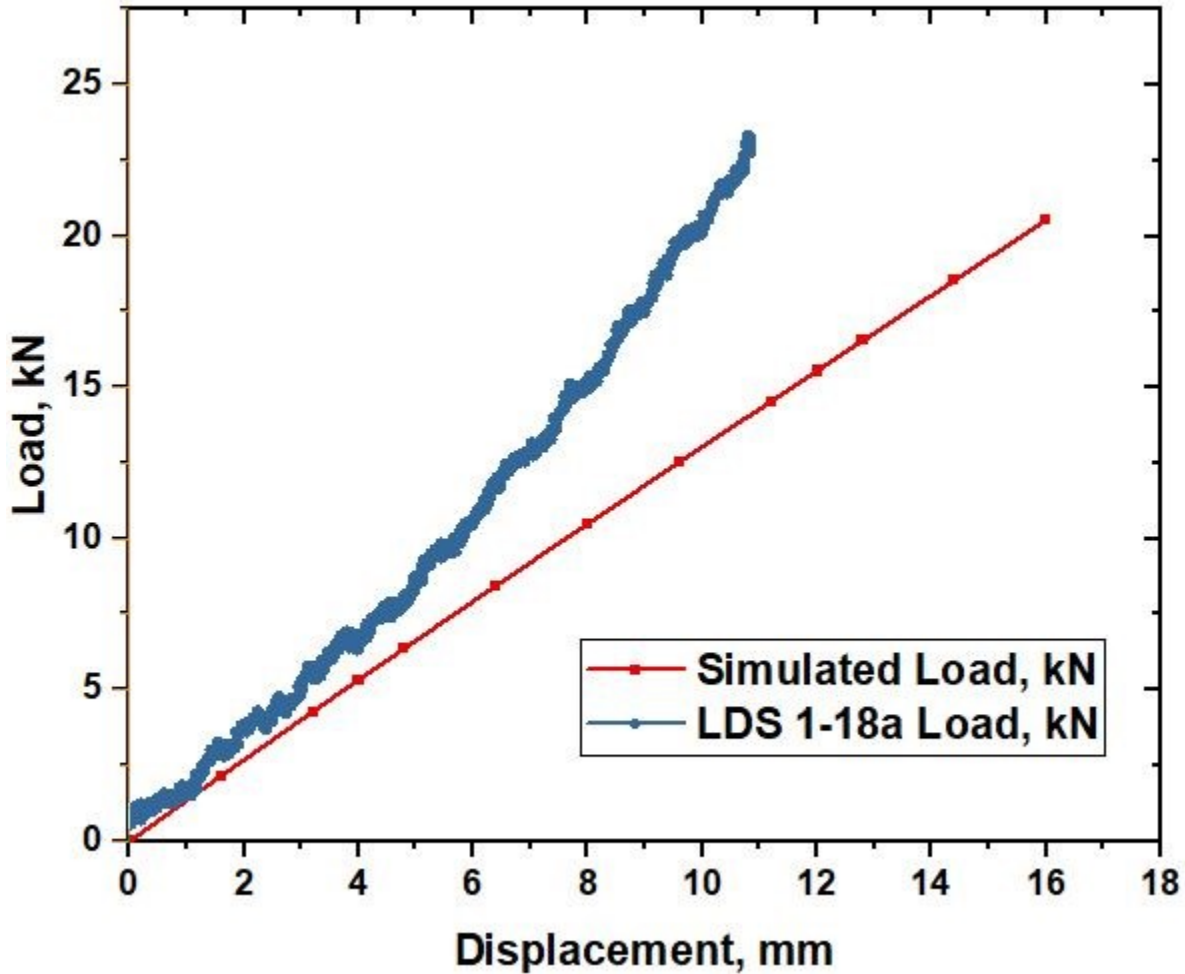
Figure 6.10:Comparison of the simulation with compression test result of the "1-18,9712k31" spring

6.8. Recommendations

This paper proposes a new simplified mechanical analysis with simulation results to emulate the force-displacement relationship of Belleville springs as a vibrational element of LDS-pVARD. For simulation, this calculation is designed for Belleville springs without machined contact surfaces. Furthermore, the calculation does not consider the effect of friction, whose effect is noticed in compression results in Figure *6.9* and Figure *6.10*. But for the mechanical testing, the friction factor is dominant and increases with the increase of the contact area between the springs as the load increases.

The annular ring of the empty trimmed cone can be able to absorb external axial forces counteracting against each other. The spring section is generally rectangular. Large size springs (t> 6 mm) are made with machined contact flats. Belleville springs are laid out for higher loads of low displacements that are used individually or in sets. While using springs in a set, the effects of friction need to be considered. The set contains 3 - 5% loading per friction level therefore the working load must be increased. The working load must then be increased forcefully [77], [79].

From Figure *6.9* and Figure *6.10*, the theory of the effect of the friction factor is approved. Frictional losses in the springs are dependent on the type of spring stacking. When the number of springs stacked in parallel is less, edge friction accounts for most of the frictional loss. In addition, there is friction loss due to geomechanics loading frame operations with the springs. Similarly, as observed from Figure *6.9* and Figure *6.10*, frictional loss is also dependent on the spring load or spring deflection. For the high load and standard Belleville springs, frictional loss increases proportionally with spring deflection. So, if the friction factor can be calibrated, then the accuracy of this approach goes toward improving or validating its accuracy. Therefore, how to control friction loss should be examined in future research.

6.9. Conclusion

The results from the simulation show that the design parameters of the LDS-pVARD tool fulfill the safety requirements with minimum FOS of 5.

The scope of this work is limited to the mechanical design and static analysis of the LDS-pVARD tool. It does not include the tasks related to the fatigue analysis, the design of experiment, selection of the spring stacking and/or the calibration of tool compliance, which will be considered in future research. However, some mechanical compression tests on various scenarios of spring stacking have been conducted and analyzed in this paper. Fatigue analysis of pVARD as well as drill string components will be involved in future studies.

The comparative analysis of the compression results of pVARD springs obtained from Geomechanics loading frame and the simulation demonstrated the need for determining the friction

factor. Such friction factor is key to producing the pVARD fundamentals and therefore, make drilling data (planned) more representative.

Chapter 7:   Investigation of the Hysteresis Effect on the LDS-pVARD Springs

7.1. Introduction

In this section, tests were conducted to determine the Hysteresis effect on the LDS Belleville springs with experimental load vs deflection cyclic analysis. The friction separates the load during loading and unloading of the coned disc spring, resulting in a hysteresis cycle. Estimation of the effects of hysteresis will be important to define the dynamic properties of disc springs as friction dissipation is related to both reduction and fretting phenomena [74]. Hysteresis is the difference between the strain energy required to generate a given stress in a material, and the material's elastic energy at that stress. This energy is dissipated as internal friction in a material during one cycle of testing (loading and unloading). Mechanical test data is plotted on the stress vs strain curve, while a component displaying hysteresis shows a path during the loading phase and a separate path during the unloading phase. The two pathways are distinctly separated due to the hysteresis loss, the portion between the curves represents the energy dissipation [80], [81].

The deflection of the spring is affected by the friction that influences the spring loads. It is added when loading the spring and subtracted when unloading the spring. There is a hysteresis loop between actual loading and unloading. Schnorr [77] reported influence of friction on spring force for various parallel stacking for cycling (+ loading, – unloading) characterization [79], [77].

The amount of friction depends on many factors: geometric, material, assembly, load dependant factors. In disc spring stacks particularly with parallel units, friction must be considered. Sliding friction occurs on the adjacent, moving surface (radial walls) of the disc spring. As a result, the spring force increases on loading and decreases on unloading, creating a hysteresis effect. This feature can be applied to shock-absorbing or vibrating systems to keep them damping. The hysteresis effect is a parallel function of the number of disc springs. In such cases, single stacked disc springs are preferred and good lubrication is essential. Schnorr [77] also showed the influence of lubrication on the friction. The choice of the lubricant is often influenced by the friction type. In addition to reducing friction, it can also prevent another spring flash when stacked in parallel. Lubricants such as: oil, grease, slip paints etc. are selected depending on the use or purposes. Grease is most compatible if re-lubrication is difficult or cannot be regularized [74], [82], [83] , [84].

7.1.1. Selection of the Spring

A group of the lab scale LDS-pVARD commercial Belleville springs with 1" ID and 2" OD with part reference number 9712K31 (Table 2.1) was selected for the experiment.

7.1.2. Selection of the Lubrication

Commercial grade-2 type grease was used as lubricant (Figure 7.1) in the spring configurations for cyclic operation. Grade 2 has stiffness like peanut butter [83].

Figure 7.1: Commercial grease using 1-18 parallel springs configuration.

7.2. Experimental Apparatus

Displacement Transducer, Geomechanics Loading Frame, commercial grade-2 type Grease.

7.3. Design of Experiment

The number of spring configurations were selected for the tests. It was selected by trial and error method. The details of the test matrix for the experiments are given in Table 7.1.

Table 7.1: Matrix of the LDS-pVARD springs load-displacement cyclic test

No of Parallel Spring in a stack	No of Series	Lubrication	Operation Cycle
10	1	No	Single
14	1	No	Single
16	1	No	Single
18	1	No	Single
18	1	Grease	Single
10	1	No	Multi
18	1	No	Multi
18	1	Grease	Multi

7.4. Experimental Process and Methodology

The Experiments were conducted using commercial geomechanics loading frames with a compression tool set described in Figure 7.2. The maximum loading capacity of this frame is 490 kN. This loading frame is a manually operated machine, so the loading rate is not regulated constantly. The equations proposed by Almen-Laszlo [57] have been used to govern the load-deflation relationship of the Belville Spring stack.
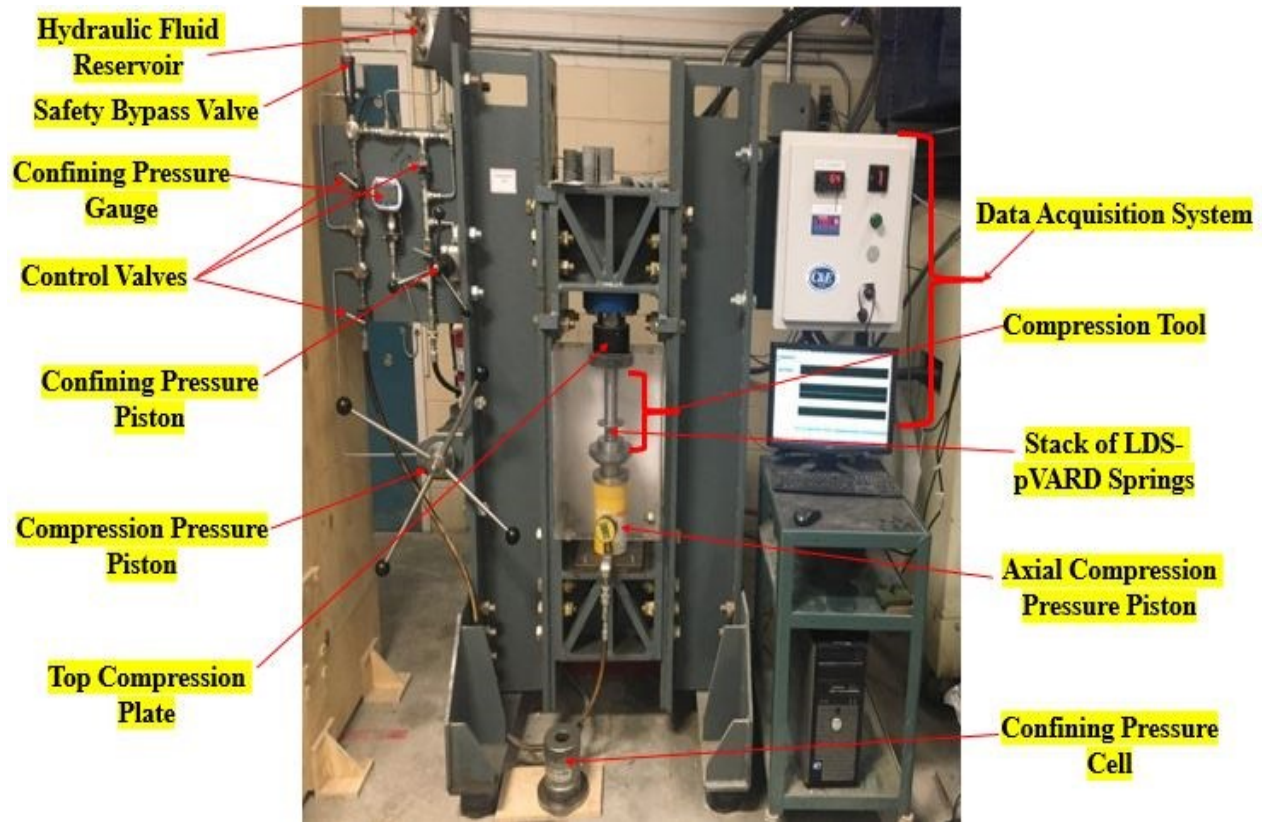
Figure 7.2: Load-Displacement Cyclic test on LDS-Spring configuration

The friction factor and hysteresis effect are highly influenced using parallel stacked springs and lubrication [74], [82]. Determined the LDS-pVARD spring hysteresis through the following steps: Place the lower platen on the base or actuator rod of the loading device. Swab the spring specimen and the upper and lower platens. Start the axial load until determined LDS-pVARD spring maximum flat load 22 kN. Then, calculate the compressive stress and stress of the test spring specimen from the compressive load-displacement data using the following equations 7.1 and 7.2.

$$Normal\ Stress\ (\sigma) = \frac{P_{max}}{A} \dots\dots\dots\dots\dots\dots7.1$$

$$Normal\ Strain\ (\epsilon) = \frac{(L - L_0)}{L_0} \dots\dots\dots\dots\dots\dots7.2$$

Where

σ = Normal Stress (MPa)

ϵ = Normal Strain (Unit Less)

P_{max} = Maximum load, (kN)

A= Cross sectional area

L_0= The original length

L= Extension length

7.5. Result and Discussion

Cyclic experimental analysis was conducted, and the results are consistently discussed.

7.5.1. Number of Parallel Spring

7.5.1.1. Single Cycle Operation

Figure 7.3 shows the load vs time relationship for four various parallel spring configurations: 1-10;1-14;1-16;1-18 [10 series in a single parallel configuration: 1-10; 14 series in a single parallel configuration: 1-14; 16 series in a single parallel configuration: 1-16; 18 series in a single parallel configuration: 1-18].
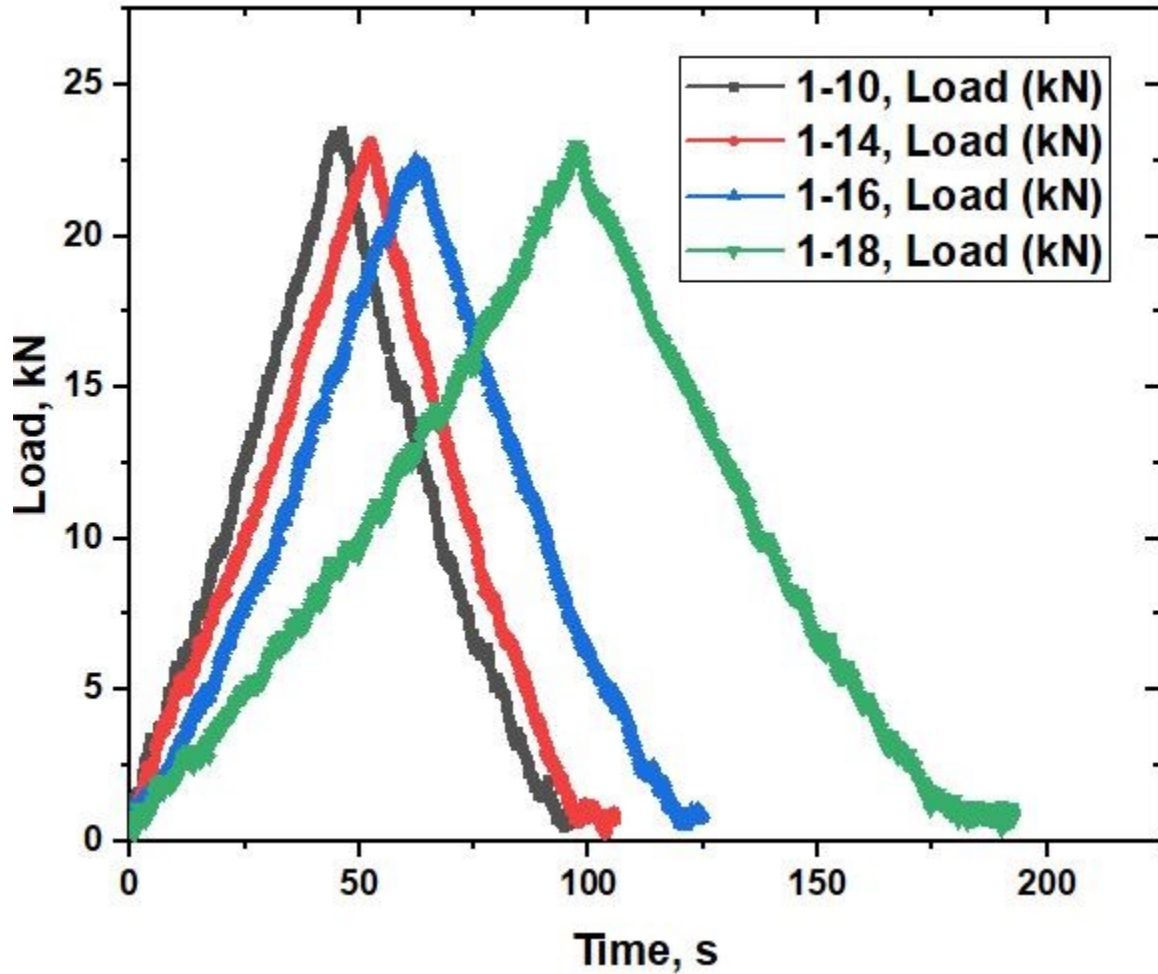
Figure 7.3: Load vs Time graph of single cycle operations for various parallel spring configuration

Figure 7.4 shows the principal load variations for four various parallel spring configurations. This figure also demonstrates the influence of the friction on the compression load for four various spring stacks. Figure 7.3 and Figure 7.4 indicate the same load for each single operation. According to the Almen-Laszlo [57] ,where discs are stacked in parallel, the total load capacity of the stack equals the load for one disc multiplied by the number of discs. But the total travel of the stack equals the travel of just one disc. The load-deflection curves are regressive to nearly linear. Parallel stacks are often used to provide friction damping in dynamic load applications [85]. Figure 7.4 shows the friction is significantly increased in proportion to the number of the parallel springs
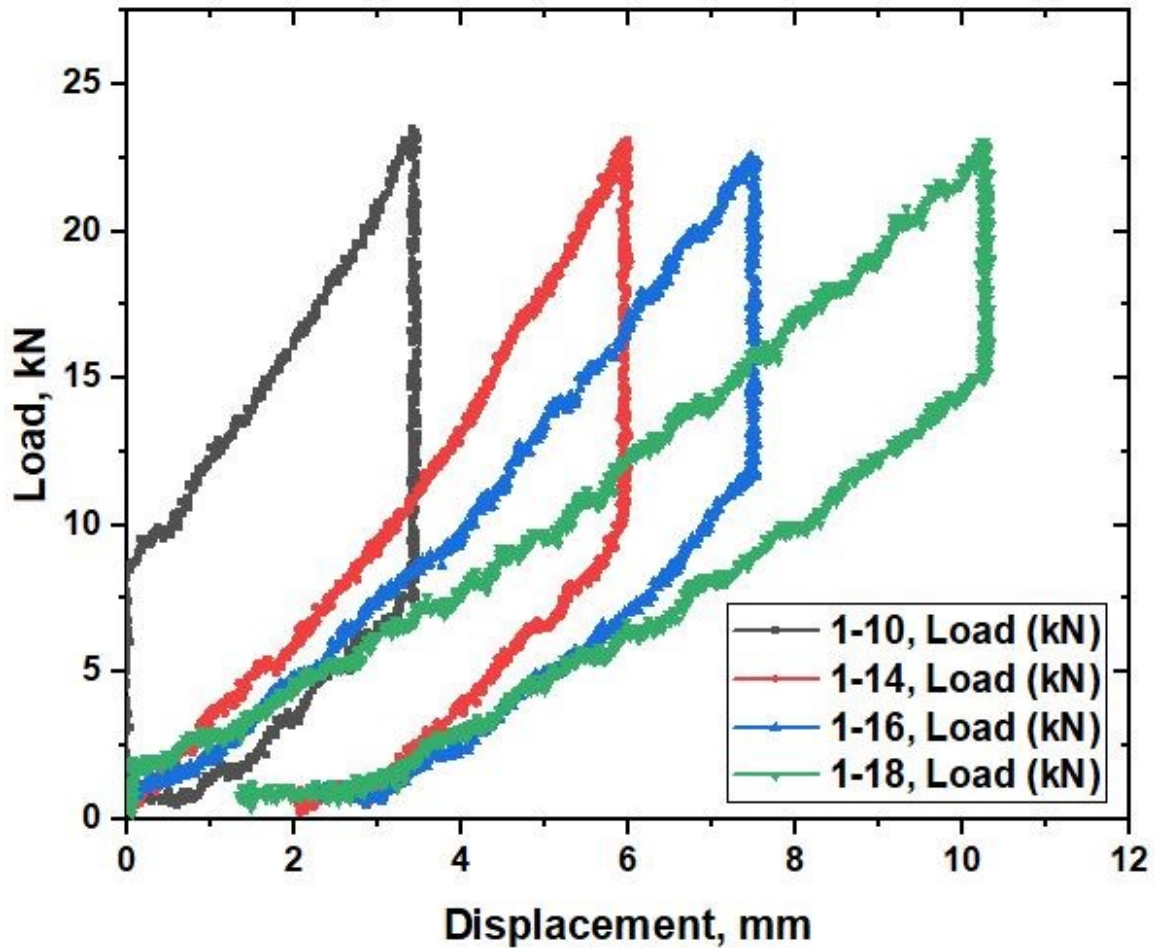
Figure 7.4: Influence of friction on spring force for four various parallel stacking for single-cycle operation

The effect of the number of parallel springs on the hysteresis effect is shown in Figure 7.5. The figure indicates that the height number of the parallel spring stacking produces the maximum friction. It is highlighted that the hysteresis effect of 10 parallel springs is more than 18 of the parallel springs.
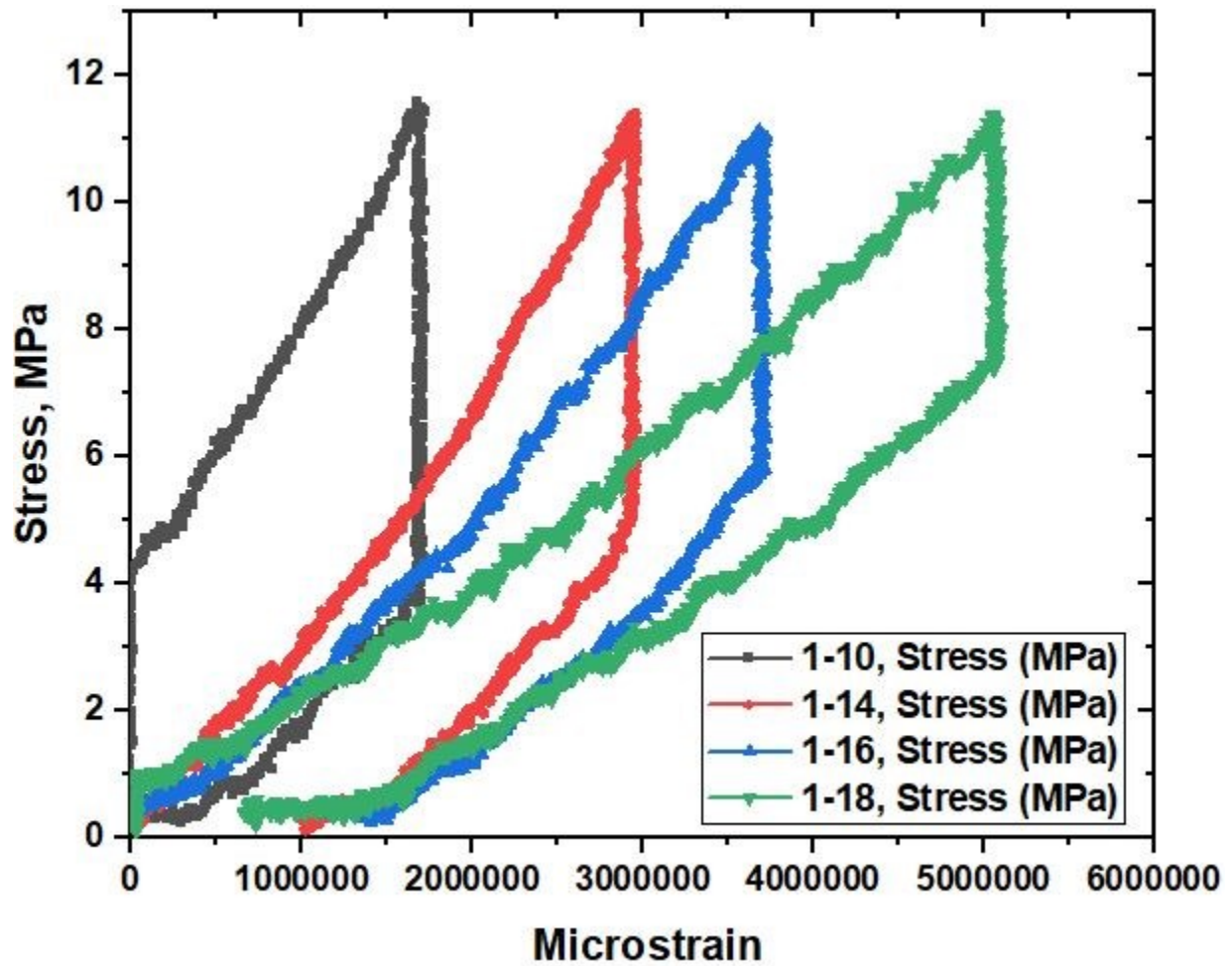
Figure 7.5: Comparison of the hysteresis effect among the various number of parallel spring configurations for single cycle operation

7.5.1.2.   Multi Cycle Operation

The lowest and highest spring stack out of four spring stacks were selected for multi-cycle operation. Figure 7.6 shows load vs time curve for 1-10 and 1-18 parallel spring configurations.
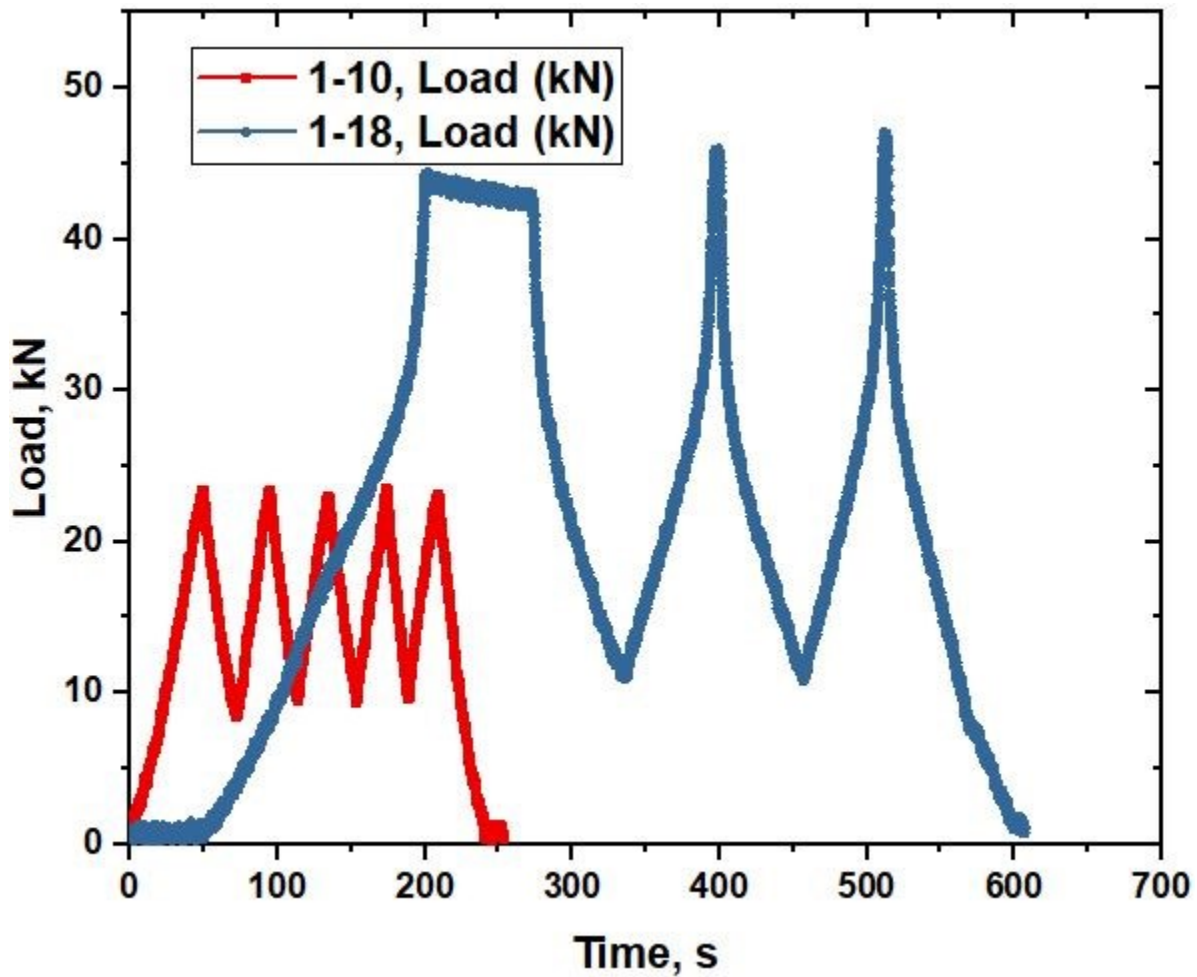
Figure 7.6: Load vs Time relationship of multi-cycle operation for 1-10 and 1-18 parallel spring configurations

Figure 7.7 shows the load variations for 1-10 and 1-18 spring configurations that indicates the influence of the friction on force for parallel spring stacking for multi-cyclic operation. It also shows that the friction is significantly increased in proportion to the number of the parallel springs for multi-cycle operation. Almen-Laszlo's equation *[57]* shows that the number of the disc springs are stacked in parallel standing the load, the deflection of the whole stack is equal to that of one disc spring divided by the number of springs, to have the same deflection of a single disc spring the load to apply has to be the times that of a single disc spring *[84]*. In addition, the sliding displacements on the disc surfaces can also be evaluated as a function of the deflection. Here, coned disc springs stacked in parallel come into contact at only the upper and lower parts of the surface because the bending moment has an effect *[74]*.
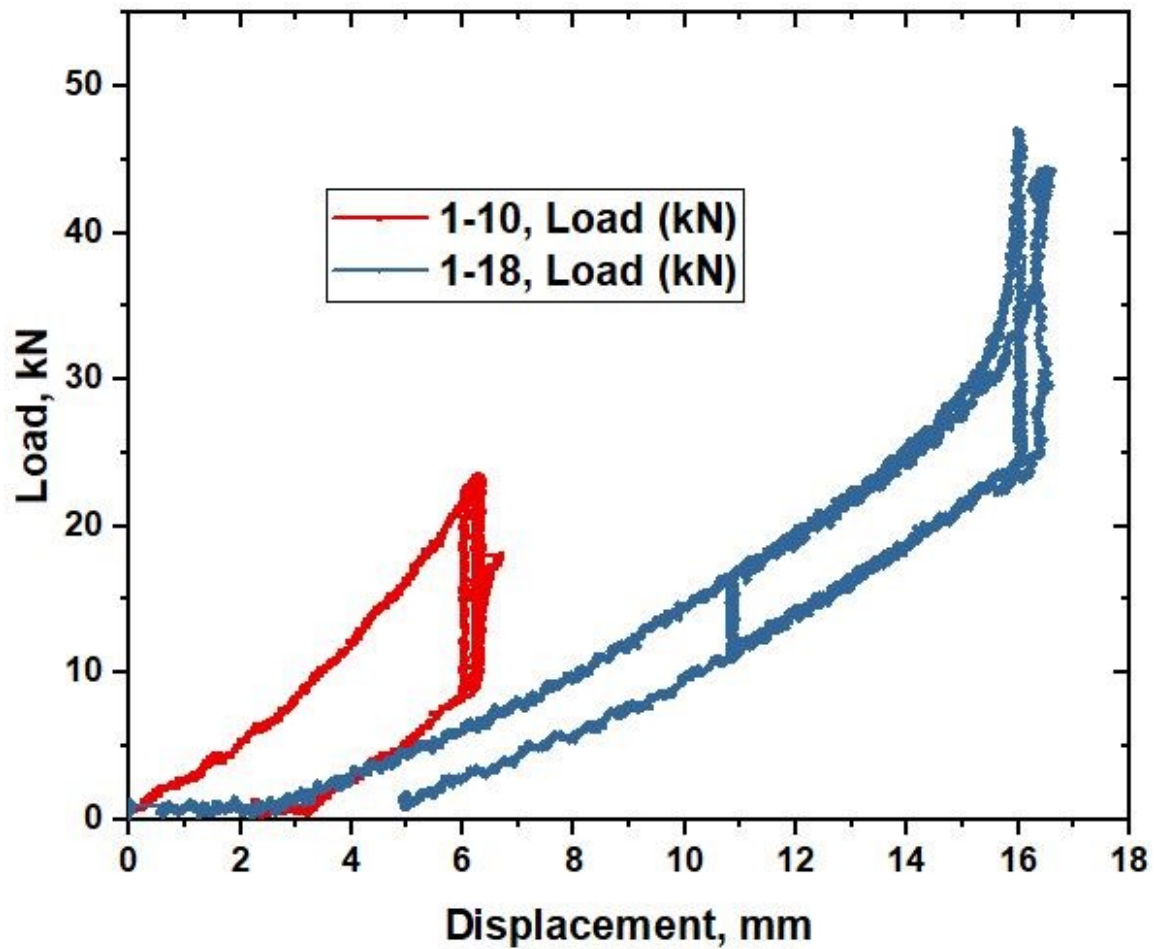
Figure 7.7: Friction impact on spring force for 1-10 and 1-18 spring stacking for multi-cycle operation

Figure 7.8 illustrates that the 1-10 spring stacking produces the maximum hysteresis effect than 1-18 spring stacking. This supports that the friction is significantly increased in proportion to the number of parallel springs.
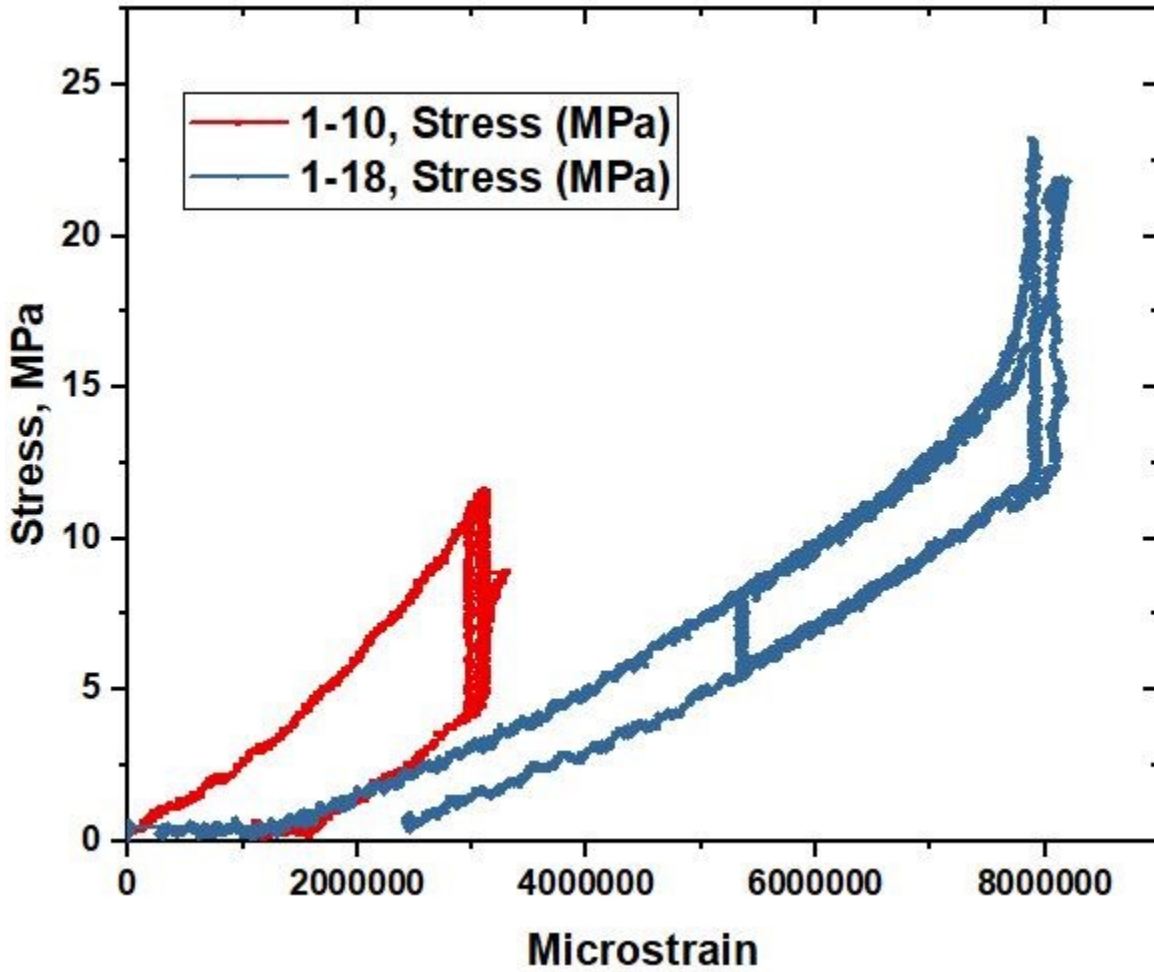
Figure 7.8: Hysteresis effect between the 1-10 and 1-18 spring configurations for multi-cycle operation

7.5.2. Lubrication Impact

When the lubricant is added to the spring sets it spreads between the two surfaces flushing with each other and removes the irregularities present on the surface, creating a thin layer between the contact surfaces. As a result, the contact between the two hard surfaces is replaced by the lubricant layer because it significantly reduces the frictional strength [86].

7.5.2.1.   Single Cycle Operation

Since the 1-18 spring stacking indicated the highest friction between the spring stacks, single cyclic testing was performed using lubricants in this spring configuration. Figure 7.9 shows the load vs. time relationship for the 1-18 spring configuration without lubrication and with lubrication.

Figure 7.9: Load vs Time graph of 1-18 spring configurations between without lubrication and with lubrication for single-cycle operation

The larger variation of Figure 7.10 shows the effect of lubrication on friction for the 1-18 spring configuration. It demonstrates that the friction is significantly reduced after the use of lubrication for single-cycle operation.
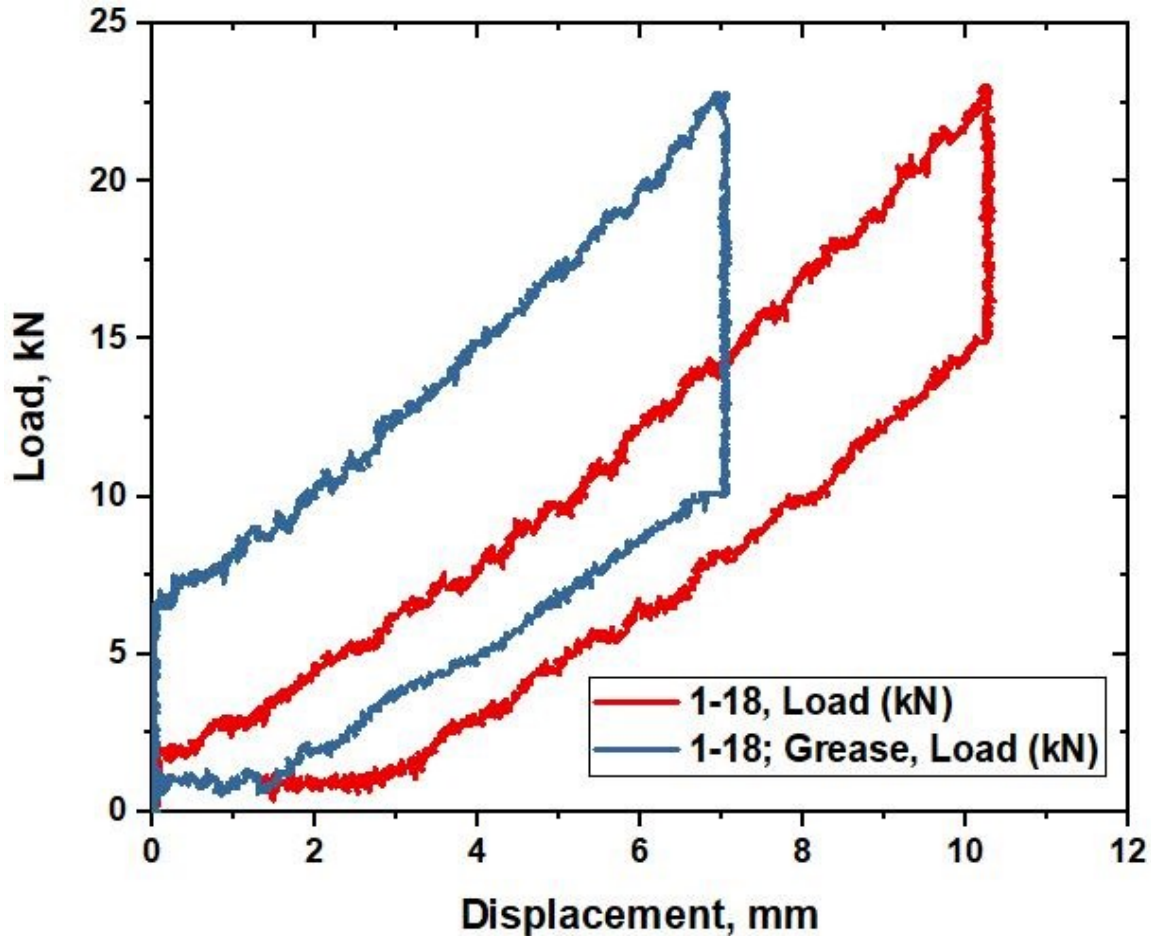
Figure 7.10:The effect of lubrication on the friction of the 1-18 spring stack for single-cycle operation

The potential influence of the lubrication on the hysteresis effect shows in the Figure 7.11. This indicates that the friction is significantly reduced after the use of grease as lubrication in the 1-18 spring stacks compared to not using lubrication.
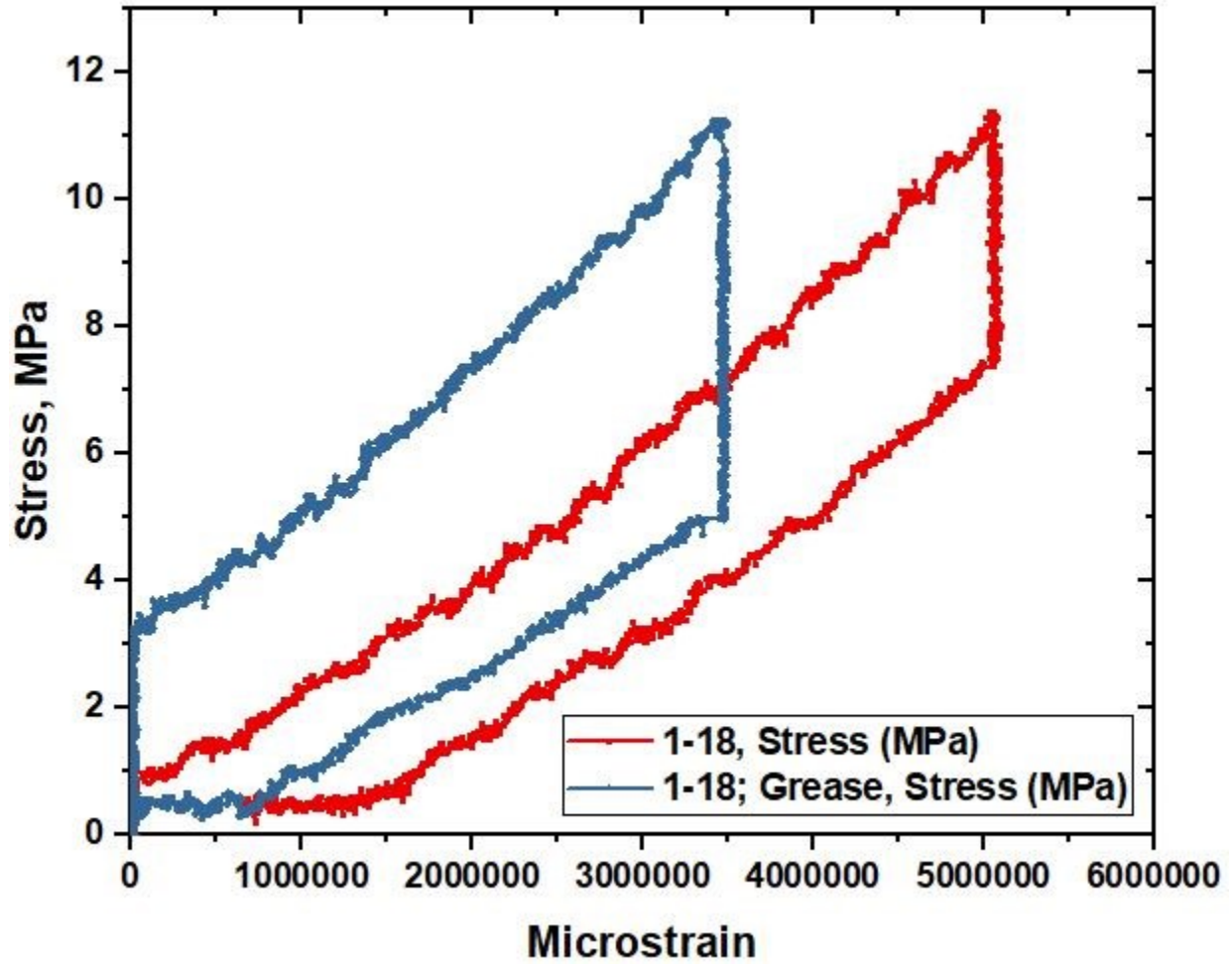
Figure 7.11:The influence of lubrication on the hysteresis effect of 1-18 parallel spring configuration for single-cycle operation

7.5.2.2.   Multi Cycle Operation

Figure 7.12 shows the load vs time graph for the 1-18 spring configuration between without lubrication and with lubrication.
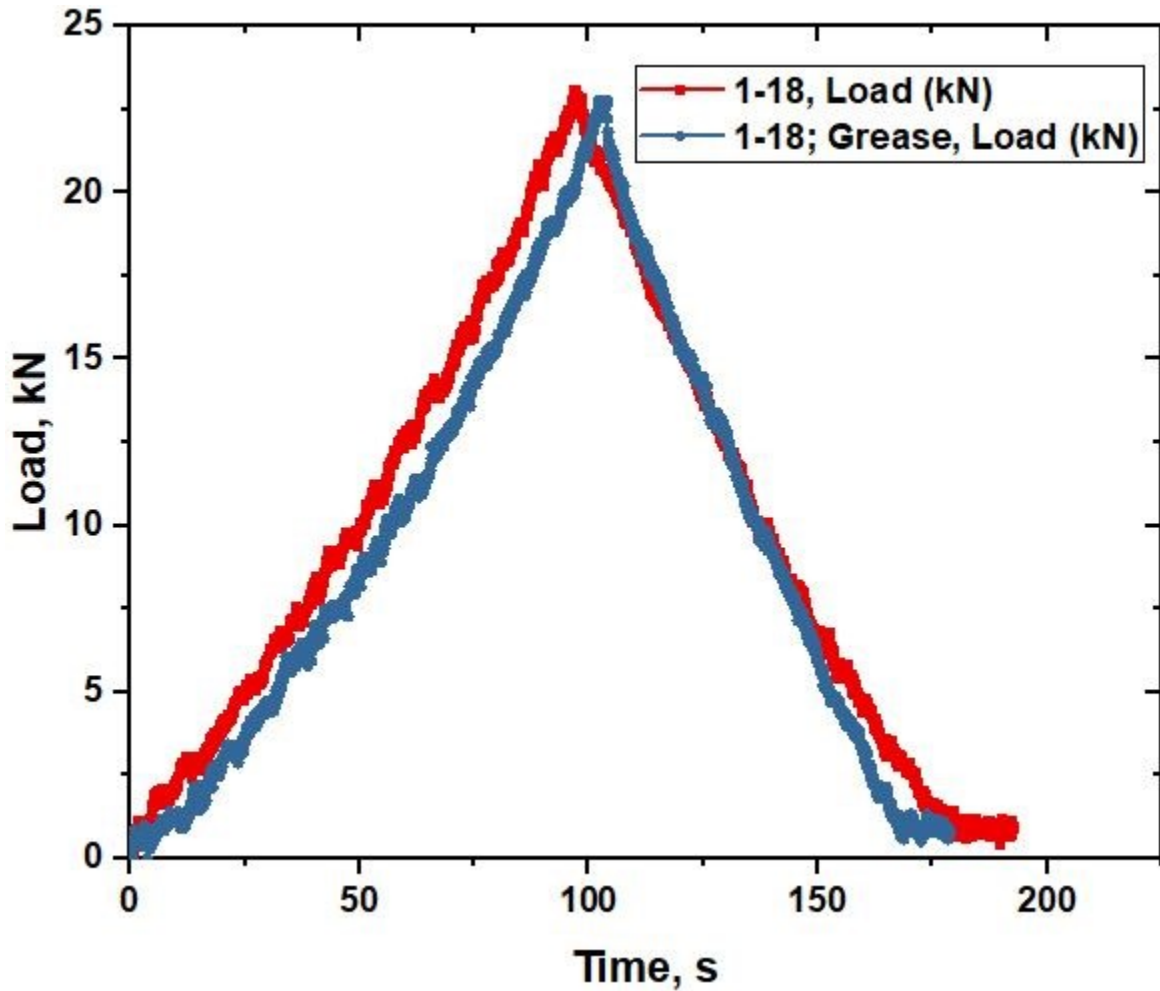
Figure 7.12: Load vs Time relationship of 1-18 spring configurations between without lubrication and with lubrication for multi-cycle operation

Figure 7.13 demonstrates load vs displacement relationship for the 1-18 parallel spring configurations using lubrication and no lubrication for multi-cycle operations. Figure 7.13 and Figure 7.12 both show the same load for each multi-cycle operation.
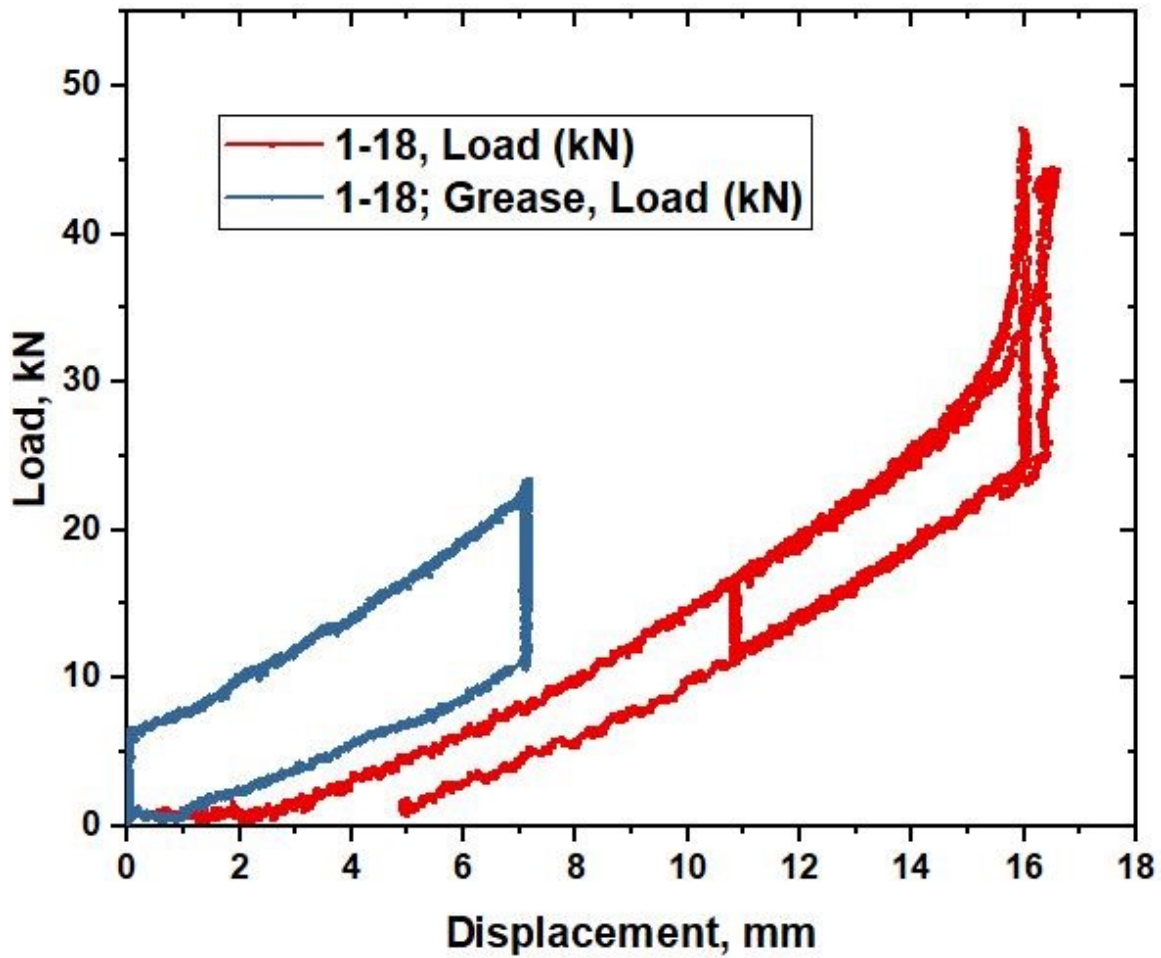
Figure 7.13: Impact of lubrication on the hysteresis effect of 1-18 parallel spring configuration for multi-cycle operation

Figure 7.14 illustrates the effects of hysteresis without lubrication and lubrication on the 1-18 parallel spring stacks. This indicates that the 1-18 spring stacks with grease increases the hysteresis effect compared to the same stacking without grease.
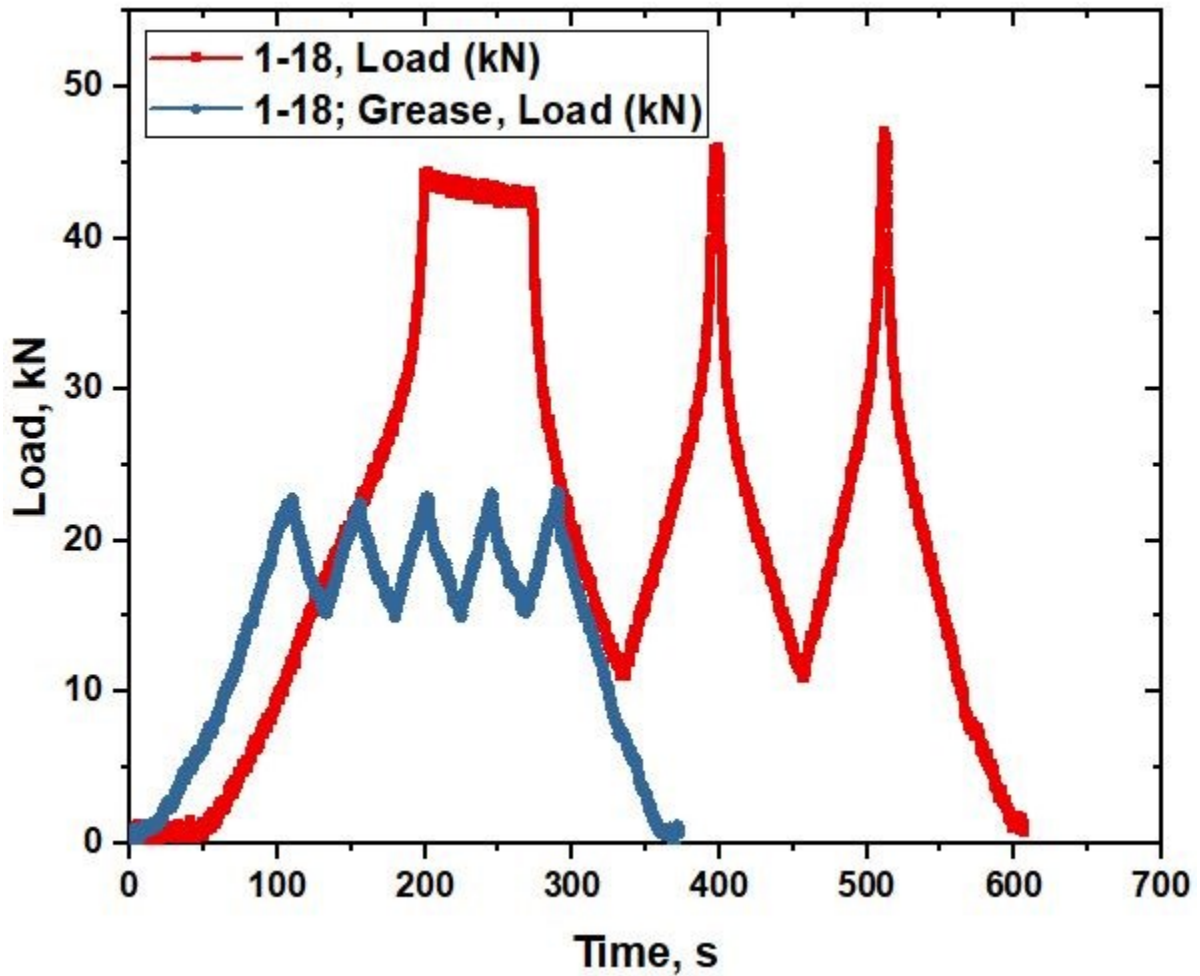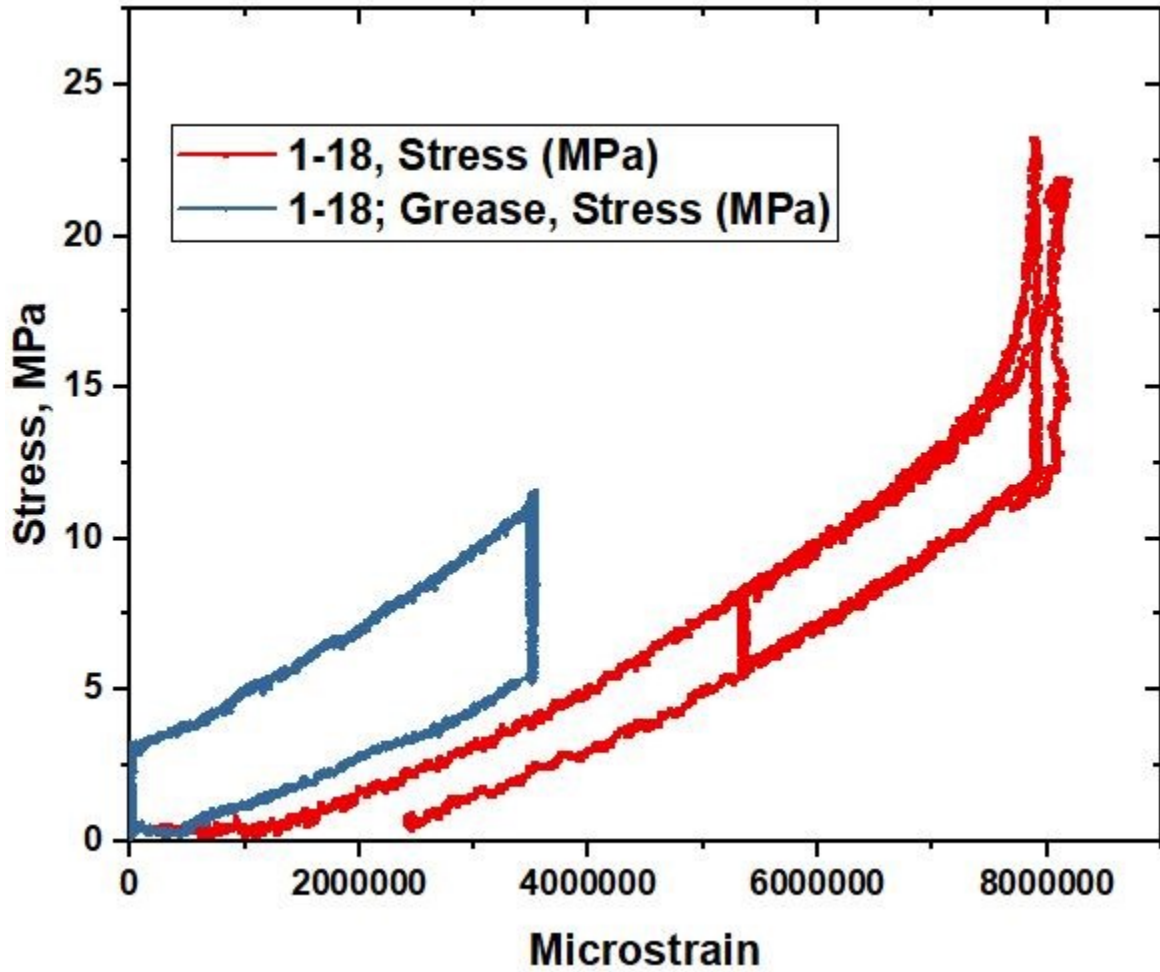
Figure 7.14: Hysteresis effect of the 1-18 spring configurations between without lubrication and with lubrication for multi-cycle operation

7.6. Conclusion

The effect of hysteresis is induced by increasing friction. The maximum friction with parallel stacking is between the springs that increase in proportion to the number of parallel springs that proved the Almen-Laszlo's [57] equations. Thus, the force on the loading side is higher than the actual force and lower than the unloading side. However, using suitable lubrication maximizes the hysteresis effect. Furthermore, this study is also introducing as a fundamental guideline procedure for the hysteresis effect evaluation of the LDS-pVARD spring that can be used as a basis for further research.

Chapter 8: Investigation of Drilling Performance in Core Bit Drilling using passive-Vibration Assisted Rotary Drilling (p-VARD) Technology

This chapter is based on the conference paper "Investigation of Drilling Performance in Core Bit Drilling using passive-Vibration Assisted Rotary Drilling (p-VARD) Technology" authored by Md. Shaheen Shah, Yingjian Xiao, Syed Imtiaz and Stephen Butt, and presented at the Geo St. John's 2019 the Canadian Geotechnical Conference, St. John's, Newfoundland, Canada, September 29 – October 2, 2019.

8.1. Co-authorship Statement

The contributions of this collaborative work are described in the following six parts. 1) Identification of research topic is collaborative between all co-authors. 2) Design of experiments are contributed by Md. Shaheen Shah, Dr. Yingjian Xiao and the main supervisor Dr. Stephen Butt. 3) Md. Shaheen Shah and Dr. Yingjian Xiao is responsible of conducting drilling experiments. 4) Data analysis and discussion of results is a collaborative work contributed by all co-authors, 5) Manuscript preparation is mainly contributed by Md. Shaheen Shah, 6) Dr. Yingjian Xiao, Dr. Syed Imtiaz and Dr. Stephen Butt provided technical knowledge and reviewed the manuscript.

8.2. Abstract

Diamond core drilling is the primary means of exploration drilling for mineral deposits and in Canada is stipulated to the meet legislative requirements for mineral deposit evaluation. However, it is the slowest and thus most expensive form of drilling in the mineral industry, and economic analysis has shown that increase in drilling Rate of Penetration (ROP) can have a significant impact on drilling costs and overall levels of exploration. The passive-Vibration Assisted Rotary Drilling (p-VARD) technology was developed to improve the ROP for drilling with the roller cone and PDC drill bits used in the oil and gas industry, and the purpose of this investigation was to evaluate the potential for p-VARD to improve ROP for natural diamond coring bit. In the Drilling Technology Laboratory (DTL) of Memorial University of Newfoundland (MUN), a Small Drilling Simulator (SDS) was used to conduct experiments using 26 mm diameter coring bit drilled into a 168.4 MPa hard rock material. Drill-off tests were conducted by applying a series of weight-on-bit (WOB) and evaluating the drilling ROP at various p-VARD tool configurations and comparing these with

drilling without the p-VARD technology. Rate-of-penetration (ROP) was well correlated with WOB and drill string compliance. From results, an increase of ROP was observed using two p-VARD configurations, with a maximum increase of 28% using p-VARD configuration compared to drilling without p-VARD. This study demonstrates the potential of decreasing the time for core drilling in hard rock using p-VARD technology.

8.3. Introduction

Drilling activities at the depth are often affected by the lower rate of penetration (ROP). In many cases, similar rocks can be drilled at a higher ROP under atmospheric conditions. The most important distinction among drilling situations at surface and depth are the stresses acting on the rock, which embody the pore pressure, borehole pressure and the geostatic overburden pressure [87]. Khorshidian et al. [52] investigated the effect of the stresses on drilling response. The Drilling Technology Laboratory (DTL) of Memorial University of Newfoundland (MUN) introduces the technology that provides higher penetration rates and greater monetary value in drilling by utilizing Vibration Assisted Rotary Drilling (VARD).

During the drilling process, vibrations are typically undesirable and exertions are done to mitigate them. There are three types of vibrations exemplary; axial vibration, torsional vibration and lateral vibration that are linked to whirl, stick-slip and non-uniform dynamic loading, which causes damage to bits and down-hole equipment [35]. Institute of Technical Mechanics, National Academy of Sciences of Ukraine experimented devices that work on the principle of excavation which resulted in two to three times of increase in ROP [88]. Alali and Barton [89] studied an Axial Oscillation Generator Tool (AOGT) which was observed to significantly reduces stick-slip. Forster [90] developed a small-scale vibration test-rig to simulate stick-slip and study stick slip reduction methods which effects in an enhancement in ROP and better Mechanical Specific Energy (MSE). Using a coring bit, Li et al. [47] experimental results showed that the combined effect of vibrations and rotation increases the rate of penetration. Babatunde et al. [49] investigated the influence of vibration frequency on penetration rates using natural diamond drag bits that consequence the VARD improved the penetration rates. To further study the effect of vibrations on drilling performance, a lab scale p-VARD tool was designed and tested. Rana et al. [35] used the SDS setup using p-VARD tool to enhance the drilling ROP approximately 50% for fine-grained concrete

sample using Poly-crystalline Diamond Compact (PDC) drill bits by modulating the rock-bit interactions.

In this paper, the p-VARD technology is incorporated into drilling tests using a coring bit aiming to study the drilling performance or ROP on hard rock drilling.

8.4. Experimental Equipment and Procedure

8.4.1. Drill-off Tests

Drill-off Tests (DOTs) are the drilling experiments where drilling parameters are systematically varied and the impact on ROP is measured (Xiao et al. [55]). Figure *8.1* shows the setup for DOT using a laboratory drilling setup, i.e. Small Drilling Simulator (SDS) which was used by previous researchers and described in detail by Khorshidian et al. [52]. A suspended weight is applied through a wheel which transmits the torque to drive the rig top move down. In this way, a Weight on Bit (WOB) is obtained and applied on the drill bit which makes the drilling penetration process possible. Drilling parameters include WOB, rotary speed, rock strength, bit type, flow rate, and drill string compliance, p-VARD tool etc. Generally, drilling parameters are confirmed during this drilling process except WOB. A series of WOB is solely applied which correspondingly lead to a series of ROP. The "Perfect-Cleaning Theory" describes this relationship between ROP and WOB, rotary speed and rock strength for roller cone bit [5]. A maximum ROP is then found as the "founder point", which describes the best drilling performance under the specific conditions.
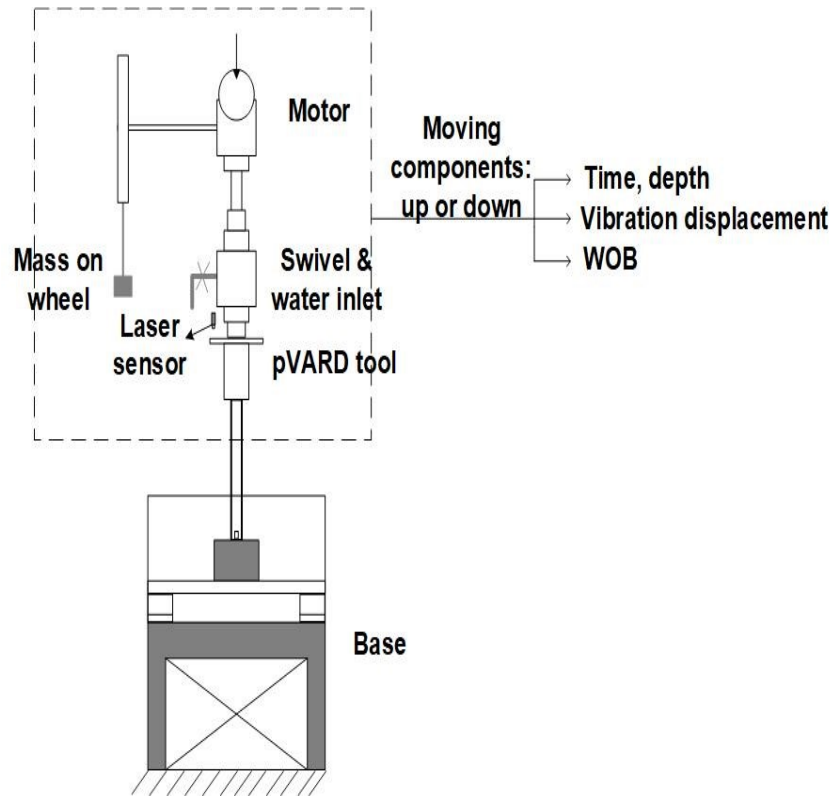
Figure 8.1:Schematic of the SDS with p-VARD tool

In this experiment, a 26 mm Outside Diameter of coring bit is utilized. Rotary speed is set at 300 Revolutions Per Minute (RPM). Drilling parameters and the process are also shown in Figure *8.1*.

8.4.2. Drill String Compliance

The p-VARD tool has been schemed that turns to advantages of the bit-rock interactions and creates axial vibrations, providing full rotary speed and torque to the drill-bit. The tool has been designed to be continuously functioning above the drill bit. It has three segments: a compliant segment, a dampening segment, and a torque transmitting unit [35]. The compliance of the tool can be modified for various measurements.

Figure 8.2:Configurations of the Belleville spring setting in the p-VARD tool, with 8 sets of single parallel soft springs (left), 8 sets of single parallel stiffer springs (middle) and 4 sets of double parallel stiffer springs (right).

For this experiment, three configurations of p-VARD have been exercising including SinSoft, SinStiff and DouStiff that are given in *Figure 8.2*.

*T*able 8.1: Details of spring configurations

p-VARD configurations	Details	Stiffness (N/mm)
SinSoft	Single Soft-8 Springs+ 2 SPACERS	278.4
SinStiff	Single Stiff-8 Springs+ 2 SPACERS	840.7
DouStiff	Double Stiff-8 Springs+ 3 SPACERS	2438.6

Table *8.1* shows the details of three p-VARD settings. There are two types of Belleville springs: "soft" and "stiff", which indicate one is stronger to the other. For the SinSoft configuration there

are eight single-soft springs with two spacers. Similarly, SinStiff and DouStiff configurations are eight single-stiff springs with two spacers and eight double-stiff springs with three spacers, respectively. In every test, the p-VARD springs were lubricated with hydraulic oil decrease the friction effect. From the load-deflection tests under a loading machine, the stiffness of these configurations is respectively 278.4, 840.7 and 2438.6 N/mm.

8.4.3. Rock Specimen

A granite block specimen with dimensions of 304.8 mm (12 inches) x 304.8 mm (12 inches) x 203.2 mm (8 inches) was used, as shown in Figure *8.3*, to conduct DOT aiming to investigate the effective functionality of p-VARD tool. The Unconfined Compressive Strength (UCS) of this granite was obtained at 168.4 MPa from a standard strength test, following an ASTM standard (ASTM D7012-14e1) [60].
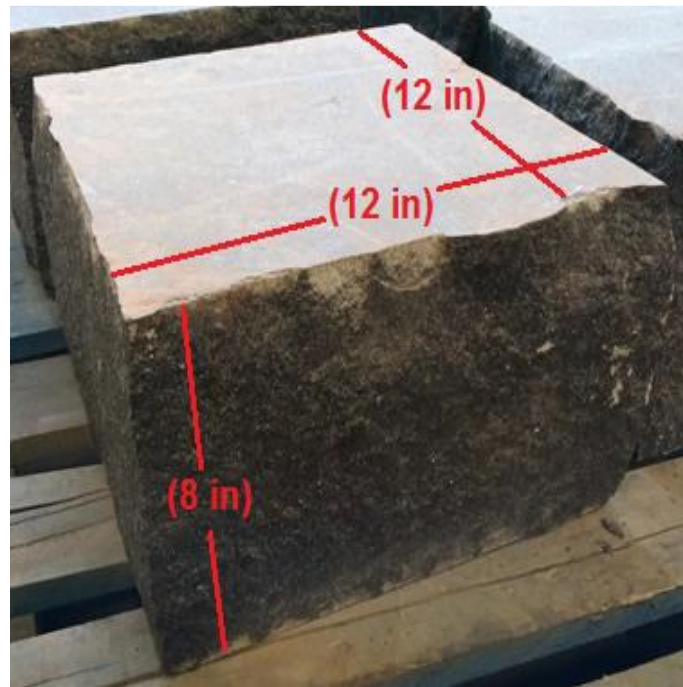

Figure 8.3:Granite block specimen (12 x 12 x 8 inches)

8.4.4. Pump off Tests

To figure out the parameters for DOT, the flow rate has to be determined. Generally, a Pump off Test (POT) is used to study the ROP with respect to flow rate. The optimized flow rate would

produce the maximum ROP. In DTL, POTs have been performed at a series of incremental flow rates with the drill string have varying compliance (i.e. Rigid and soft p-VARD configurations). Figure *8.4* shows the assembly of POT test results. The optimized flow rate is taken an average of 18.31 L/min for various drilling conditions.
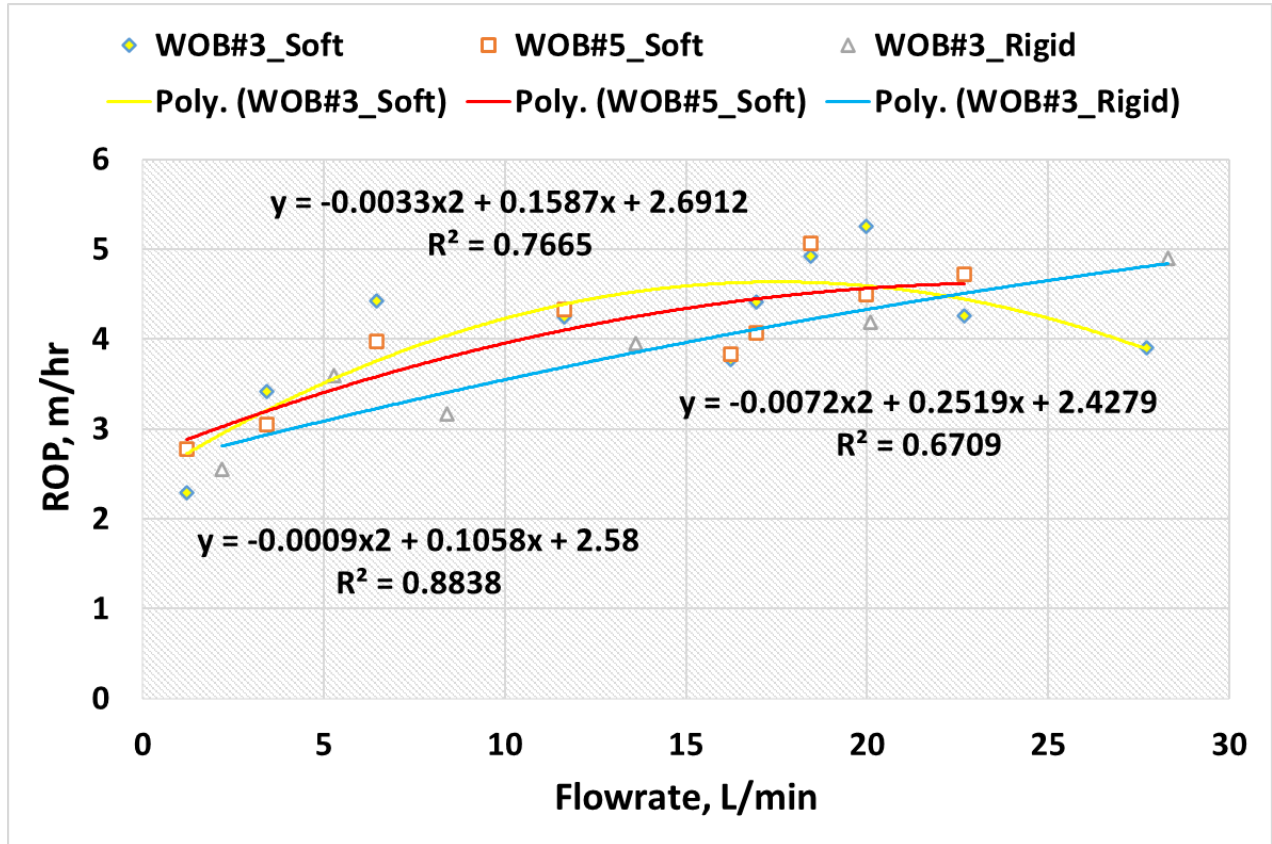

Figure 8.4:POT curves using different WOBs

8.5. Results and Discussions

8.5.1. Data Acquisition and Processing

There are four types of DOT with four different drill string compliance, i.e. rigid, SinSoft, SinStiff and DouStiff. For all tests, tap water is used with a constant flow rate of ~18.31 L/min and the rated rotary speed is set at 300 RPM. For each type of DOT, a series of incremental WOB are used. The test matrix is listed in Table *8.2*.

Figure *8.5*.a. provides sample data of a single DOT. Note that the bit depth is recorded versus time and the linear trend can be obtained with the slope as ROP. A laser sensor was used to detect and precisely record the relative motion of SDS and the drill string. For each revolution, six peaks of signal were recorded which corresponded to six machined groves. The rotary speed then can be calculated by picking the time difference for specific revolutions. For example, Figure *8.5*.b shows the laser sensor recordings of displacement peaks and two pulses at the same grove are picked for one revolution. Due to the difference in rotary speed for different runs of DOT, a normalized ROP is then obtained for the 300 RPM condition.
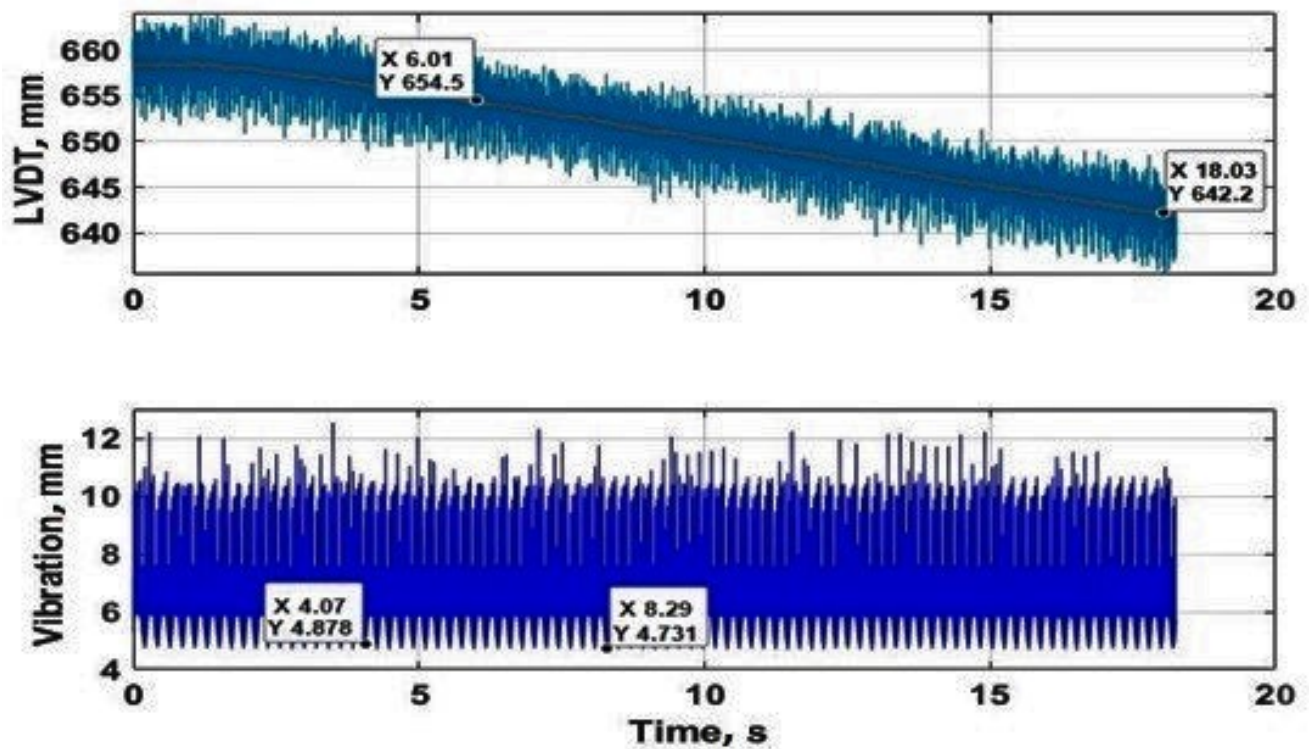

Figure 8.5:a. Demonstration of DOT data: a. bit depth versus time (top) ;b. drill string displacement versus time (bottom)

Table 8.2: Matrix for DOTs

Drill string setting	WOB (KN)	ROP (m/hr)	Rotary speed (RPM)	Normalized ROP (m/hr)
Rigid	0.842	2.99	288	3.11
	1.007	3.70	286	3.88
	1.172	3.32	279	3.57

	1.337	3.20	277	3.47
	1.502	3.52	272	3.88
	1.667	3.42	264	3.89
	1.832	3.41	264	3.87
	1.997	4.03	263	4.59
	2.162	3.94	259	4.57
	2.327	3.50	252	4.17
SinSoft	0.842	3.68	284	3.89
	1.007	4.63	282	4.93
	1.172	4.25	277	4.61
	1.502	4.57	269	5.10
	1.832	3.99	263	4.55
	1.997	4.18	263	4.77
	2.162	4.42	259	5.12
	2.237	3.59	259	4.17
SinSoft later	0.842	2.97	288	3.09
	1.172	4.01	281	4.29
	1.502	4.85	279	5.23
	1.832	5.31	272	5.85
	2.162	4.67	268	5.24
SinStiff	0.842	2.97	289	3.08
	1.007	3.73	285	3.93
	1.172	4.72	282	5.01
	1.337	4.84	277	5.25
	1.502	4.22	275	4.61
	1.667	3.81	270	4.24
	1.832	3.65	264	4.15
	1.997	3.59	261	4.13
	2.162	3.80	257	4.43
	2.327	5.01	257	5.84
DouStiff	0.842	2.99	287	3.13
	1.007	2.96	285	3.13
	1.172	3.67	276	3.98
	1.337	3.90	273	4.29
	1.667	3.54	269	3.95
	1.832	3.45	266	3.89
	1.997	3.54	263	4.04
	2.162	3.17	259	3.67
	2.327	3.40	260	3.92

8.5.2. Results

Figure 8.6 demonstrates the processed data in Table 8.2.
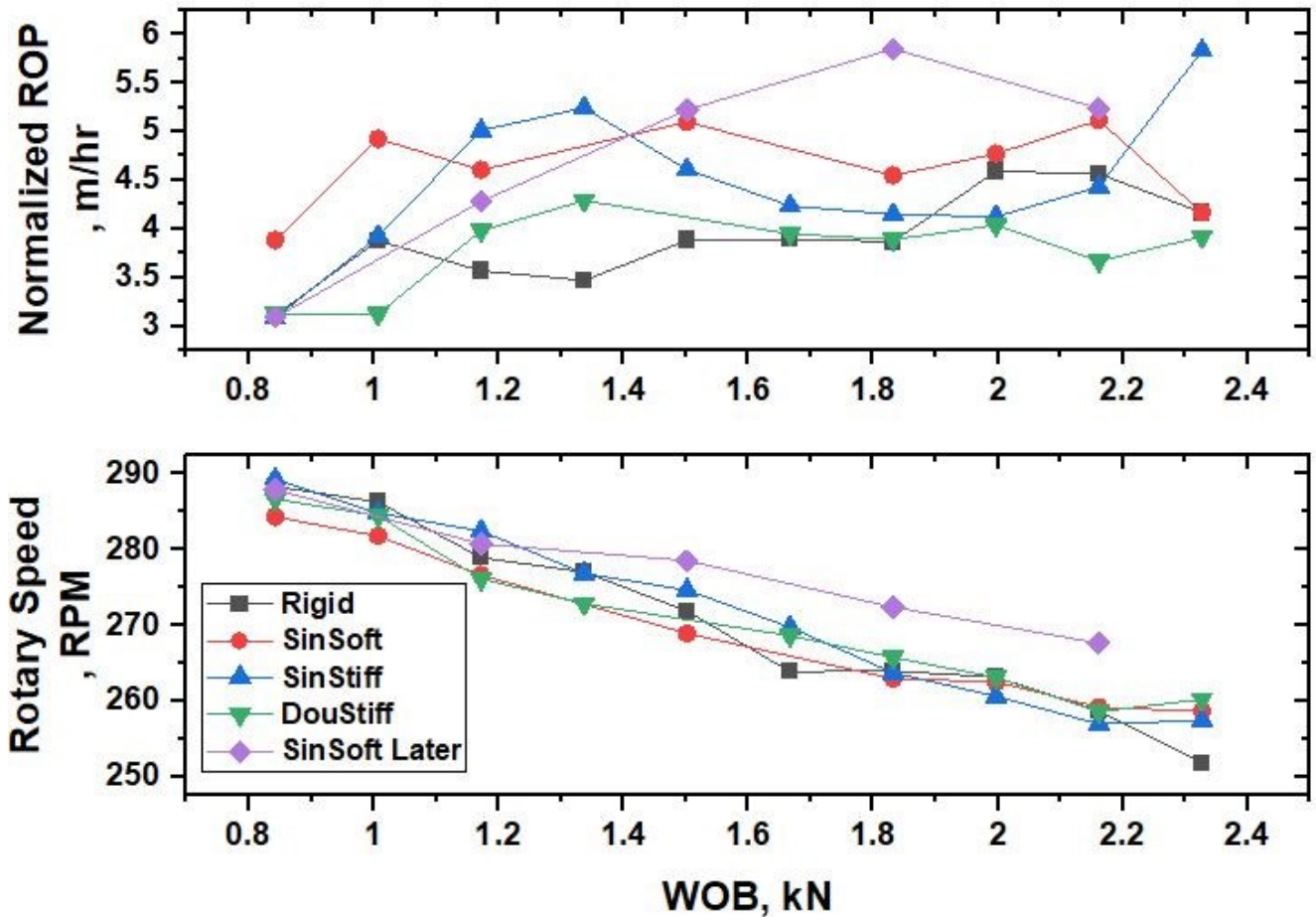

Figure 8.6:ROP versus WOB for various compliance settings

For rigid drilling, ROP generally increases with increasing WOB which complies with the Perfect-Cleaning Theory. The DouStiff provide no visual improvement on ROP. In the case of SinSoft configuration, the highest ROP is obtained compared to other configurations. A founder point is observed at high WOB. A 28% increase is obtained compared to rigid or conventional drilling. This indicates that the SinSoft of lowest stiffness works the best on hard rock drilling. The ROP from the SinStiff setting ranks in the middle compared to rigid and SinSoft situations. Finally, it is concluded that the ROP for p-VARD is found to be higher than the traditional drilling methods.

8.6. Conclusions

Drill string with different compliance has been achieved by using the p-VARD technology. The p-VARD technology is studied on drilling hard rock and results are novel compared to previously conducted experiments on soft rocks. A lower stiffness of drill string causes the highest ROP regarding drilling performance on hard rock drilling. This was contrary to what was found for soft rock.

Chapter 9:   Summary and Recommendation for Future Work

9.1.   Summary and Conclusion

The study began as part of a study by Memorial University of Newfoundland's Drilling Technology Laboratory (DTL) to expand the study of the effect of vibration on ROP. The study was started with the introduction of Vertical Assisted Rotary Drilling (VARD) technology and then was applied to passive Vertical Assist Rotary Drilling (pVARD). The first prototype pVARD laboratory scale was planned for use with the drilling scale. Promising results from the first prototype led to the development of a second prototype for use in field trials.

From the overall studies of the vibration effect on the ROP for both VARD and pVARD indicate the visual improvement on ROP. More recent research in DTL using different scale pVARD tools shows significant improvements for ROP. From lab and field experiments it is obvious that a pVARD tool can increase ROP which can only be noticed after applying a certain amount of WOB. An operational range has been reported for the effective use of the pVARD tool based on WOB.

Early in this thesis, the unconfined compressive and indirect tensile strength of the granite were measured by the mechanical loading frame following the ASTM standard. The ultimate compressive strength of the rock is the most significant property of the drilling that affects the rate of penetration. Indirect tensile strength tests provide the strength results of the granite rock which are consistent with the results obtained at the rule of thumb with compressive strength results. Due to higher compressive strength, it decreases the rate of penetration that directly influences the drilling efficiency.

As part of thesis, mechanical and simulation investigation has been performed on the vibrating components of the LDS-pVARD tool for drilling performance applications. The hysterics effect has been determined on the various LDS spring stacking as well as done some case studies by using lubrication. The hysteresis effect minimizes in proportion to the number of parallel springs but using suitable lubrication maximizes the hysteresis effect. Based on the results of laboratory and field trials conducted with pVARD equipment, some designs may be modified to suit the equipment in oil and gas drilling operations. In addition to this information, the knowledge gained from

laboratory and field tests have been used to design third-generation LDS-pVARD and will be used to design next-generation pVARD for use in industry.

In the laboratory, POTs have been performed by selecting an optimal flow rate among different types of rigid and SDS-pVARD configurations with different WOB. Drill-off-tests have performed a series of WOBs, a constant fluid flow rate with different SDS-pVARD and rigid configurations. In the drilling, it is seen that compliance performance plays a major role with hard rock. The compliant pVARD tool configuration enhances the rate of penetration on granite. The performance enhancement due to the compliance of the pVARD tool improves with increasing WOB for the cases rather than with rigid drilling. The performance of the tool depends upon the flow rate, the stiffness of the springs and the WOB.

Since the effect of the pVARD tool on the ROP varies with different drilling parameters, it is possible to modulate the tool to the given drilling parameters. The performance enhancement due to the compliance of the pVARD tool improves with increasing WOB and higher compared with rigid drilling. The performance of the tool depends upon the flow rate, the stiffness of the springs and the WOB. The evaluation of the drilling parameters as well as the relationship with pVARD tool performance could not be determined in this thesis.

The drilling performance focuses on the Rate of Penetration (ROP) that is the main interest and demand for oil and gas companies to achieve the hydrocarbon target effectively and economically. ROP has been mainly affected by two factors: the drill string factor and the formation factor. For the drillstring factor, this thesis used a newly designed tool as passive Vibration Assisted Rotary Drilling (pVARD) tool with the coring bit for increasing ROP against conventional drilling for the rotary drilling.For the formation factor, Granite rocks were the rock types used for the research of this thesis. This study has set a benchmark for improving drilling efficiency that can be helpful for oil and gas companies make their decisions.

9.2. Recommendations

The work of this research has been taken as a baseline for standard mechanical measurements of hard rocks material granite. The future work will be extended to cover the physical measurements of rocks material and drilling tests under the various levels of pressures of well bottom-hole pressure while drilling and confining pressures while conducting the Confined Compressive Strength (CCS) tests. This will be also intended to evaluate drilling experiments in isotropic and anisotropic hard rock materials to determine the significance of the isotropy and anisotropy on drilling performance.

This study demonstrates the effectiveness of the axial compliance component in increasing ROP on a laboratory scale on hard rocks. Although these SDS-pVARD experimental data show instances where the pVARD tool increases the rate of penetration but still a defined relationship between operational ranges has not been determined. The current research is conducted with three various compliance settings. Different types of spring constants in the test matrix can get more indications of putting into action the pVARD tool.

This research is conducted with a coring bit and shows great results. However, testing different types of full-scale bits with different geometries and numbers of cutters may be a good next step to explore. A subsequent study is still needed for various fluid flow conditions for drilling performance

Although RPM was kept constant in this study, future tests should be analyzed by changing the compliance settings, flow rates, or WOB with different ranges of RPM. The different ranges of RPM seem to be particularly important because the rotational speed is the major booster to bit vibration and bit-rock interaction which is the key strength of the pVARD tool.

Finally, the next goal for the third generation pVARD is to produce an index for optimal LDS-pVARD operational range. Drilling performance can be considered the recommendations of the pVARD's spring compression tests and the stress-strain analysis of rock samples conducted prior to drilling experiments. In addition, it can be considered by analyzing the cut size distribution and evaluating the drilling parameters applied as a function of WOB.

To make an optimal index, first calculate the properties of the springs mainly loaded with displacement in conformity with 25%, 50%, 75% and 100% stiffness. Then measure the UCS of the rock samples and build the relationship between the UCS-WOB-ROP. Thereafter, calculate the geomechanical properties (mainly Stress vs Strain) of the rock sample by 25%, 50%, 75% and 100%. Consequently, rigid drilling is performed based on the UCS of the sample. Afterward, the drilling is performed by using the LDS-pVARD based on the different spring configurations and UCS of the rock sample. These results are compared with those obtained from drilling without pVARD, which represents the typical rigid BHA of the conventional drilling.

References

[1] A. J. Bourgoyne, K. Millheim, M. Chenevert and F. J. Young, Applied Drilling Engineering, Richardson, TX, US: Society of Petroleum Engineers, 1991.

[2] P. Vieira, C. Lagrandeur and K. Sheets, "Hammer Drilling Technology - The Proved Solution to Drill Hard Rock Formations in the Middle East," in *SPE Middle East Oil and Gas Show and Conference*, Manama, Bahrain, 25-28 September,2011.

[3] A. L. Jedick and A. L. Ohio, "Diamond Core Drill Bit". United States Patent 5,996,571;, 07 December 1999.

[4] M. Klempa, P. Bujok, L. Struna and J. Pinka. [Online]. Available: http://158.196.10.120/DRILLING/drilling/theory.html. [Accessed 19 June 2020].

[5] W. Maurer, "The 'Perfect – Cleaning' Theory of Rotary Drilling," in *Society of Petroleum" 37th Annual Fall Meeting of SPE*, Los Angeles, California, USA, 7-10 October, 1962.

[6] A. Bauer and P. N. Calder, "Open Pit Drilling-Factors Influencing Drilling Rates," in *4th Rock Mechanics Symposium*, Mines Branch, Department of Energy, Mines and Resources, Ottawa, 29-30 March 1967.

[7] A. T. Bourgoyne Jr and F. S. Young Jr, "A Multiple Regression Approach to Optimal Drilling and Abnormal Pressure Detection," *Society of Petroleum Engineers Journal,* vol. 14, no. 4, pp. 371 - 384, August , 1974.

[8] T. M. Warren, "Drilling Model for Soft-Formation Bits," *Journal of Petroleum Technology,* vol. 33, no. 06, pp. 963 - 970, June, 1981.

[9] E. Detournay, T. Richard and M. Shepherd, "Drilling response of drag bits: Theory and experiment," *International Journal of Rock Mechanics & Mining Sciences,* vol. 45, no. 8, pp. 1347-1360, 2008.

[10] M. Taylor, A. Murdock and S. Evans, "High Penetration Rates and Extended Bit Life Through Revolutionary Hydraulic and Mechanical Design in PDC Drill Bit Development," in *SPE Annual Technical Conference and Exhibition*, Denver, Colorado, U.S., 6-9 October,1996.

[11] G. Mensa-Wilmot, S. P. Langdon and Y. Harjadi, "Drilling efficiency and rate of penetration: Definitions influencing factors relationships and value," in *IADC/SPE Drilling Conference and Exhibition*, New Orleans, Louisiana, USA, 2-4 February, 2010.

[12] R. Teale, "The Concept of Specific Energy in Rock Drilling," *International Journal of Rock Mechanics and Mining Sciences & Geomechanics Abstracts,* vol. 2, no. 1, pp. 57-73, March, 1965.

[13] J. Cochener, "Quantifying Drilling Efficiency," Office of Integrated Analysis and Forecasting,U.S. Energy Information Administration, June 28, 2010.

[14] J. P. Germiquet and R. Minnitt, "Rock Strength and Geometallurgical Modelling, Mogalakwena Mine," *Journal of the Southern African Institute of Mining and Metallurgy,* vol. 116, no. 3, pp. 247-250, 2016.

[15] R. Pessier, S. Walace, H. Oueslati and B. Hughes, "Drilling Performance is a Function of Power at the Bit and Drilling Efficiency," IADC/SPE Drilling Conference and Exhibition, San Diego, California, USA, 6-8 March, 2012.

[16] J. Brantly and E. Clayton, "A Preliminary Evaluation of Factors Controlling Rate of Penetration in Rotary Drilling," in *Drilling and Production Practice*, New York, USA, 1 January, 1939.

[17] A. Garnier and N. Van Lingen, "Phenomena Affecting Drilling Rates at Depth," *Transactions of the AIME,* vol. 216, no. 1, pp. 232 - 239, December ,1959.

[18] N. Garner, "Cutting Action of a Single Diamond Under Simulated Borehole Conditions," *Journal of Petroleum Technology,* vol. 19, no. 7, pp. 937 - 942, July, 1967.

[19] "Changsha Drilling Machinery CO., LTD," [Online]. Available: https://www.diamondcorebitmfg.com/waterway-configuration-channel-flushing/. [Accessed 02, July 2020].

[20] "Diamond Core Drill Bits," TMG Manufacturing, [Online]. Available: https://tmgmfg.com. [Accessed 26, June 2020].

[21] "Professional Diamond Driller's Handbook - Practical guide," Atlas Copco, Fagersta,Sweden, 2015.

[22] E. Guttenkunst, "Study of the wear mechanisms for drill bits used in core drilling," Department of Engineering Sciences,Applied Materials Sciences,Uppsala University, Sweden, 2018.

[23] D.Miller and A.Ball, "Rock drilling with impregnated diamond microbits—An experimental study," *International Journal of Rock Mechanics and Mining Sciences & Geomechanics Abstracts,* vol. 27, no. 5, pp. 363-371, October, 1990.

[24] M. Karakus and S. Perez, "Acoustic emission analysis for rock–bit interactions in impregnated diamond core drilling," *International Journal of Rock Mechanics and Mining Sciences,* vol. 68, pp. 36-43, June, 2014.

[25] M. Mostofi, L. Franca and T. Richard, "Drilling Response of Impregnated Diamond Bits: An Experimental Investigation," in *47th U.S. Rock Mechanics/Geomechanics Symposium*, San Francisco, California,US, 23-26 June,2013.

[26] Feenstra.R and J. Van Leeuwen, "Full-Scale Experiments on Jets in Impermeable Rock Drilling," *Journal of Petroleum Technology,* vol. 16, no. 3, March ,1964.

[27] D. Ashley, X. McNary and J. Tomlinson, "Extending BHA Life with Multi-Axis Vibration Measurements," in *SPE/IADC Drilling Conference*, Amsterdam, The Netherlands, 27 February–1 March, 2001.

[28] M. Biggs and J. Cheatham, "Theoretical Forces for Prescribed Motion of a Roller Bit," *Society of Petroleum Engineers Journal,* vol. 9, no. 4, December ,1969.

[29] M. Sheppard and M. Lesage, "The Forces at the Teeth of a Drilling Rollercone Bit: Theory and Experiment," in *SPE Annual Technical Conference and Exhibition*, Houston, Texas, 2-5 October,1988.

[30] D. Glowka, "Use of Single-Cutter Data in the Analysis of PDC Bit Designs: Part 1 - Development of a PDC Cutting Force Model," *Journal of Petroleum Technology,* vol. 41, no. 8, August ,1989.

[31] R. Reyes, "Bit-Rock Interaction in Rotary Drilling: Numerical and Experimental Study,Master of Engineering Dissertation," Memorial University of Newfoundland, St. John's, Canada, 2017.

[32] T. Richard, C. Germay and E. Detournay, "Self-excited Stick-slip Oscillations of Drill Bits," *Comptes Rendus Mécanique,* vol. 332, no. 8, pp. 619-626, August, 2004.

[33] Q. Gao, "Development of Laboratory and Field Drilling Tools to Measure Bit Operating,[Master of Engineering Dissertation]," Memorial University of Newfoundland, St. John's, Canada, 2014.

[34] R. Rahman, "Development and Interpretation of Downhole Data from Downhole, Master of Engineering Dissertation," Memorial University of Newfoundland, St. John's, Canada, 2015.

[35] P. Rana, A. Abugharara, S. Butt and J. Molgaard, "Experimental and Field Application of Passive-Vibration Assisted Rotary Drilling (pVARD) Tool to Enhance Drilling Performance," in *49th US Rock Mechanics / Geomechanics*, San Francisco, CA, USA, 2015.

[36] Y. Xiao, "Evaluation of drilling performance and penetration mechanisms using seismic while drilling and acoustic emission methods,Doctor of Philosophy Dissertation," Memorial University of Newfoundland, St. John's,Canada, September, 2017.

[37] S. Butt, B. Gillis and P. Rana, "Vibration Assisted Rotary Drilling". U.S.A Patent 10,214,972 B2, 26 February 2019.

[38] B. Gillis and S. Butt, "Comparison of Field and Laboratory Vibration Assisted Rotary Drilling," in *52nd US Rock Mechanics / Geomechanics Symposium*, Seattle, Washington, USA, 17–20 June, 2018.

[39] J. Zhong, "Investigation of Bit-Rock Interaction for Rotary Drilling and Influence on Penetration Rate," Master of Engineering Dissertation,Memorial University of Newfoundland, St. John,s, Canada, 2016.

[40] B. Gillis, "Development of Laboratory and Field Scale Passive Vibration Assisted Rotary Drilling Tools, Master of Engineering Dissertation," Memorial University of Newfoundland, St. John's, Newfoundland, Canada, October, 2019.

[41] M. Eskin, W. C. Maurer and A. Leviant, In Maurer Engineering (1st Ed.), Former-USSR R&D on novel drilling techniques, pages 8-21, 1995.

[42] D. D. Barkap, In Maurer Engineering (1st Ed.), Former-USSR R&D on novel drilling techniques, Page.22, 1957.

[43] B. Baidyuk, "Former-USSR R&D on Novel Drilling Techniques," in *Maurer Engineering (1st Ed.)*, 1993, pp. 18-22.

[44] A. Izosimov, A. Volokhin and Y. F. Khacharuridze, "Well Drilling Device," USSR Authorship Certificate No. 899836, applied for January 23, 1980.," 1980.

[45] Y. A. Sintsov and et al., "``Drilling Tool," USSR Authorship Certificate No. 1469086, applied for November 27, 1985.," 1985.

[46] J. V. Pennington, "Some results of DRI investigation-rock failure in percussion," in *Drilling and Production Practice*, New York, USA, 1 January,1953.

[47] H. Li, S. Butt, K. Munaswamy and F. Arvani, "Experimental investigation of bit vibration on rotary drilling penetration rate," in *44th US Rock Mechanics Symposium and 5th U.S.-Canada Rock Mechanics Symposium*, Salt Lake City, UT, June 27–30, 2010.

[48] H. Li, "Experimental investigation of the rate of penetration of vibration assisted rotary drilling, Master of Engineering Dissertation," Memorial University of Newfoundland, St. John's, Newfoundland, Canada, Junary, 2011.

[49] Y. Babatunde, S. Butt, J. Molgaard and F. Arvani, "Investigation of the Effects of Vibration Frequency on Rotary Drilling Penetration Rate Using Diamond Drag Bit," in *45th US Rock Mechanics/Geo Mechanics symposium*, San Francisco, CA, June 26-29, 2011.

[50] Y. Babatunde, "The Effect of Varying Vibration Frequency an Amplitude for Drilling Optimization,Master of Engineering Dissertation," Memorial University of Newfoundland, St. John's, Newfoundland, Canada, November, 2011.

[51] A. Abtahi, "Bit Wear Analysis and Optimization for Vibration Assisted Rotary Drilling (VARD) using Impregnated Diamond Bits,Master of Engineering Dissertation," Memorial University of Newfoundland, St.John's, Newfoundland,Canada, September, 2011.

[52] H. Khorshidian, S. Butt and F. Arvani, "Influence of High Velocity Jet on Drilling Performance of PDC bit under Pressurized Condition," in *48th US Rock Mechanics/ GeoMechanics Symposium*, Minneapolis, MN, USA, 2014.

[53] L. Wang, S. Butt and J. Yang, "Dynamic Analysis of Bottom Hole Assembly With External Vibrating Force Excitation," in *International Mechanical Engineering Congress and Exposition*, San Diego, California, USA, November 15-21, 2013.

[54] M. Khademi, "Laboratory Study of the Effect of Axial Compliance on Rock Penetration of PDC Bits," Master of Engineering Dissertation,Faculty of Engineering and Applied Science, Memorial University of Newfoundland, St. John's, Newfoundland, Canada, October, 2014.

[55] X. Xiao, J. Zhong, C. Hurich and S. Butt, "Micro-Seismic Monitoring of PDC bit drilling performance during Vibration Assisted Rotary Drilling," in *49th US Rock Mechanics/Geo-Mechanics Symposium*, San Francisco, USA, June ,2015.

[56] J. Zhong, S. Butt and J. Yang, "DEM Simulation of Enhancing Drilling Penetration Using Vibration and Experimental Validation," in *Summer Simulation Multi-Conference*, Montreal, Quebec, Canada., 2016.

[57] J. Almen and A. Laszlo, "The Uniform-section Disk Spring," *Transactions of the American Society of Mechanical Engineers,* vol. 58, p. 305–314, 1936.

[58] M. Giuliodori, H. Lujan, W. Briggs, G. Palani and S. DiCarlo, "Hooke's law: applications of a recurring principle," *The Journal of Advances in Physiology Education,* vol. 33, p. 293–296, 2009.

[59] Z. T. Bieniawski, "Estimating the Strength of Rock Materials," *Journal of the Southern African Institute of Mining and Metallurgy,* vol. 74, no. 8, pp. 312-320, March,1974.

[60] D7012-e1, "Standard Test Methods for Compressive Strength and Elastic Moduli of Intact Rock Core Specimens under Varying States of Stress and Temperatures," ASTM International, West Conshohocken, PA,www.astm.org, May 01, 2014.

[61] D3967-16, "Standard Test Method for Splitting Tensile Strength of Intact Rock Core Specimens," ASTM International, West Conshohocken, PA, 2016.

[62] G. Faure and J. Powell, "Granitic Rocks," in *Strontium Isotope Geology. Minerals, Rocks and Inorganic Materials (Monograph Series of Theoretical and Experimental Studies)*, Berlin, Heidelberg, Springer, 1972.

[63] D4543-08, "Standard Test Method for Preparing Rock Core as Cylindrical Test Specimens and Verifying Conformance to Dimensional and Shape Tolerances," ASTM International, 2008, West Conshohocken, PA.

[64] E122-17, "Standard Practice for Calculating Sample Size to Estimate, With Specified Precision, the Average for a Characteristic of a Lot or Process," ASTM International, West Conshohocken, 2017.

[65] S. Reza, B. Mostafa and B. Tikou, "Development of an Artificial Neural Network (ANNs) Model for Estimating Cemented Paste Backfill Performance," in *Post-Mining*, Nancy, France , February 6-8, 2008.

[66] X. Wei and K. Chau, "Three dimensional analytical solution for finite circular cylinders subjected to indirect tensile test," *International Journal of Solids and Structures,* vol. 50, no. 14-15, pp. 2395-2406, July, 2013.

[67] P. Małkowski, L. Ostrowski and J. Brodny, "Analysis of Young's modulus for Carboniferous sedimentary rocks and its relationship with uniaxial compressive strength using different methodsof modulus determination," *Journal of Sustainable Mining,* vol. 17, no. 3, pp. 145-157, 2018.

[68] D. Maharjan, J. M. Junior, G. Rideout and Butt.S, "Bond graph analysis of p-VARD," in *Progress in Canadian Mechanical Engineering*, Charlottetown, PE, Canada, 2020.

[69] J. Shigley, C. Mischke and T. Brown, Standard Handbook of Machine Design, Third Edition, The McGraw-Hill Companies, Inc., 2004.

[70] N. L. Pedersen and P. Pedersen, "Stiffness and design for strength of trapezoidal Belleville springs," *Journal of Strain Analysis for Engineering Design,* vol. 46, no. 8, pp. 825-836, 2011.

[71] Y. Zhiming and Y. Kaiyuan, "A Study of Belleville Spring and Diaphragm Spring in Engineering," *Journal of Applied Mechanics, Transactions,* vol. 57, no. 4, p. 1026–1031, December 1, 1990.

[72] "Stiffness of Variable Thickness Belleville Springs," *Journal of Mechanical Design,* vol. 123, no. 2, p. 294–299, June, 2001.

[73] G. Curti and R. Montanini, "On the Influence of Friction in the Calculation of Conical Disk Springs," *Journal of Mechanical Design,* vol. 12, no. 4, p. 622–627, December, 1999.

[74] S. Ozaki, K. Tsuda and J. Tominaga, "Analyses of static and dynamic behavior of coned disk springs: Effects of friction boundaries," *Thin-Walled Structures,* vol. 59, pp. 132-143, October, 2012.

[75] M. Hamidon, M. T. H. Sultan and A. H. Ariffin, "Investigation of mechanical testing on hybrid composite materials," in *Failure Analysis in Biocomposites, Fibre-Reinforced Composites and Hybrid Composites*, Woodhead Publishing Series in Composites Science and Engineering, 2019, pp. 133-156.

[76] M. Paredes, "Analytical and Experimental Study of Conical Telescoping Springs With Nonconstant Pitch," *Journal of Mechanical Design,* vol. 135, no. 9, 2013.

[77] "Handbook for Disc Springs," Adolf Schnorr GmbH + Co. KG, Ann Arbor, Michigan, 2003.

[78] "Mechanical and Product Testing Equipment & Applications Experts," TestResources, Inc., [Online]. Available: https://www.testresources.net/. [Accessed 19 February 2020].

[79] M. Paredes, "Methodology to build an assistance tool dedicated to preliminary design: application to compression springs," *International Journal on Interactive Design and Manufacturing,* vol. 3, 2009.

[80] "Associated Spring Barnes Group (ASBG) Inc.," Associated Spring Barnes Group (ASBG) Inc., [Online]. Available: https://www.asbg.com. [Accessed 28 July 2020].

[81] "Elastic Hysteresis," [Online]. Available: https://www.instron.us/. [Accessed 28 July 2020].

[82] "Century Spring Corporation (CGS), MW Industries," [Online]. Available: www.CenturyDiscSprings.com. [Accessed 22 July 2020].

[83] R. Scott, J. Fitch and L. Leugner, The Practical Handbook Of Machinery Lubrication - 4th Edition, Noria Corporation, 2012.

[84] " Disc Springs," SPIROL International Corporation , [Online]. Available: https://www.spirol.com/. [Accessed 29 July 2020].

[85] J. Brown, "MachineDesign," 01 May 2000. [Online]. Available: https://www.machinedesign.com. [Accessed 2020 October 2020].

[86] "Shield Lubricants (Kuwait Dana Lubes)," [Online]. Available: https://shieldoils.com/. [Accessed 19 October 2020].

[87] R. A. Cunningham and J. G. Eenink., "Laboratory Study of Effect of Overburden Formation and Mud Column Pressures on Drilling Rate of Permeable," *Petroleum Transaction AIME,* vol. 217, no. 1, pp. 9-17, 1959.

[88] V. Pilipenko, I. Man'ko, S. Dolgopolov and O. Nikolayev, "Characteristics of a high-frequency cavitation hydrovibrator for setting up dynamic loads on the rock cutting tool of a drilling assembly," *Naukovy Vistnyk NDU,* no. 1, pp. 66-70, 2005.

[89] A. Alali and S. P. Barton, "Unique Axial Oscillation Tool Enhances Performance of Directional Tools in Extended Reach Applications," in *Brasil Offshore*, Macaé, Brazil, 14-17 June, 2011.

[90] I. Forster, "Axial Excitation as a Means of Stick Slip Mitigation - Small Scale Rig Testing and Full Scale Field Testing," in *SPE/IADC Drilling Conference and Exhibition*, Amsterdam, The Netherlands, 1-3 March, 2011.

[91] "Handbook for Disc Springs," Schnorr Corporation, Ann Arbor, MI, 2003.

Appendices

Appendix-A.   Detail Mechanical Design of Outer Shell for the LDS- pVARD
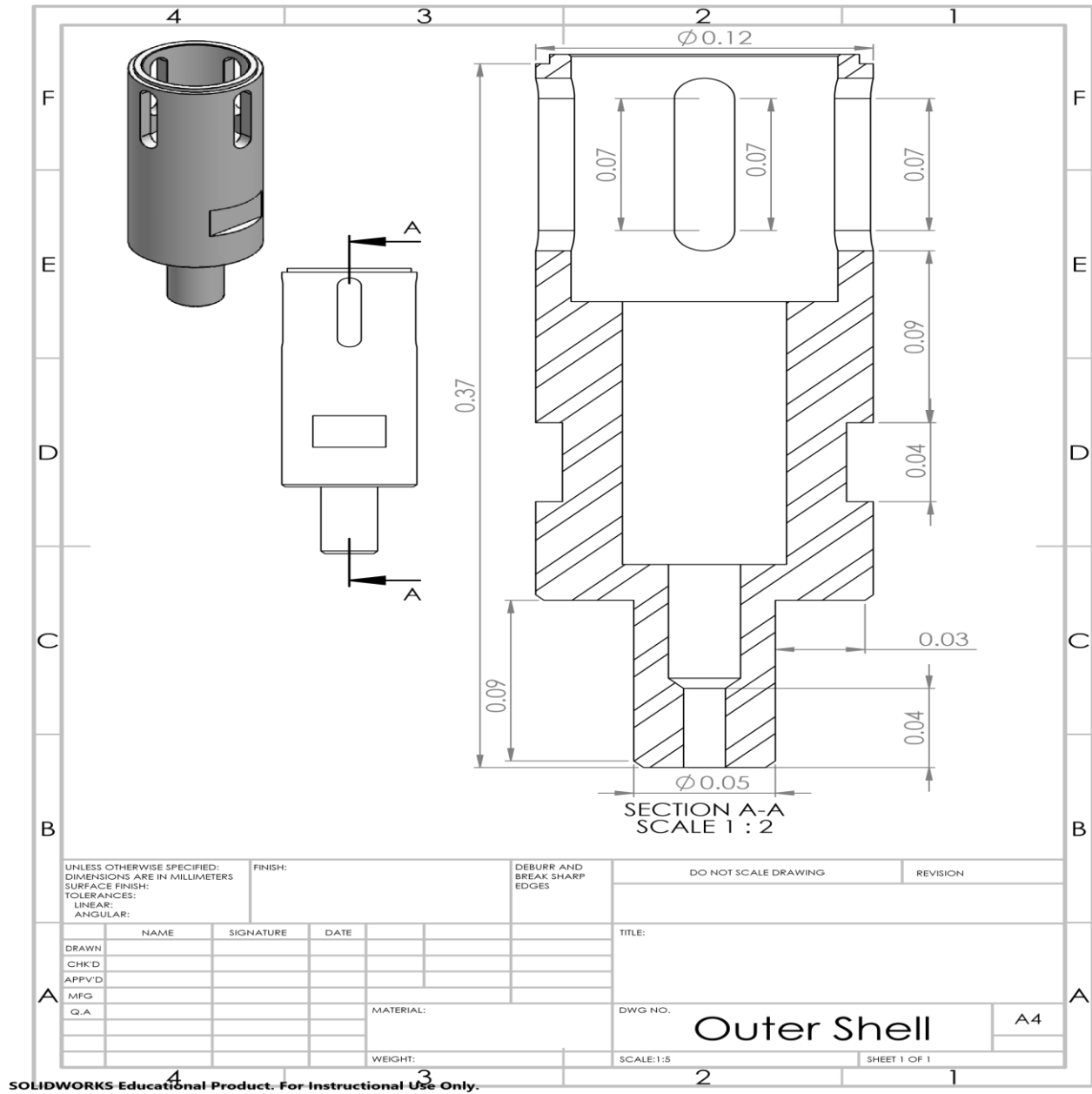
Appendix-B.   Details Mechanical Design of Inner Shaft for the LDS-pVARD

Ø0.05

Ø0.02

0.01

0.04

0.04

0.06

0.34

0.13

Ø0.02

UNLESS OTHERWISE SPECIFIED: DIMENSIONS ARE IN MILLIMETERS SURFACE FINISH: TOLERANCES: LINEAR: ANGULAR:	FINISH:		DEBURR AND BREAK SHARP EDGES	DO NOT SCALE DRAWING	REVISION

	NAME	SIGNATURE	DATE		TITLE:
DRAWN					
CHK'D					
APPV'D					
MFG					
Q.A			MATERIAL:	DWG NO.	Inside shaft A4
			WEIGHT:	SCALE:1:5	SHEET 1 OF 1
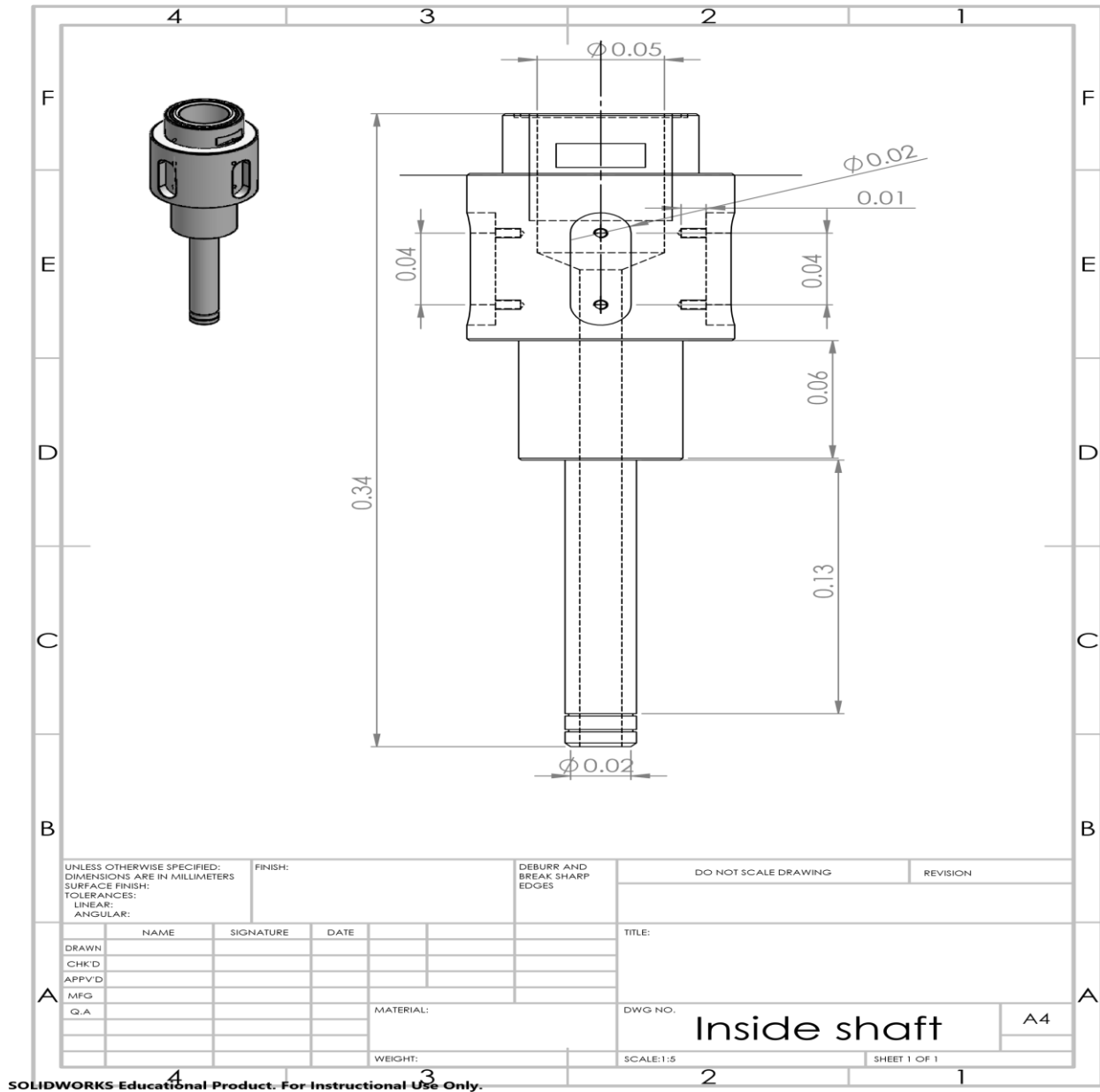
Appendix-C.   Details Mechanical Design of Key for the pVARD-LDS
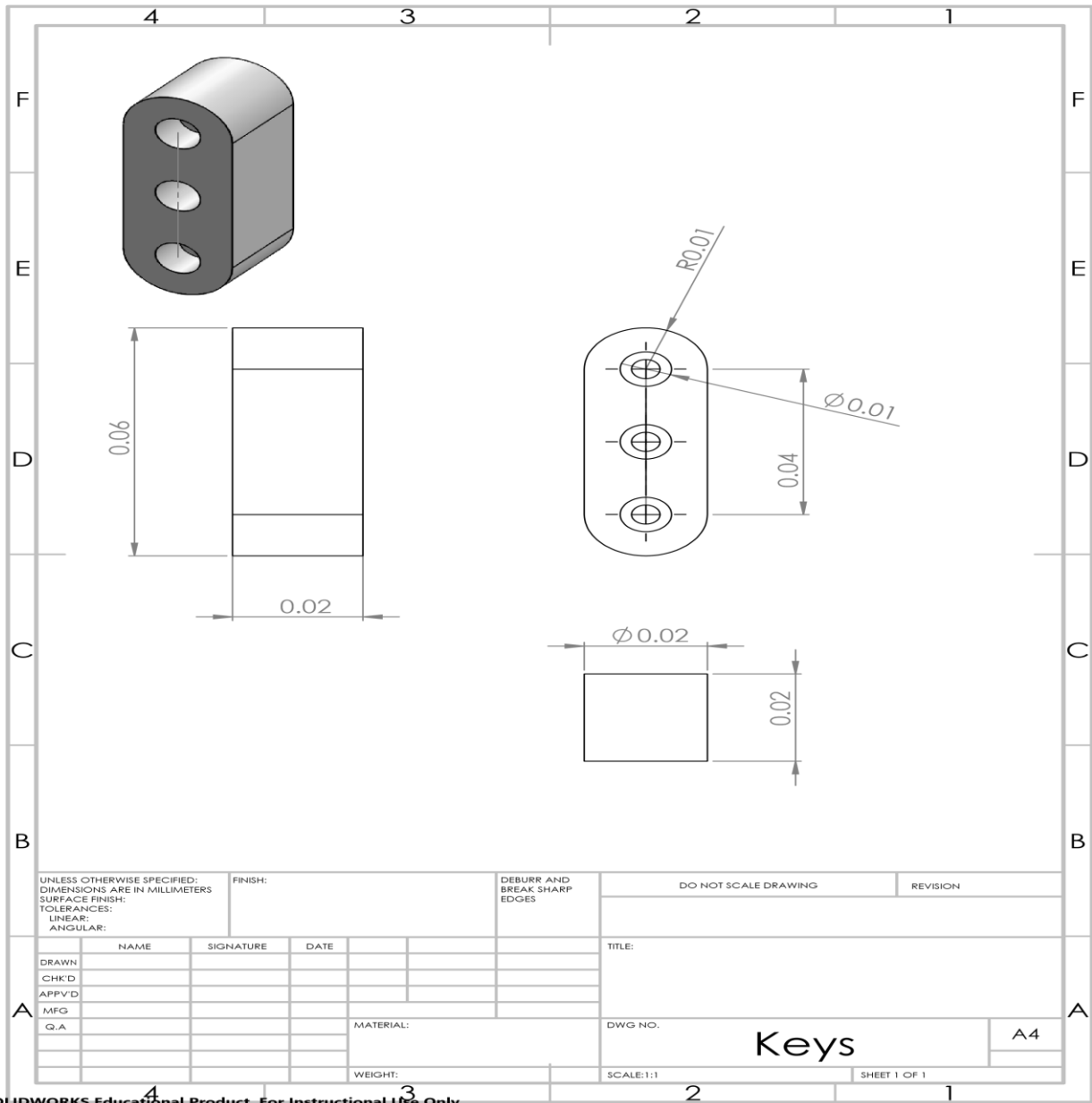
Appendix-D. **Details Mechanical Design of Sensor Plate for the pVARD-LDS**

SECTION A-A
SCALE 1 : 2

UNLESS OTHERWISE SPECIFIED:
DIMENSIONS ARE IN MILLIMETERS
SURFACE FINISH:
TOLERANCES:
  LINEAR:
  ANGULAR:

FINISH:

DEBURR AND
BREAK SHARP
EDGES

DO NOT SCALE DRAWING | REVISION

	NAME	SIGNATURE	DATE
DRAWN			
CHK'D			
APPV'D			
MFG			
Q.A			

TITLE:

MATERIAL:

DWG NO.

sensor plate

A4

WEIGHT:

SCALE:1:5 | SHEET 1 OF 1

125
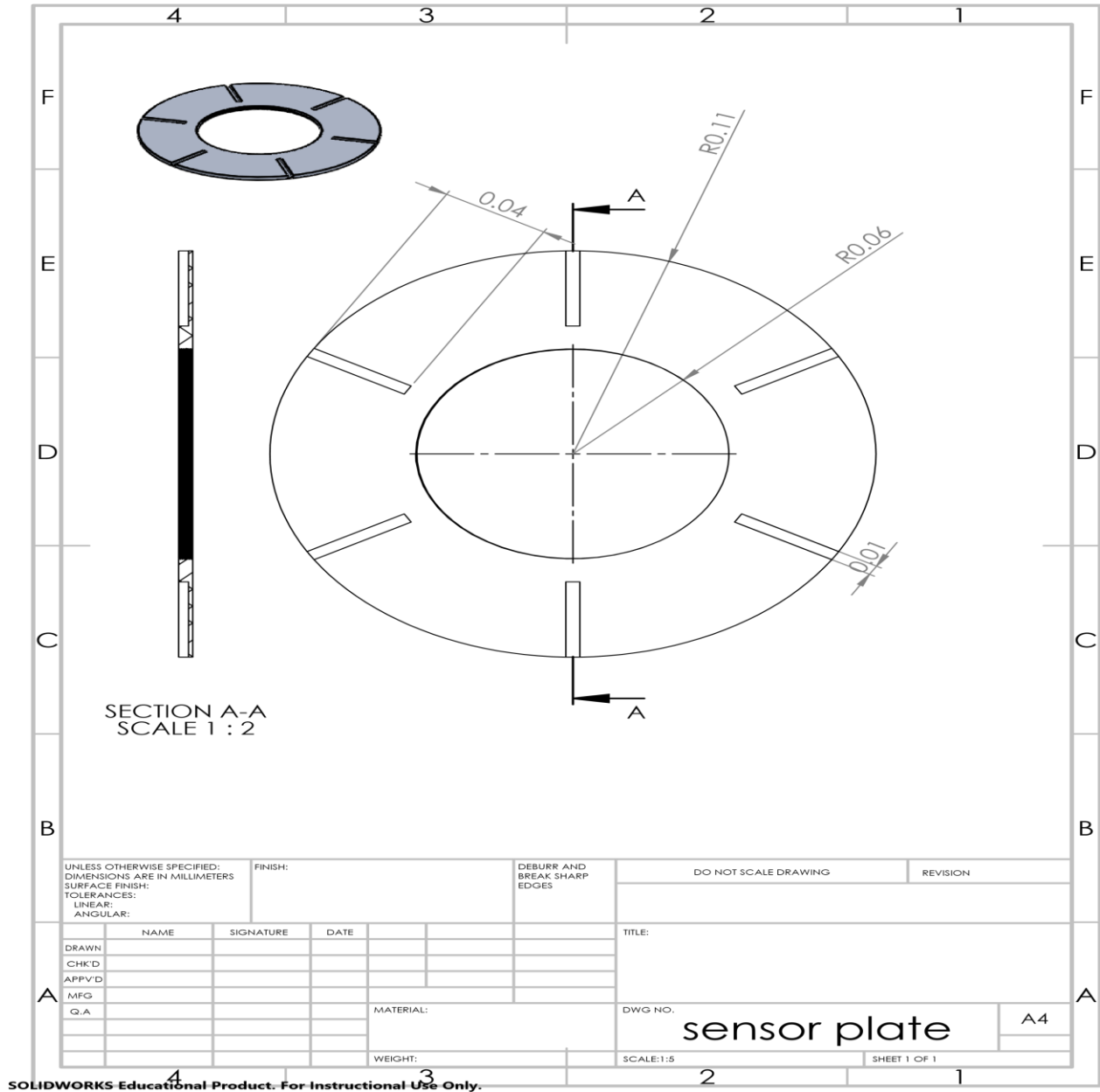
Appendix-E.   Load-Displacement and Stress-Strain Details for UCS Tests

Sample # 01: UCS Test
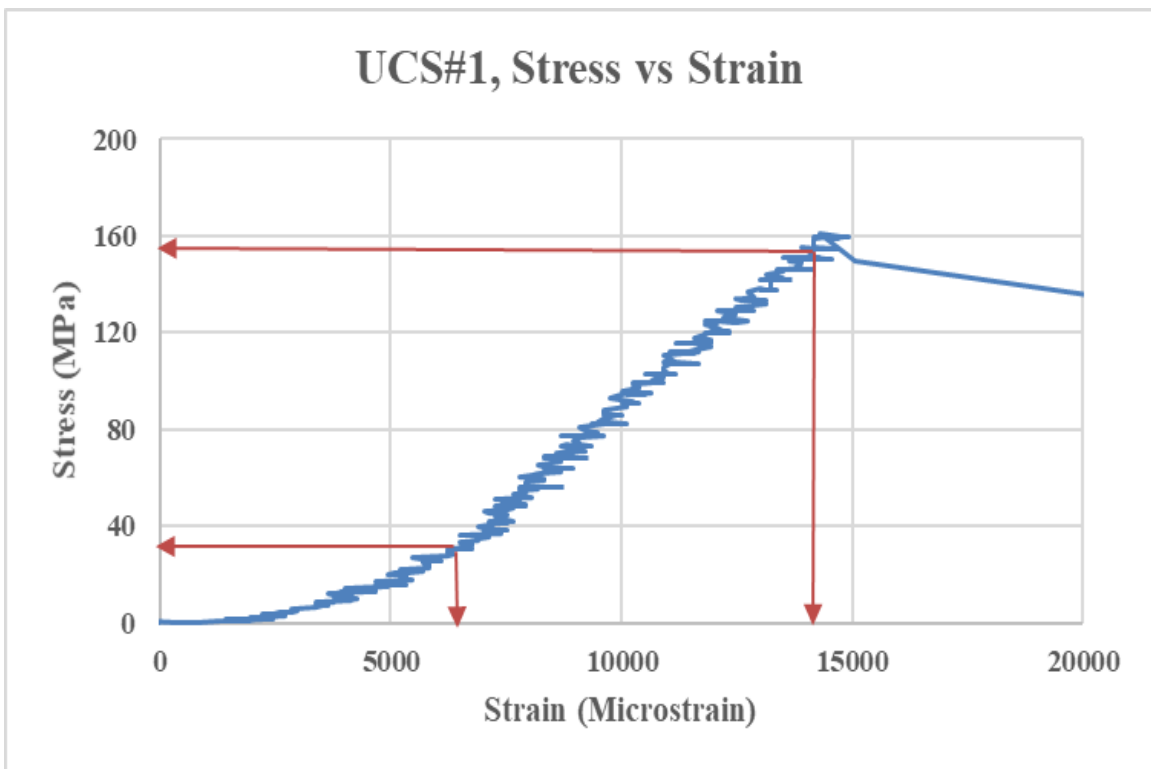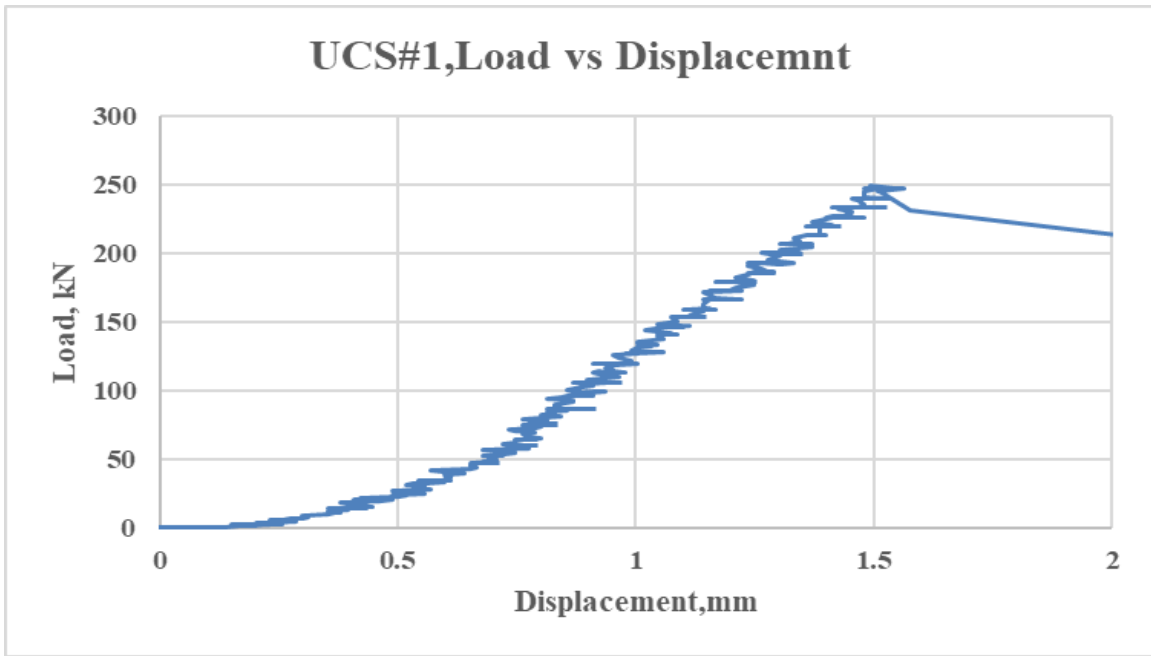
Sample # 02: UCS Test

Sample # 03: UCS Test

UCS#3, Load vs Displacement

UCS#3, Stress vs Strain

Sample # 04: UCS Test (Creep)

UCS#4,Load vs Displacement

UCS#4,Stress vs Stain
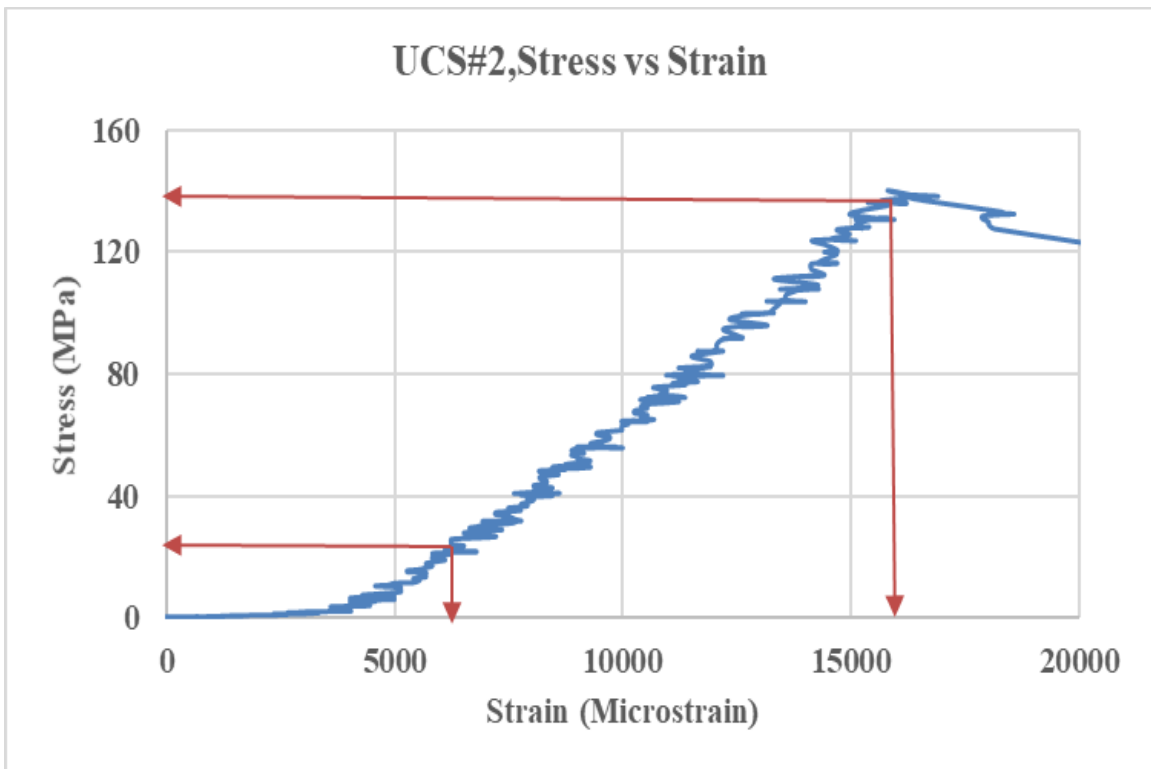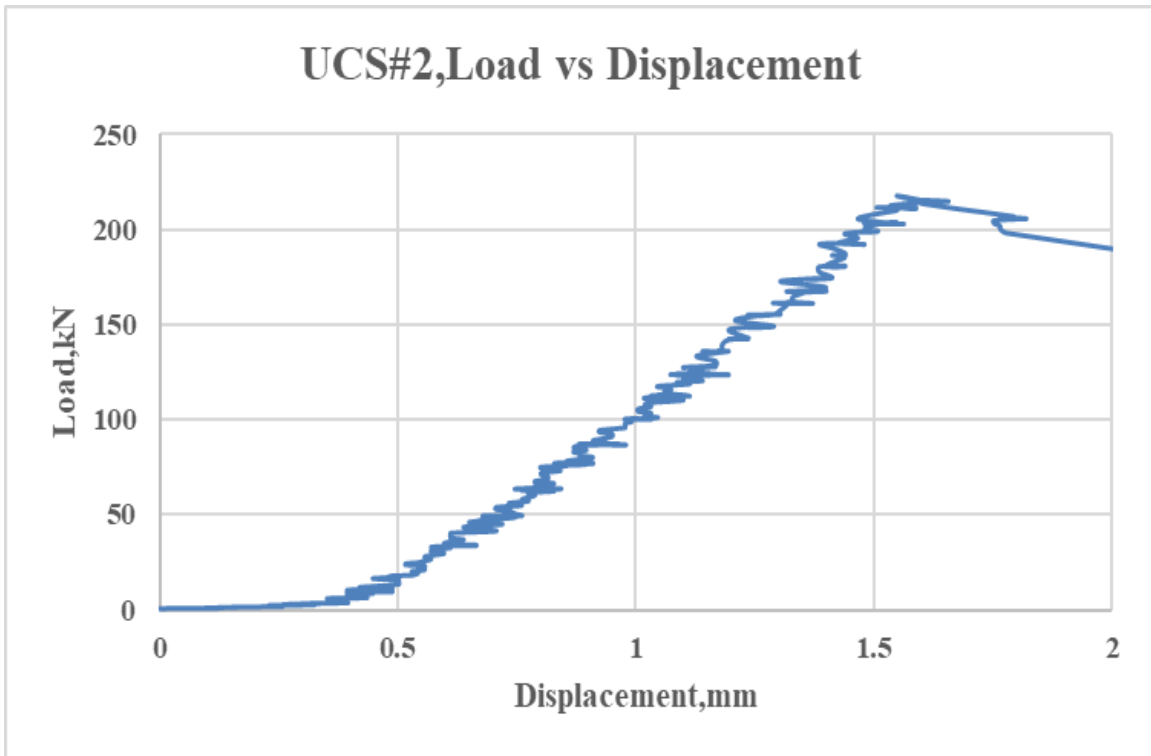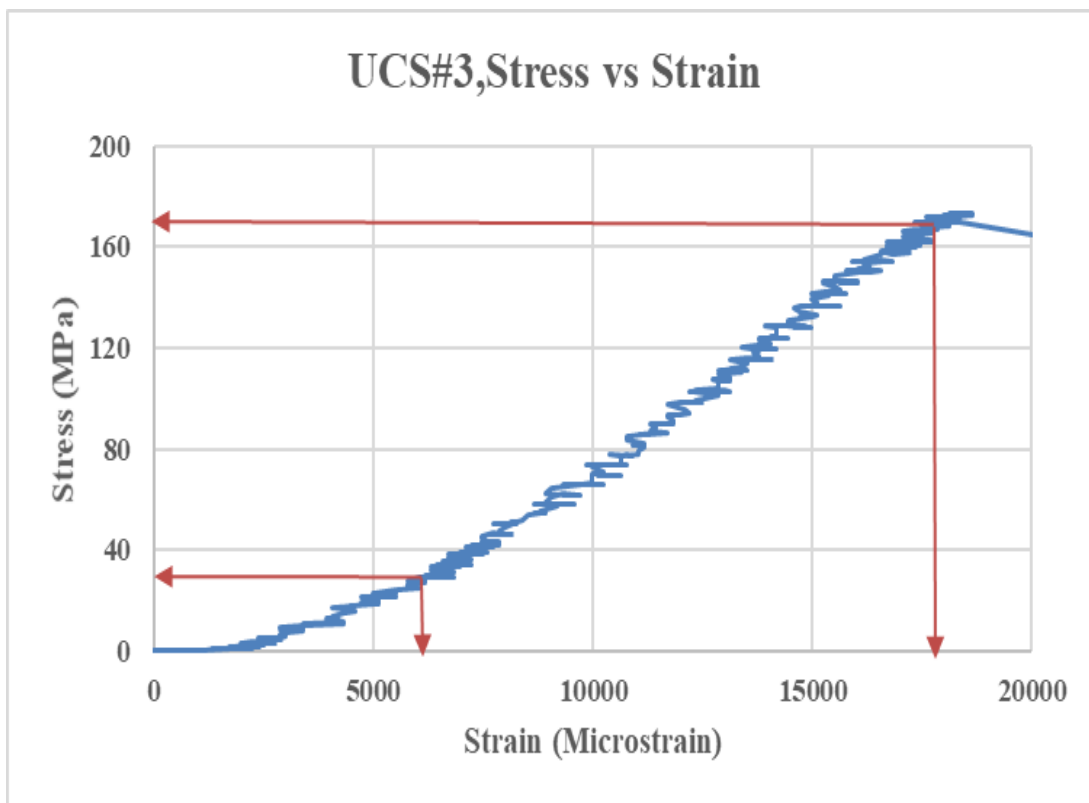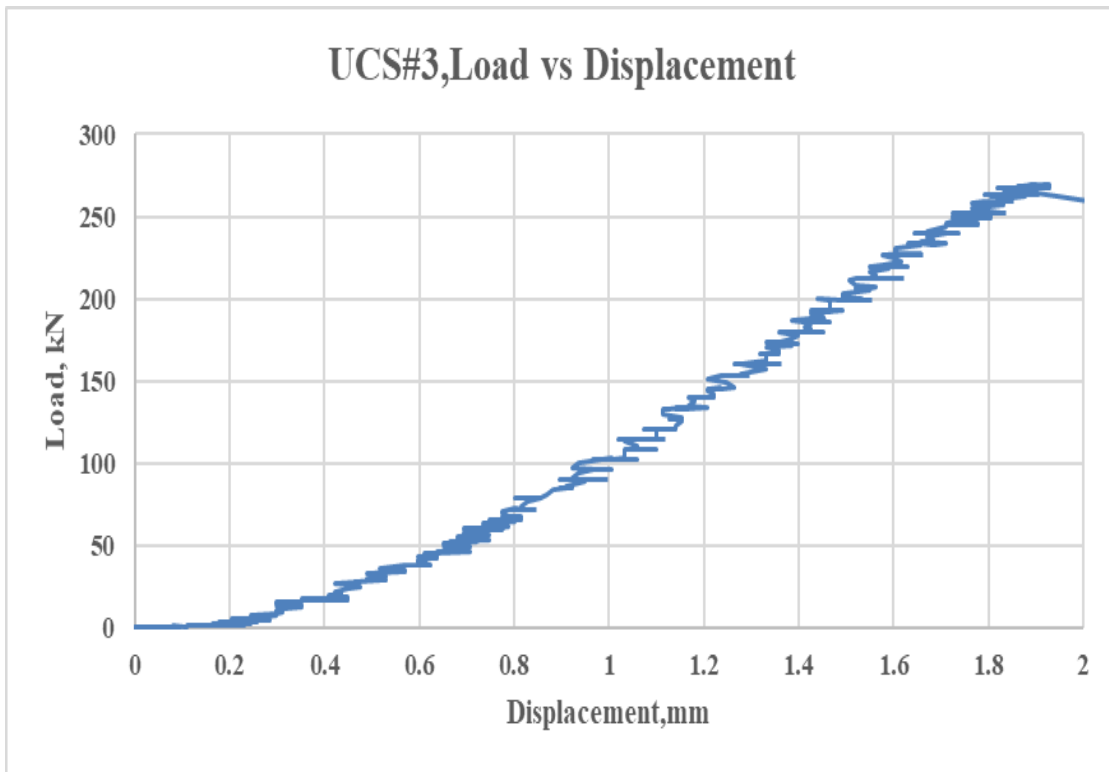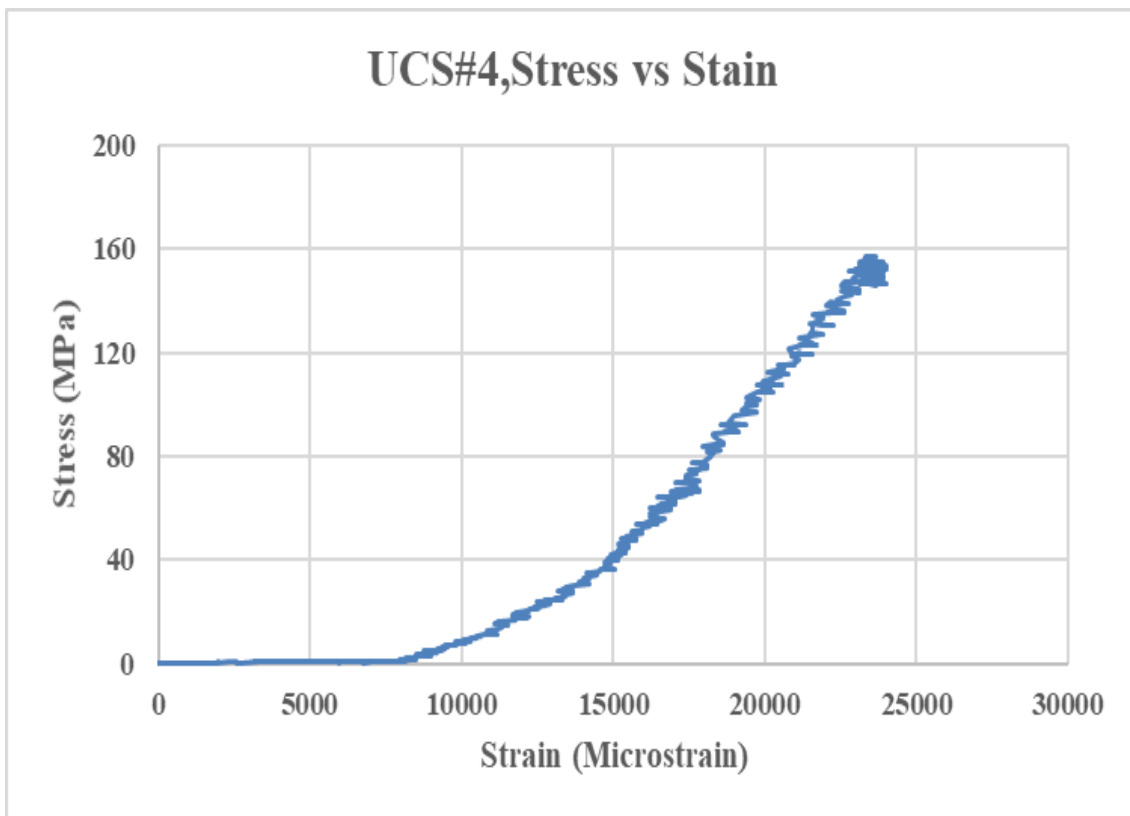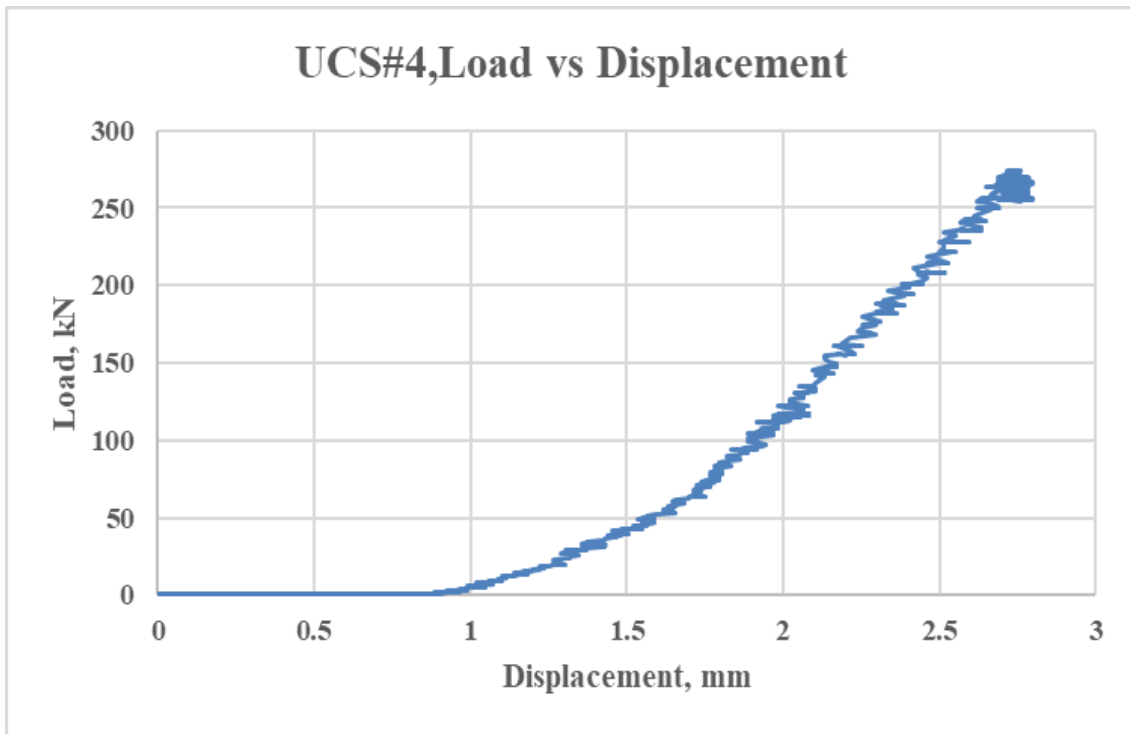
Sample # 05: UCS Test

Sample # 06: UCS Test (Creep)

UCS#6,Load vs Displacement

UCS#6,Stress vs Strain
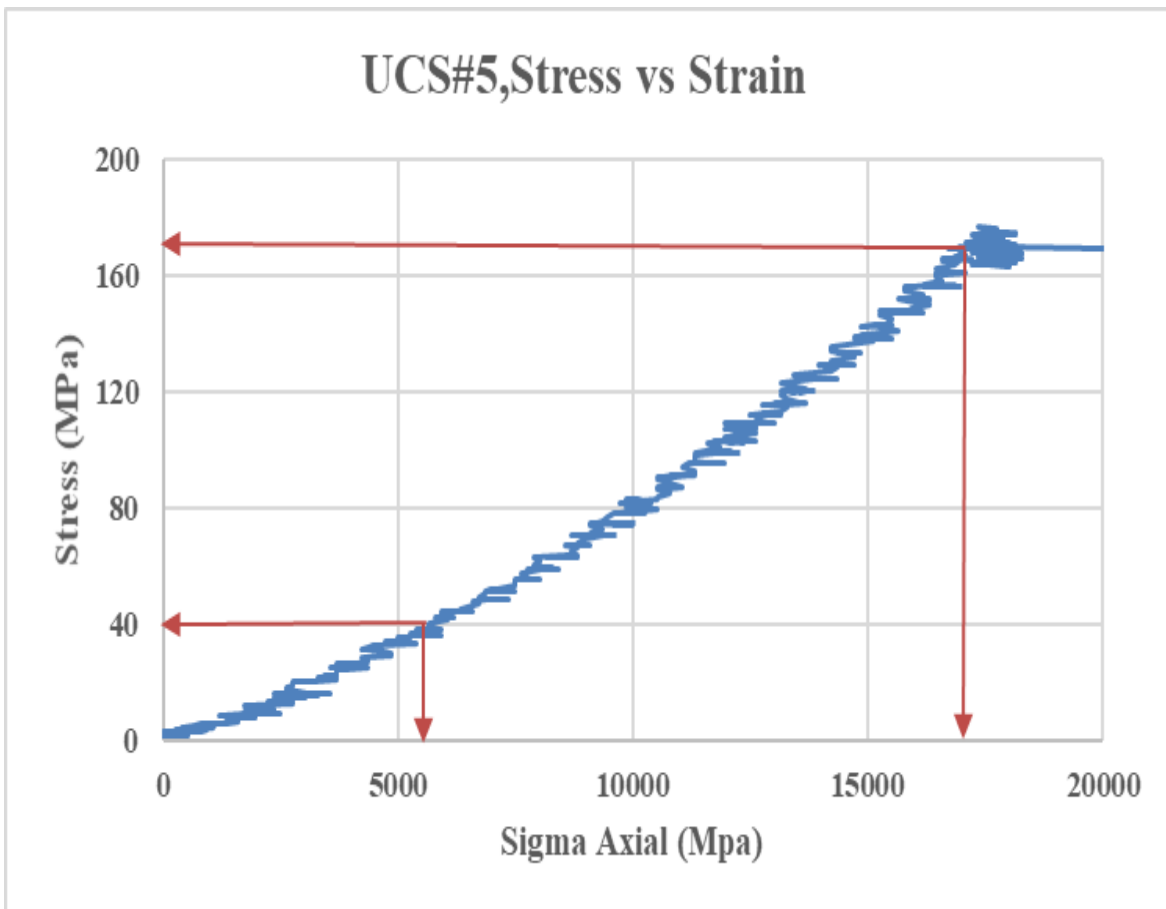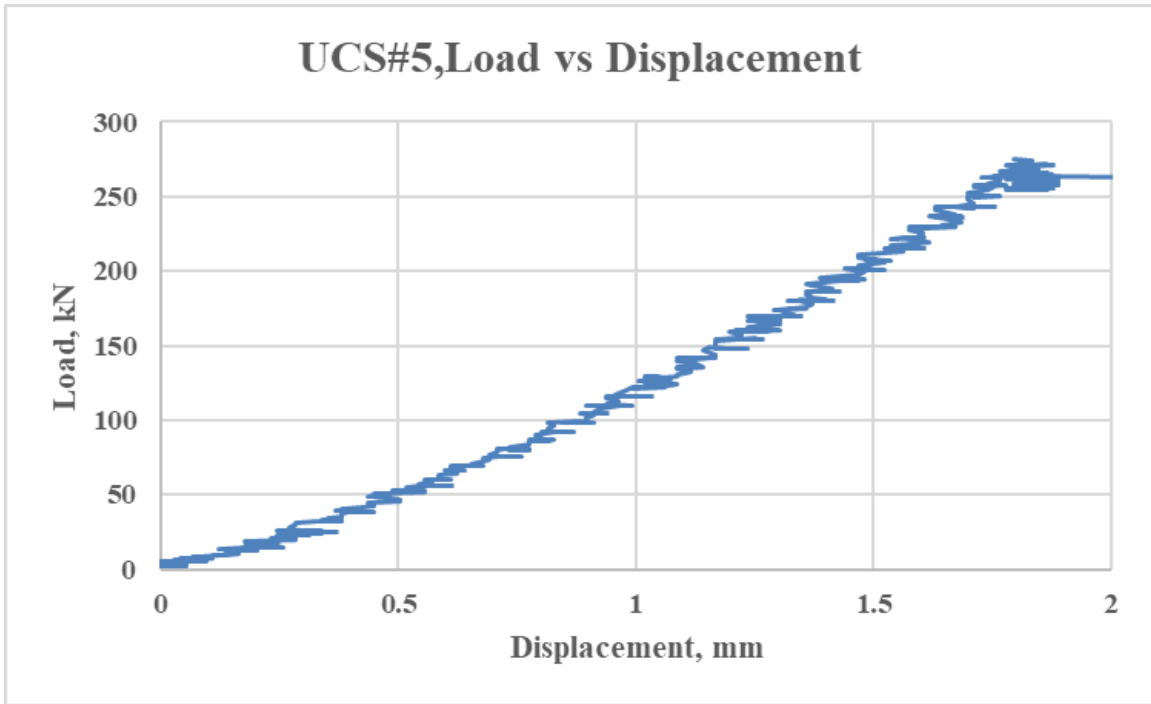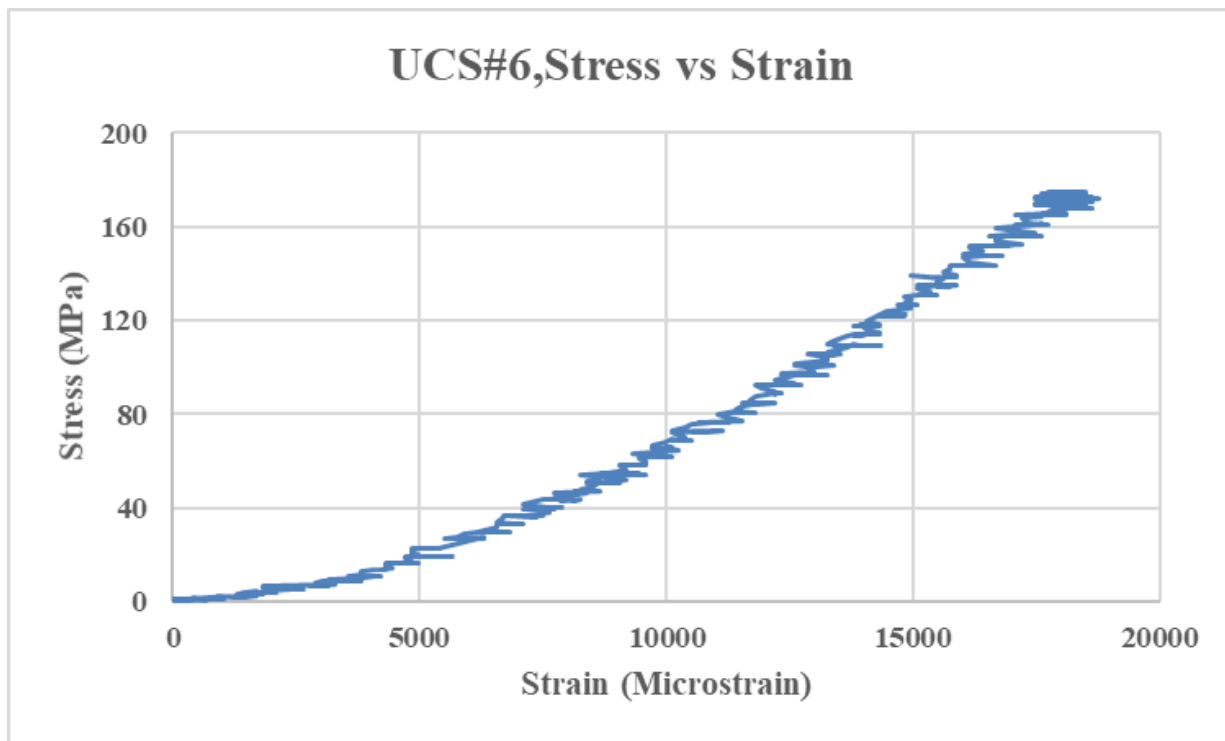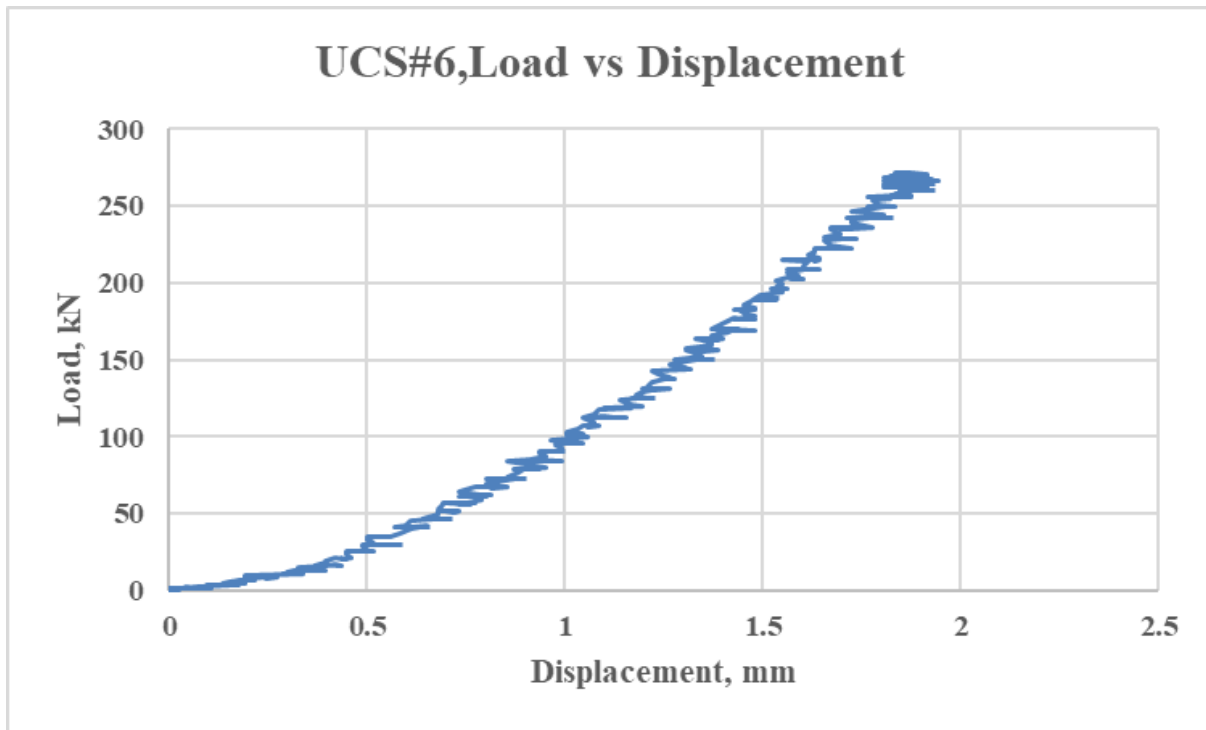
Sample # 07: UCS Test (Creep)
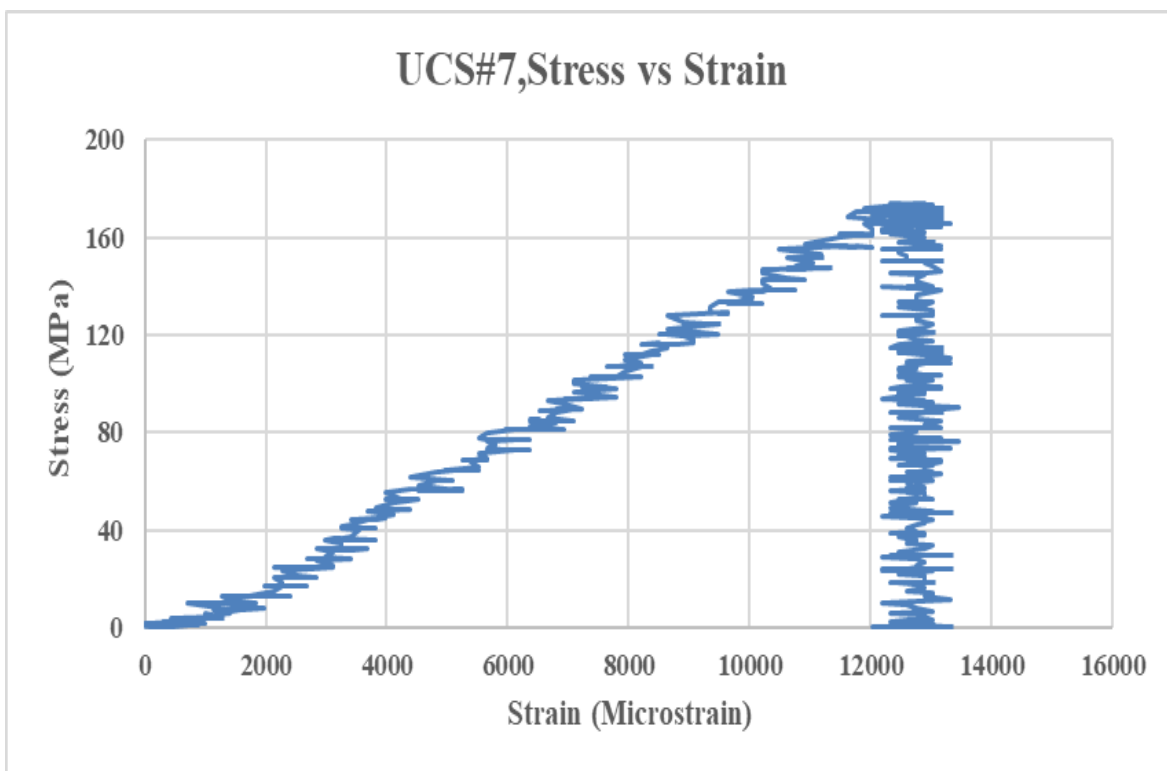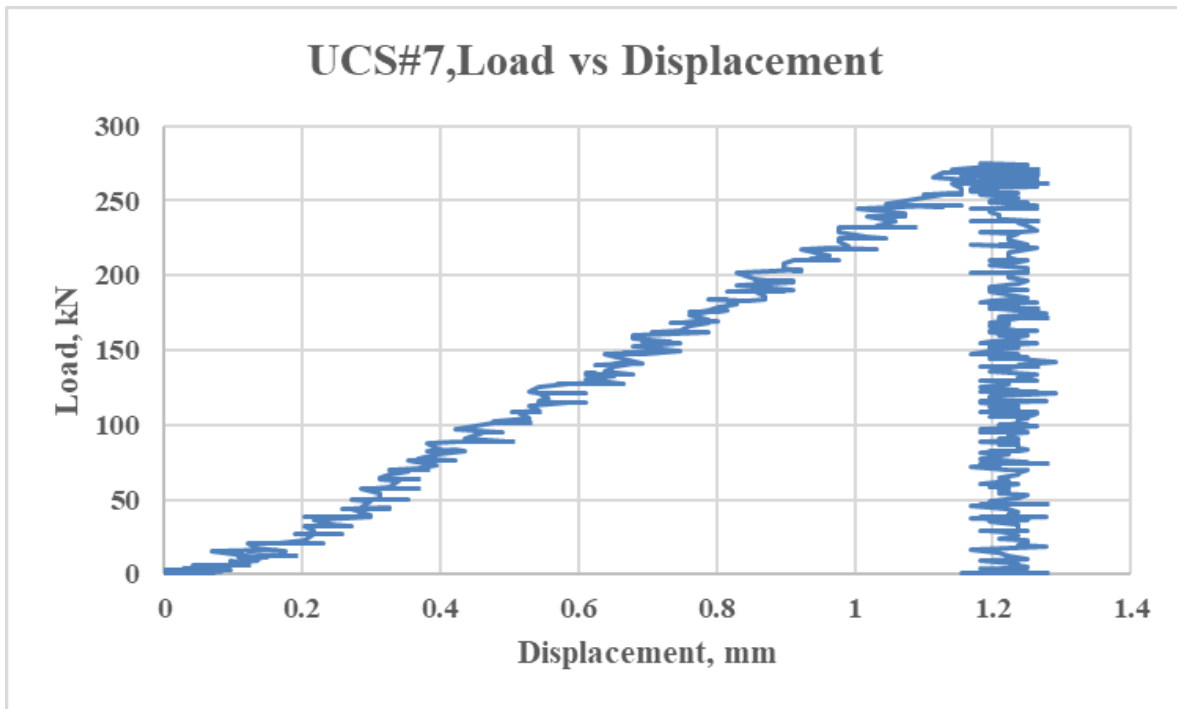
Sample # 08: UCS Test
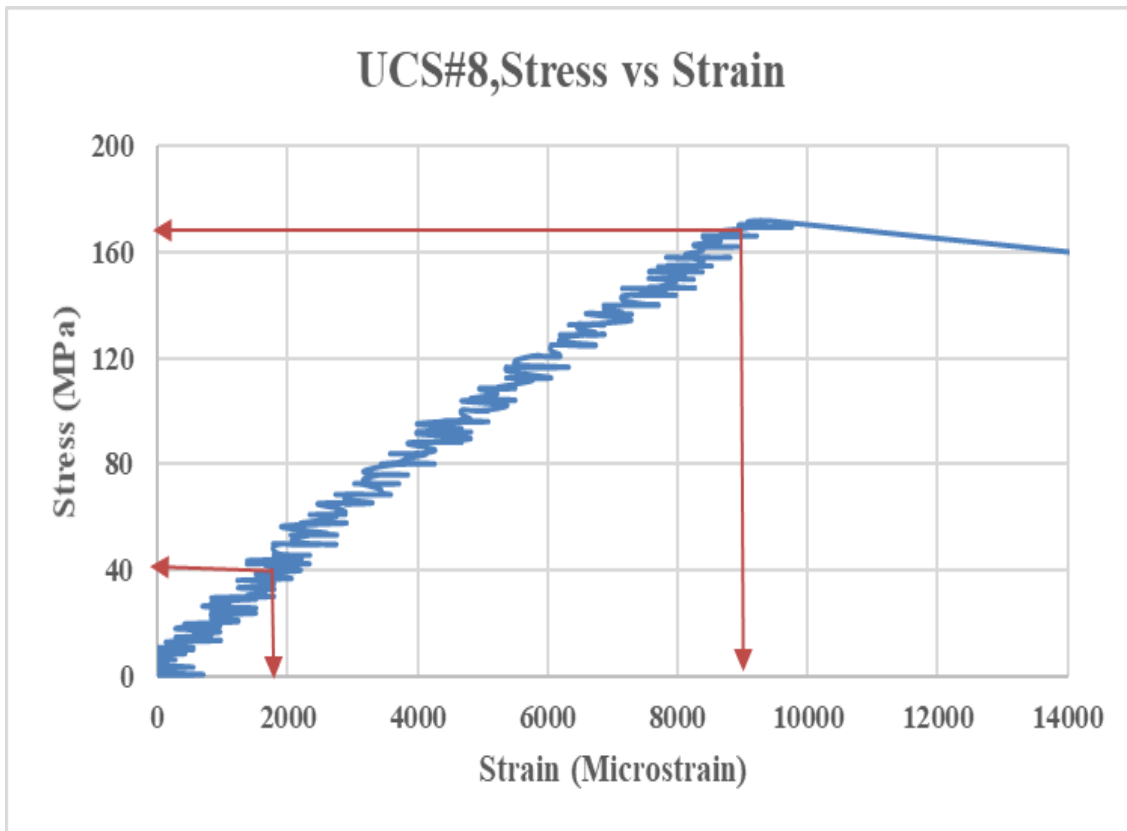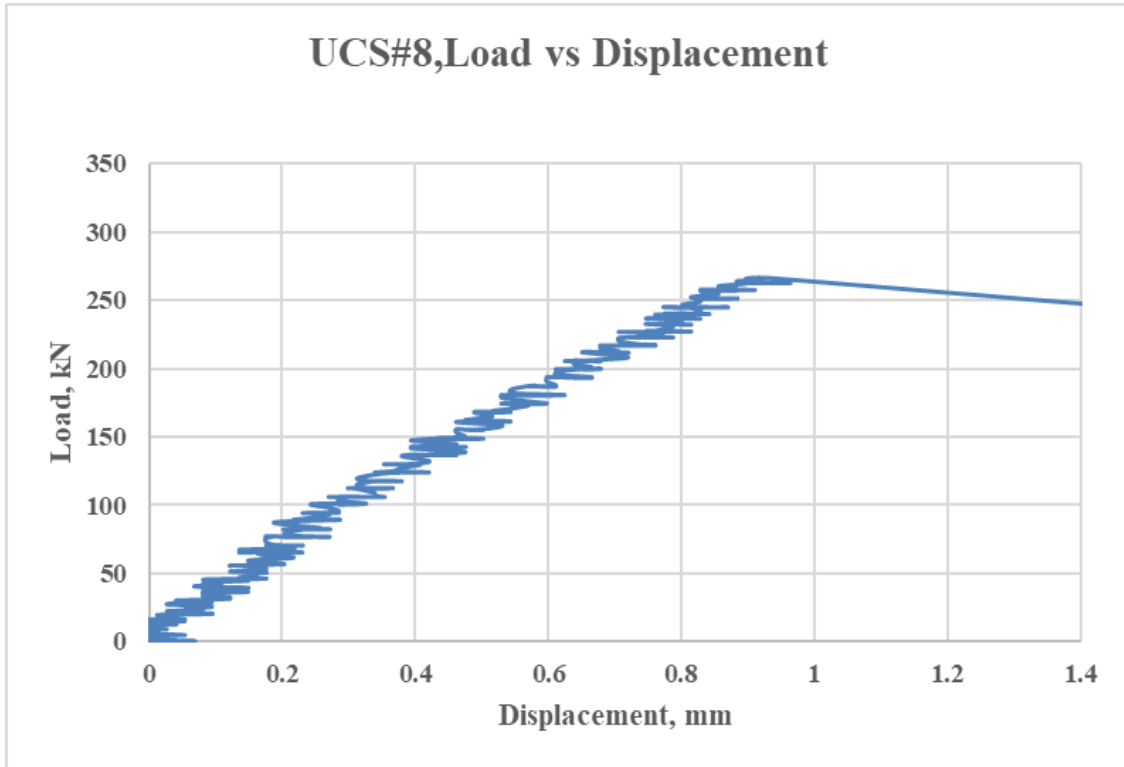
Sample # 09: UCS Test
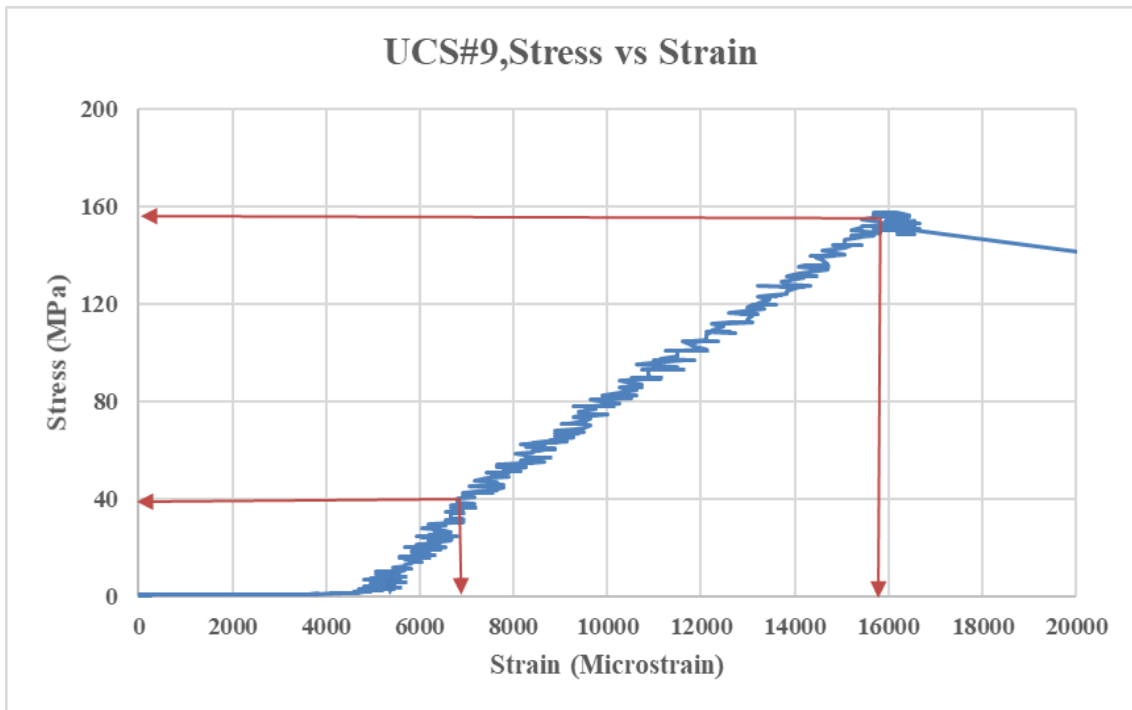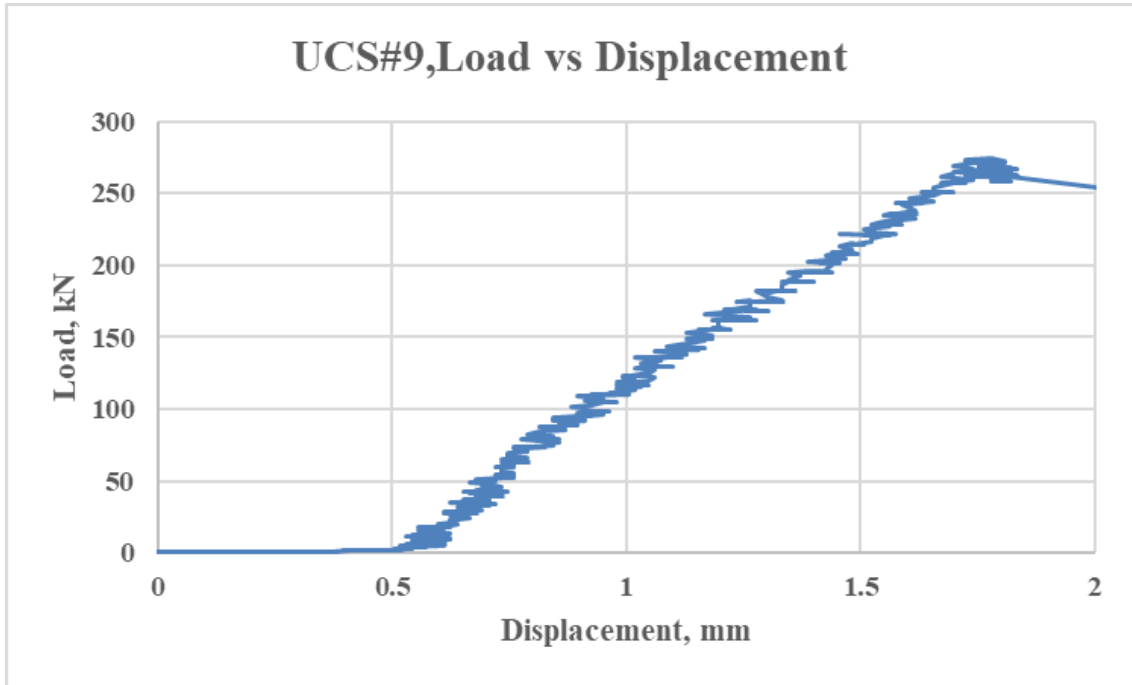
Sample # 10: UCS Test
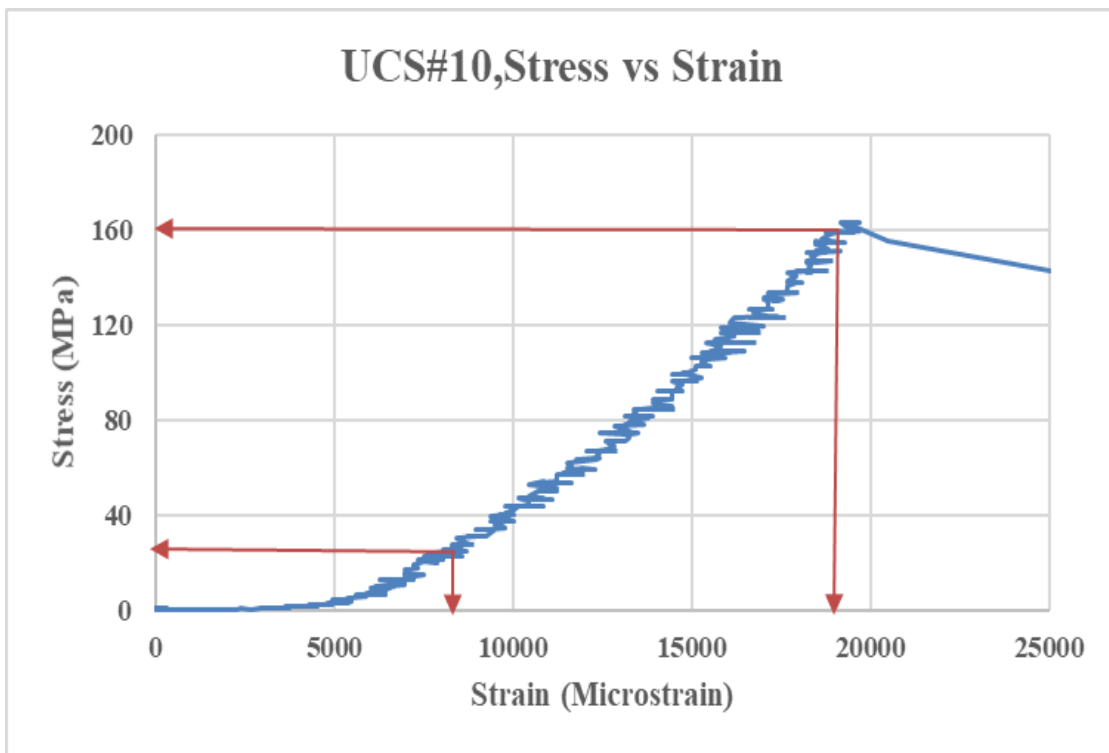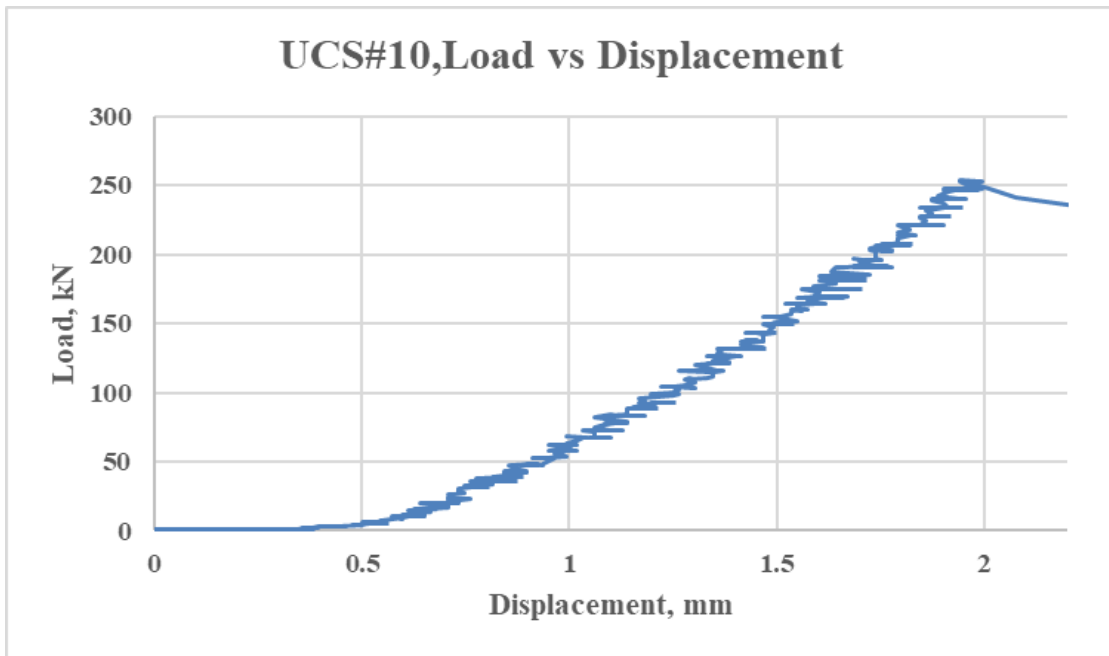
Appendix-F.   Load-Time Details for ITS Tests

Sample # 01: ITS Test
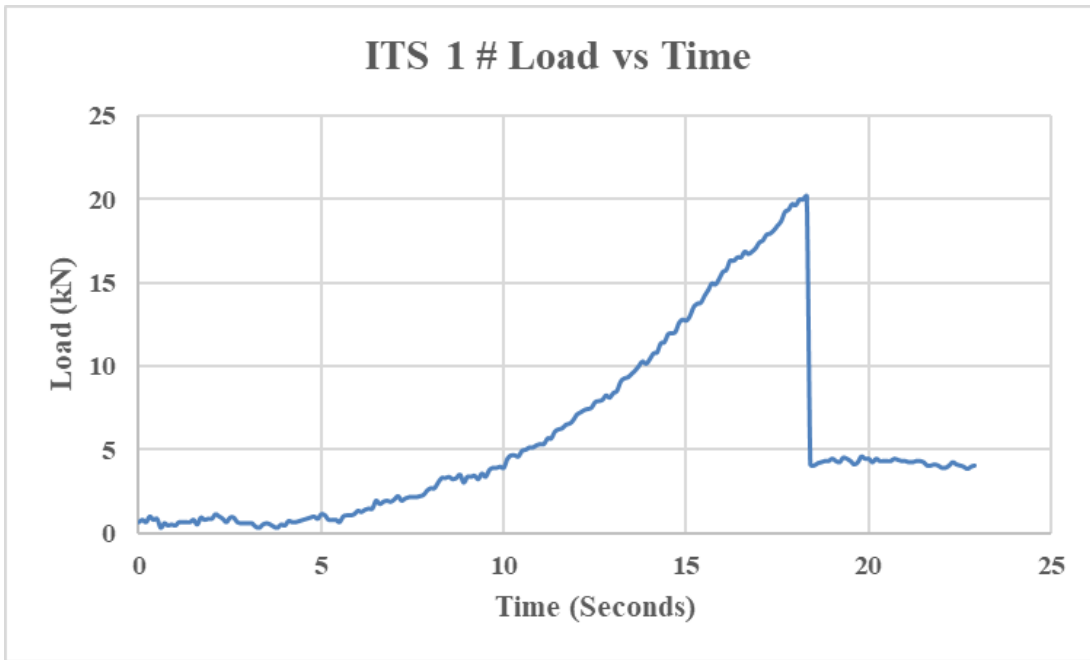
Sample # 02: ITS Test
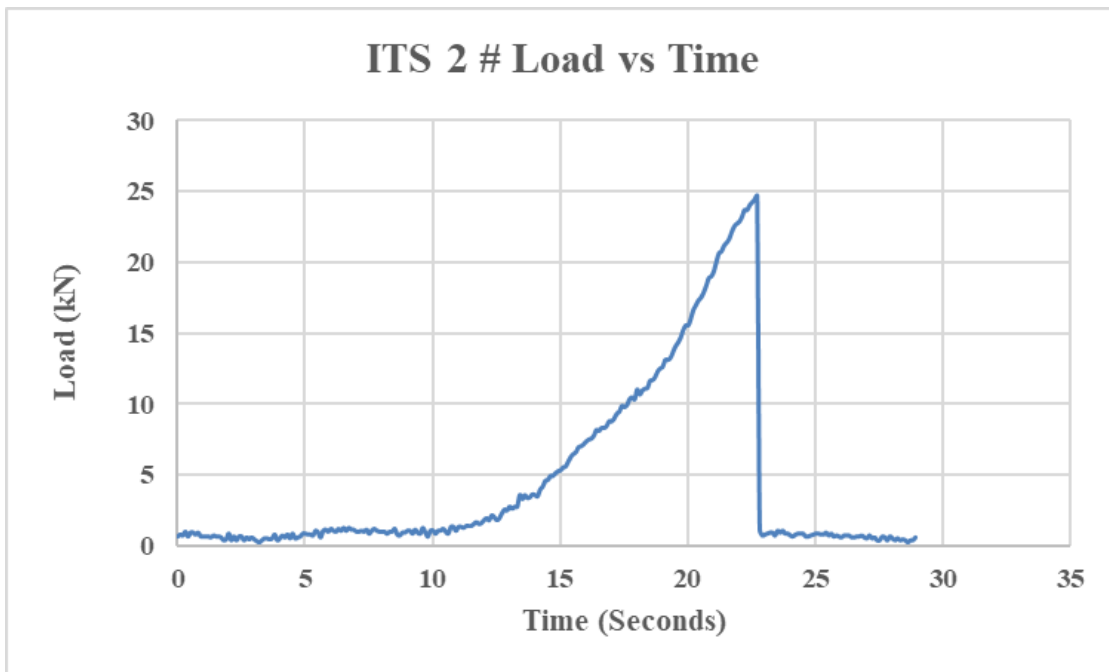
Sample # 03: ITS Test
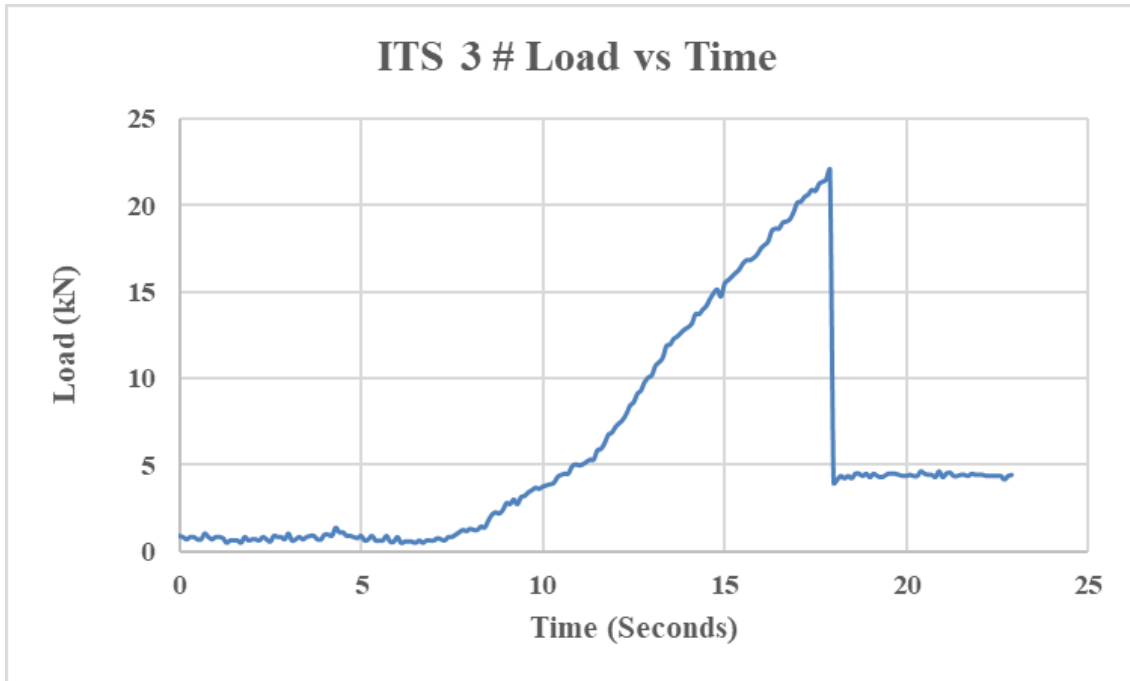
Sample # 04: ITS Test
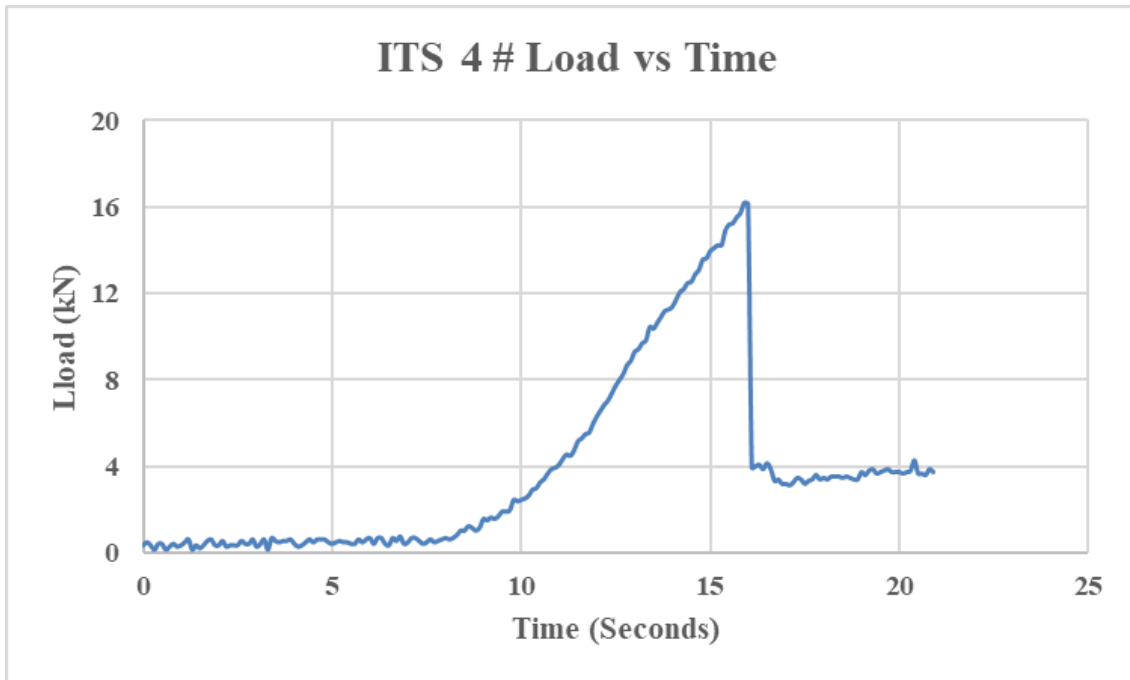
Sample # 05: ITS Test
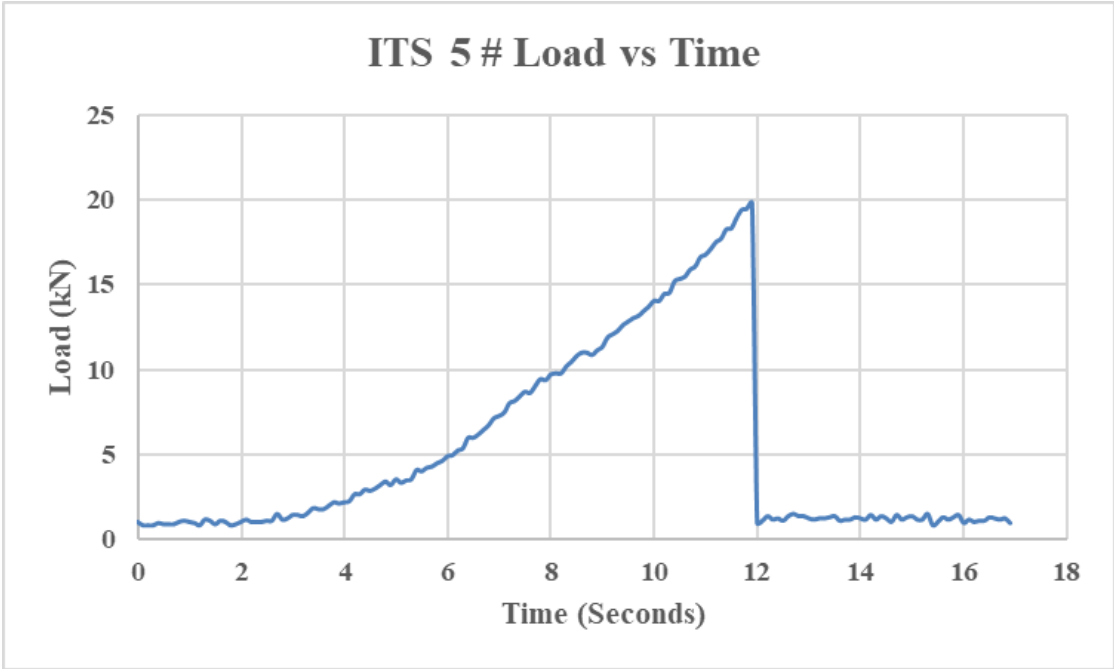
Sample # 06: ITS Test
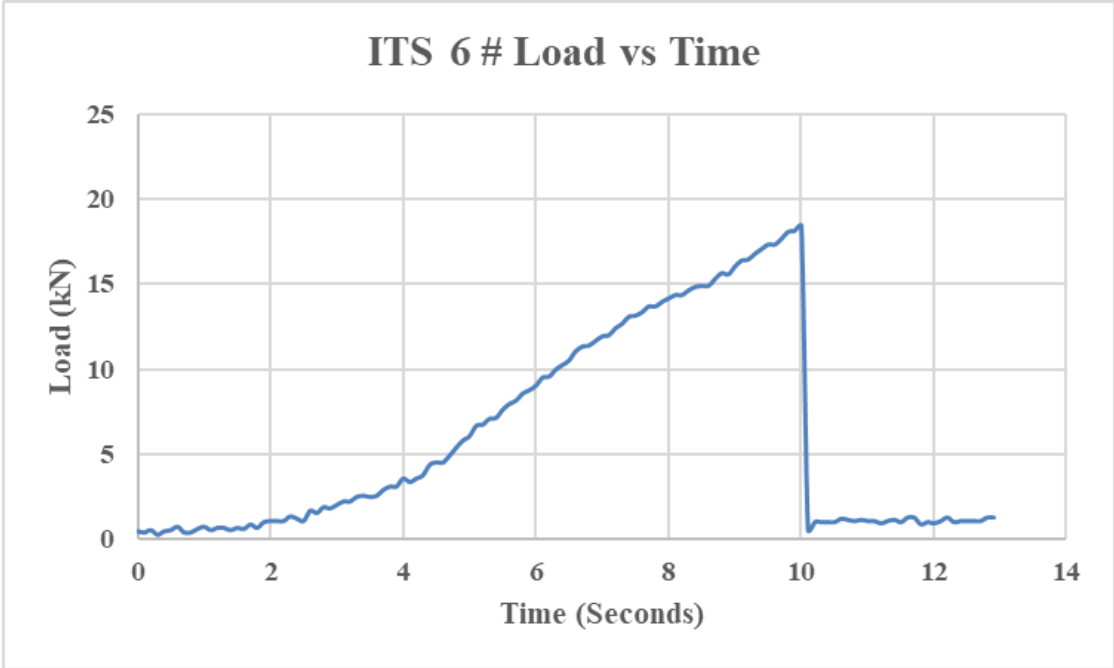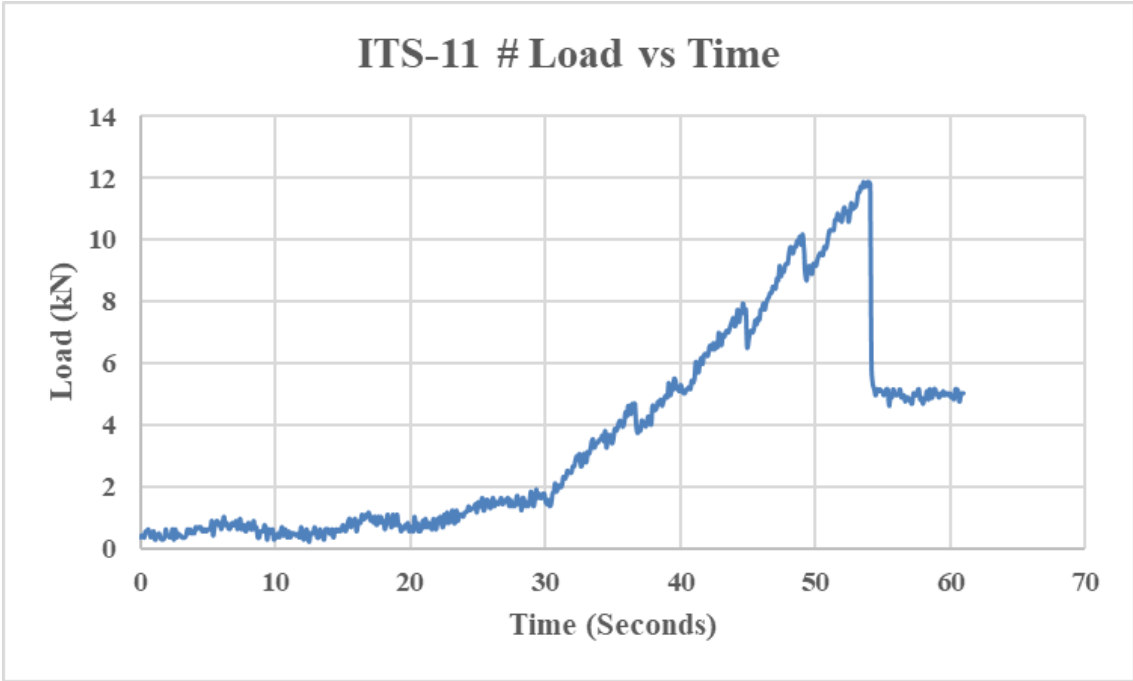
Sample # 07: ITS Test
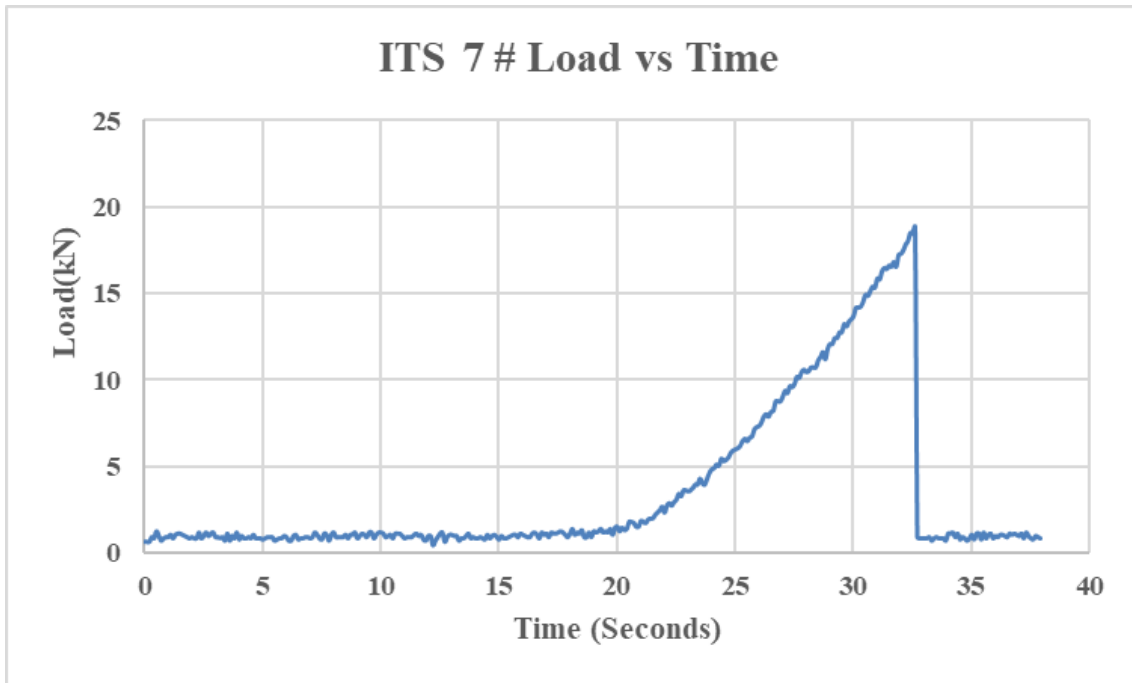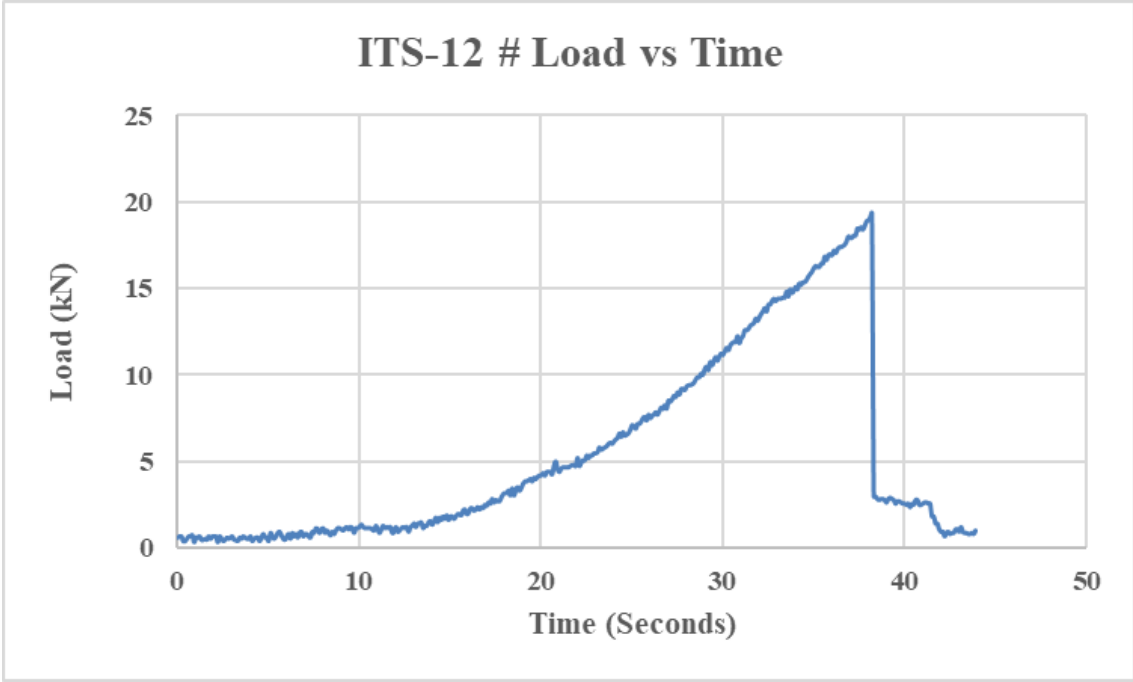

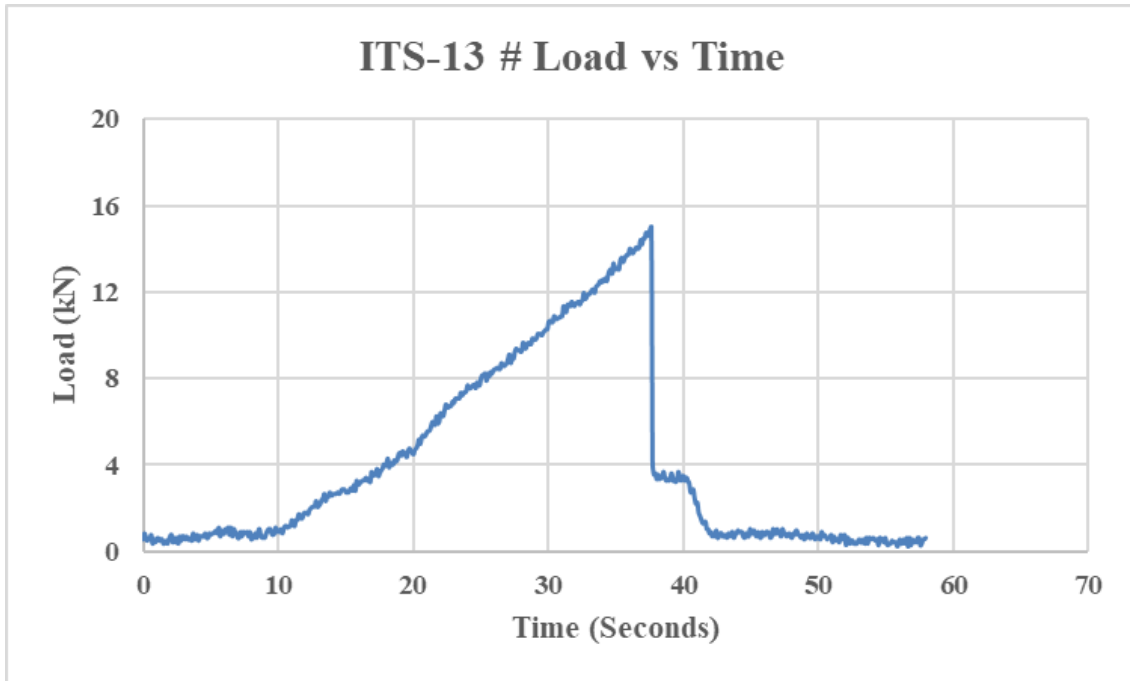**Sample # 08: ITS Test**
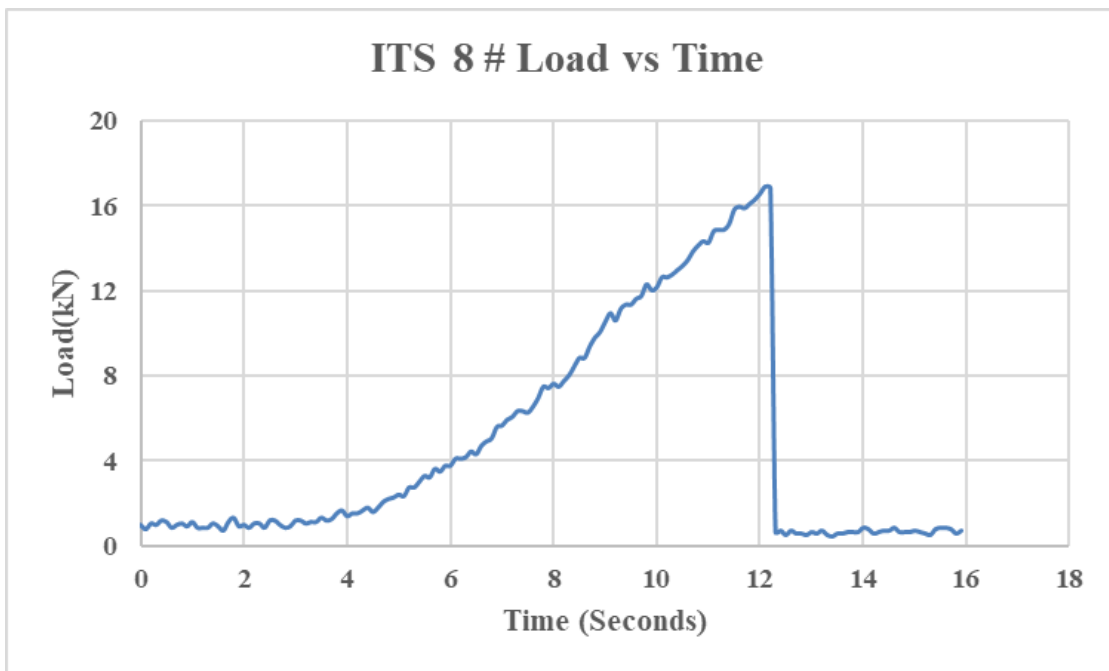
Sample # 09: ITS Test
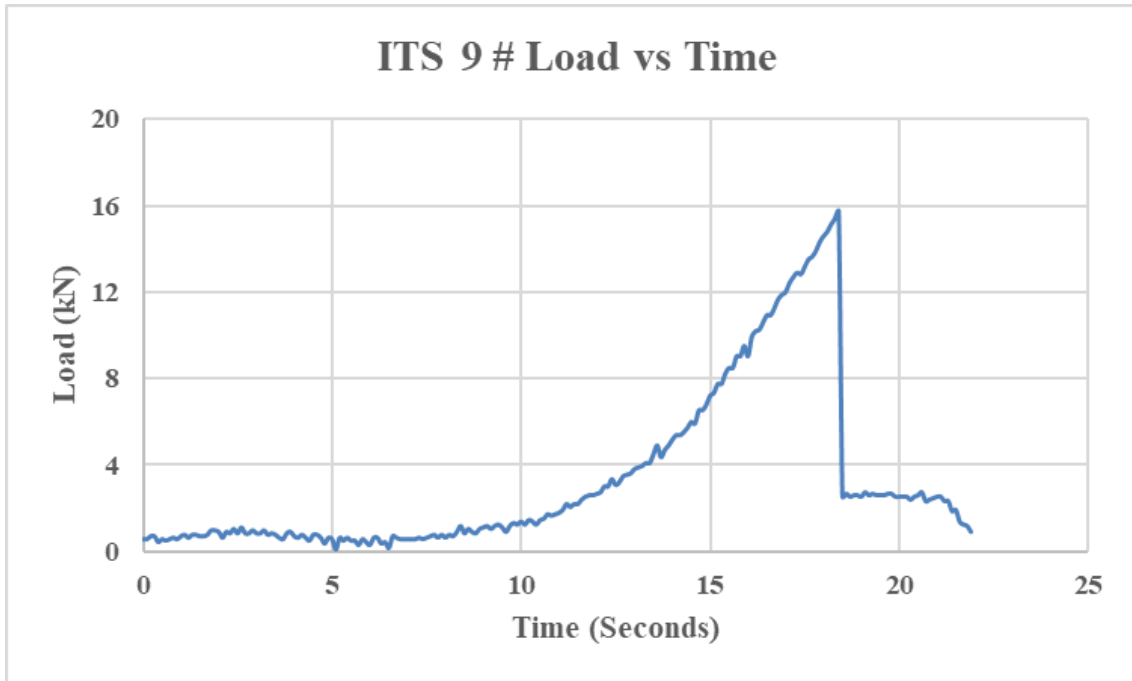
Sample # 10: ITS Test
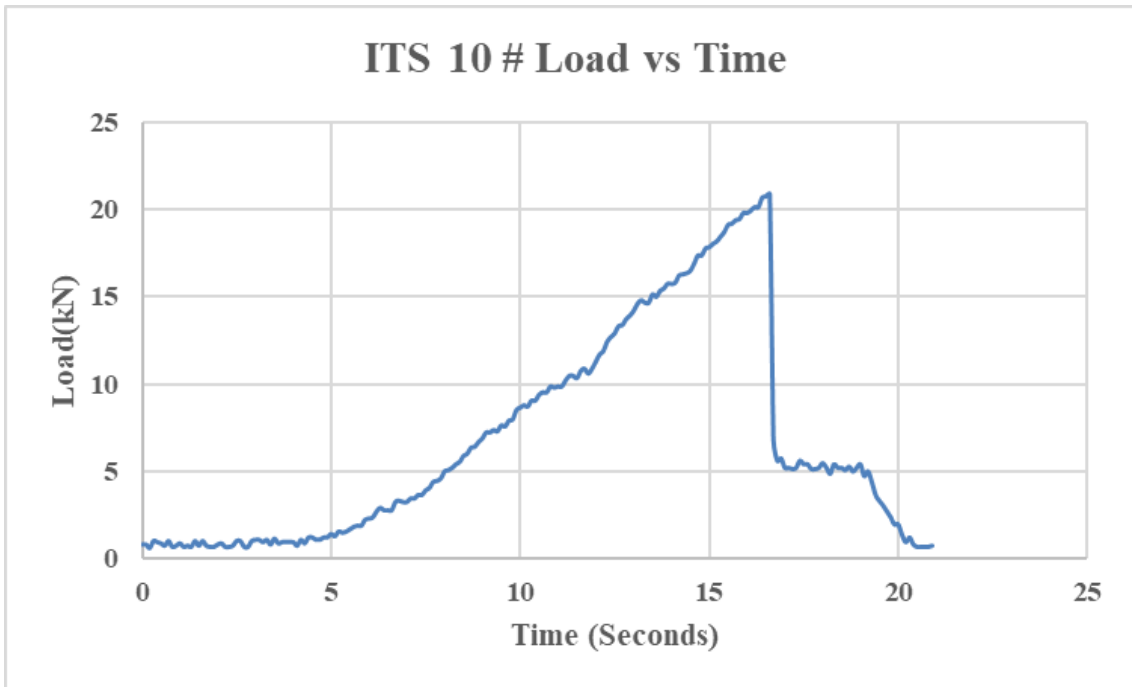
Sample # 11: ITS Test

Sample # 12: ITS Test

Sample # 13: ITS Test

Sample # 14: ITS Test